Assessment of flow and sediment transport in rivers and on floodplains ecosystem based on hydraulic modeling

Dissertation

Zur Erlangung des Doktorgrades
der Mathematisch-Naturwissenschaftlichen Fakultät
der Christian-Albrechts-Universität zu Kiel
vorgelegt von

MSc. Song Song

Department of Hydrology and Water Resources Management
Institute for Natural Resource Conservation
Kiel University, Kiel, Germany

April 2014

Referentin: Prof. Dr. Nicola Fohrer

Koreferent: Prof. Dr. Joachim Schrautzer

Tag der mündlichen Prüfung: 15. April 2014

Zum Druck genehmigt:

Der Dekan

Summary

Lowland river-floodplain systems are typical interactive ecosystems characterized by low altitude differences, high frequency of flooding, low flow velocity and the exchange of energy and substrate between channel and floodplain. Stream power is recognized as a force of formation and development of the river morphology and channel-floodplain interaction. The rising flood risk of Europe in future global change scenarios indicates an urgent need of the study of in-stream and floodplain flow/sediment processes in this area.

The aims of the dissertation are: 1) test the reliability of the mobile OTT Qliner with acoustic Doppler technology (ADQ) and the methodology for velocity and discharge measurement; 2) verification of the new formulas of the vertical flow profile with easy-to-determine parameters for a better understanding of the in-stream flow structure and improvement of the data accessibility; and 3) the evaluation of flow and sediment processes in the channel and on the floodplain of the lowland river-floodplain system in the German Upper Stör catchment by setting up 1-D hydraulic HEC-RAS models for every sub-catchment.

In this dissertation 366 measurements at 174 cross sections in 8 catchments of different sizes located in Northern Germany, Central Germany and South eastern China were collected with the ADQ, FlowSens and ADC from Sep 2011 to Jun 2012. The comparisons between data from different equipment were made to test of the reliability of ADQ. With vertical velocity profiles collected from Upper Stör catchment (Northern Germany), Kinzig catchment (Central Germany) and Changjiang catchment (Southeastern China), a new structure of the prediction formulas involving mean vertical velocity ($u/\bar{u}$) and dimensionless relative water depth (y/H) was proposed and verified. Three field campaigns were carried out in Sep 2011, Jan 2012 and Jun 2012 in the ten selected river sections in Upper Stör catchment, in order to set up the HEC-RAS models for each sub-basins. The discharge, velocity and geometry data of the river section and every cross section were collected during the field campaign, while the topography of the floodplain was extracted from 1m digital elevation model (DEM). Four gauge stations located in the Upper Stör catchment provided long-term discharge series (2000-2010) for the HEC-RAS model calibration and validation. The sediment series and the discharge series in the sub-basins without gauge station were generated by the SWAT model, which has been well calibrated and validated by a previous researcher.

The mobile OTT Qliner with acoustic Doppler technology (ADQ) provides a highly efficient and accurate way to collect flow discharge and velocity data. The results of flow average, profile, layer and point values of ADQ compare very well with electromagnetic or ultrasonic devices. Inner setting tests revealed that the measurement is more sensitive to cell size than to time interval setting. The cell size depth ratio between 0.1 and 0.2 meters produced the highest reliability. Longer time interval is recommended during measurement in shallow and slow flowing rivers.

The applications of the new structure of the prediction formulas show that the substitution of u_* and y with the $u/\bar{u}$ and y/H are reliable and applicable, and all three resulting curves provide satisfactory results. The parabolic curve describes the vertical flow velocity distribution in the best quality with an error of 7%, while the errors of the logarithmic and power fitting are 10% and 11%. In water depth direction, the predicted results of the middle part of the vertical profiles tend to be more reliable and precise than near the water surface area. The error in the river bed region is the highest. Higher catchment slope resulted in larger coefficients and constants in logarithmic and power fitting.

The introduction of the seasonal roughness modification to the HEC-RAS flow models of the sub-catchments of Upper Stör profoundly improves the model performance. The analysis of channelized and floodplain stream discharge and power show that under 10-years-peak discharge conditions only 1-10% of flow power was generated by floodplain flow, while 40-75% volume of water is located on the floodplain. Unit stream power is proportional to the increase of stream discharge, while the increase rate of unit in-channel power was 3 times higher than that of unit flow power on the floodplain. The variation of the increasing rate of the flow power is dominated by the local roughness height, while the flow power distributed on the floodplain mainly depends on the local slope of the catchments.

Analysis of the HEC-RAS sediment output indicates that the Upper Stör catchment is dominated by the deposition process during the study period (2000-2010), with a deposition depth of 2.85 cm in the river sections. The floodplain deposition accounts for only 1 % of the total sedimentation amount, and the rest 99% sediment deposits on the river bed. The land use/cover condition results in the different sedimentation amount in different catchments, while the granularity of the channelized sedimentation is dominated by the altitude of the river section, and the granularity of the floodplain sedimentation positively correlates with the stream power of the flood. The results yielded by the combination of HEC-RAS and SWAT model are comparable to the traditional radioactive dating or sediment trapping method in similar and nearby catchments.

The dissertation proved the accuracy of the new equipment and the measurement methodology, verified the applicability of the easy-to-determine formulas of the vertical flow velocity profiles, and revealed the basic knowledge of the lateral distribution of the flow, energy and sediment during the flood event in Upper Stör lowland river-floodplain system. The findings and the achievements of the dissertation provide a baseline and guideline for the further studies in lowland catchments, especially the river/floodplain interactive processes and nutrient and contamination related studies.

Zusammenfassung

Fluss-Auen-Systeme im Tiefland sind typische interaktive Ökosysteme, die durch geringe Höhenunterschiede, hohe Überflutungshäufigkeit sowie durch den Austausch von Energie und Stoffen zwischen Fließgewässer und Auen gekennzeichnet sind. Die Strömungsleistung ist hierbei die Kraft, durch welche die Flussmorphologie, aber auch die Interaktion zwischen Gewässerschlauch und Auenbereich definiert und entwickelt wird. Die steigende Hochwassergefahr in Europa, die in Zukunftsszenarien zum globalen Wandel immer wieder deutlich wird, zeigt auf, dass die dringende Notwendigkeit zu einem vertieftem Verständnis der Prozesse besteht, durch welche die Interaktionen von Strömung und Sedimenttransport zwischen Fließgewässer und Aue gesteuert werden.

Die Ziele dieser Dissertation sind (1) die Überprüfung der Zuverlässigkeit des mobilen OTT Qliner-Durchflussmessgerätes mit einem akustischen Doppler-Messsystem (ADQ) sowie der Methodik für Fließgeschwindigkeits- und Abflussmessungen, (2) die Verifizierung der neuen Formeln zum vertikalen Strömungsprofil anhand einfach zu ermittelnder Parameter für ein besseres Verständnis von Strömungsmustern sowie einer Verbesserung des Datenzugangs und (3) die Evaluierung von Strömungs- und Sedimentprozessen im Gewässerbett und in den Auenbereichen des Fluss-Auen-Systems im Einzugsgebiet der oberen Stör anhand von HEC-RAS-Modellen für jedes Teileinzugsgebiet.

Für diese Dissertation wurden im Zeitraum von September 2011 bis Juni 2012 insgesamt 366 Messungen an 174 Fließquerschnitten in acht Einzugsgebieten verschiedener Größe in Nord- und Mitteldeutschland, sowie im Südosten Chinas mit dem ADQ, ADH und FlowSens durchgeführt. Um die Zuverlässigkeit des ADQ zu testen, wurden hierbei Daten mit unterschiedlichen Geräten erhoben und miteinander verglichen. Anhand von vertikalen Geschwindigkeitsprofilen, die im Einzugsgebiet der oberen Stör (Schleswig-Holstein), im Einzugsgebiet der Kinzig (Hessen) und im Gebiet des Changjiang (China) gemessen wurden, konnte eine verbesserte Struktur der Formeln zur Vorhersage, welche die mittlere vertikale Geschwindigkeit ($u/\bar{u}$) sowie die dimensionslose Größe der relativen Wassertiefe (y/H) enthält, entwickelt und verifiziert werden. Um geeignete Eingangsdaten für den Aufbau von HEC-RAS-Modellen in den Teileinzugsgebieten der oberen Stör zu erheben, wurden im September 2011, Januar 2012 und Juni 2012 jeweils Messkampagnen zu zehn ausgewählten Flussabschnitten durchgeführt. Während der Kampagnen wurden der Abfluss, die Fließgeschwindigkeit sowie die Gewässergeometrie der Flussabschnitte und aller Fließquerschnitte erfasst. Die Topographie der Auenbereiche wurde mithilfe eines digitalen Geländemodells mit einer Auflösung von 1x1 Meter ermittelt. Insgesamt vier Pegelstationen innerhalb des oberen Stör-Einzugsgebiets lieferten langjährige Abflusszeitreihen (2000-2010) für die Kalibrierung und Validierung des HEC-RAS-Modells. Die Abfluss- und Sedimentzeitreihen in den Teileinzugsgebieten ohne Messpegel wurden mithilfe eines kalibrierten und validierten SWAT-Modells des Einzugsgebiets

erzeugt, welches im Rahmen einer anderen Forschungsarbeit entstanden war.

Der mobile OTT Qliner mit akustischer Dopplertechnologie (ADQ) bietet eine effiziente und genaue Möglichkeit zur Aufnahme von Durchfluss- und Fließgeschwindigkeitsdaten. Die Ergebnisse des durchschnittlichen Durchflusses sowie von Profil-, Schicht- und Punktwerten des ADQ sind vergleichbar mit denen elektromagnetischer Messungen oder von Ultraschall-Systemen. Tests der internen Einstellungen der Geräte zeigten, dass die Messungen sensitiver gegenüber unterschiedlichen Zellgrößen sind als gegenüber Änderungen der Zeitintervalle zwischen Messungen. Mit einem Verhältnis zwischen Zellengröße und Tiefe zwischen 0,1 und 0,2 Metern konnte die größte Zuverlässigkeit erzielt werden. Ein längeres Zeitintervall wird für Messungen in flachen oder langsam fließenden Gewässern empfohlen.

Die Anwendung der neuen Struktur der Formeln zur Vorhersage zeigt, dass die Ersetzung von u_* und y mit $u/\bar{u}$ und y/H zuverlässig und anwendbar ist. Alle drei Ergebniskurven zeigten zufriedenstellende Ergebnisse. Die parabolische Kurve beschreibt die Verteilung der vertikalen Fließgeschwindigkeit mit höchster Genauigkeit bei einer Abweichung von lediglich 7%, während die Fehler bei einer logarithmischen oder exponentiellen Anpassung bei 10% bzw. 11% liegen. In der Tiefenrichtung weisen die vorhergesagten Ergebnisse im mittleren Teil der vertikalen Profile eine höhere Zuverlässigkeit und Genauigkeit auf als an der Wasseroberfläche. In der Nähe des Gewässerbetts ist der Fehler am größten. Ein höheres Gefälle im Einzugsgebiet resultierte in erhöhten Koeffizienten für die logarithmische und exponentielle Anpassung.

Durch die Einführung einer saisonalen Rauigkeit als Modifikation in die HEC-RAS-Strömungsmodelle der Teileinzugsgebiete der oberen Stör konnte die Modellgüte erheblich verbessert werden. Die Analyse des Durchflusses sowie der Strömungsleistung im Fließgewässerbett sowie im Auenbereich zeigt, dass unter den Bedingungen eines 10-jährigen Spitzenabflusses lediglich 1-10% der Fließleistung durch Abfluss in der Flussaue generiert wurde, während zugleich 40%-75% der Wassermenge durch den Auenbereich fließen. Die Einheit Strömungsleistung ist proportional zum Anstieg des Abflusses im Gewässerbett, während Steigerungsraten der Einheitsleistung im Fließgewässer dreimal höher waren als jene der Einheitsleistung über der Flussaue. Die Variation der steigenden Rate der Fließleistung wird durch die lokale Rauigkeit dominiert, während die Fließleistung im Auenbereich hauptsächlich vom örtlichen Gefälle im Teileinzugsgebiet abhängt.

Die Analyse der HEC-RAS-Ergebnisse zum Sediment zeigt, dass das Gebiet der oberen Stör während des Untersuchungszeitraums zwischen den Jahren 2000 und 2010 durch Depositionsprozesse mit Ablagerungshöhen von bis zu 2,85 Zentimetern in den Flussabschnitten dominiert wird. Die Ablagerung in den Auenbereichen trägt lediglich 1% zum gesamten Sedimentationsvolumen bei, während die restlichen 99% im Gewässerbett abgelagert werden. Die Landbedeckungs- und Landnutzungsmuster in unterschiedlichen Teileinzugsgebieten resultieren in unterschiedlichen Ablagerungsmengen, während die

Körnung der Ablagerungen im Gewässerschlauch durch die Höhe des Flussabschnitts bestimmt wird, wohingegen die Körnung in der Flussaue positiv mit der Strömungsleistung des Hochwasserereignisses korreliert. Die Ergebnisse, die durch die Kombination der Modelle SWAT und HEC-RAS erzielt wurden, sind vergleichbar mit den Ergebnissen üblicher Radiokarbondatierungen oder von Experimenten mit Sedimentfallen, wie sie in benachbarten Flussgebieten durchgeführt wurden.

Die Dissertation konnte die Genauigkeit neuer Geräte und Messmethoden nachweisen, die Anwendbarkeit von einfach zu ermittelnden Formeln für vertikale Tiefenprofile verifizieren, sowie grundlegendes Wissen zur lateralen Verteilung von Strömung, Energie und Sediment während einzelner Hochwasserereignisse im Fluss-Auen-System des Tieflandeinzugsgebiets der oberen Stör schaffen. Die Ergebnisse und Leistungen dieser Dissertation bieten eine Grundlage und eine Richtschnur für die weitere Forschung in Tieflandeinzugsgebieten, insbesondere hinsichtlich der Prozesse bei der Interaktion zwischen Gewässerbett und Auenbereich, aber auch im Hinblick auf Studien zu Nährstoffen sowie der Gewässerbelastung.

Table of Contents

List of Figures

List of tables

List of appendix

Chapter 1. Introduction

This PhD thesis is composed of four papers which have been either published (Chapter 2 and Chapter 4) or revised to publication (Chapter 3 and Chapter 5). The present section first gives an introduction about the general background and the literature review. The fundamental scientific questions about flow velocity modeling, hydraulic modeling and sediment modeling both in channel and on the floodplain are then briefly discussed. The methodological framework is developed and shown in the following part to explain the technique that was developed to solve the scientific questions. Finally, four scientific papers, which have been integrated into the methodological framework, are presented to answer the main underlying scientific questions.

1.1 Motivation and literature review

Channel and floodplain flow are the key hydraulic components in lowland areas (Stewart et al., 1999). Climate change is likely to increase the risk of winter flood in Northern German areas (Lehner et al., 2006). The results from climatic and hydrological models point out that the typical 100-year flood tends to occur more frequently in large areas of Europe (Kundzewicz et al., 2010). Northern to northeastern Europe are under rising risk of flood according to the results of the global integrated water model WaterGAP (Lehner et al., 2006). The International Commission for the Hydrology of the Rhine basin (CHR) has carried out a multi-model research and shows that the increased winter precipitation and snow-melt discharge will case higher winter flood risk in Rhine basin (Middelkoop et al., 2001). These scenarios indicate a strong need to simulate the lowland flow/sediment process, especially during flood events when the interaction processes are triggered between in-channel and floodplain.

River flow velocity is crucial to simulate flow/sediment processes, including discharge hydrographs, the residence time of water in the hydrological system and the related pollution or sediment transportation process (Nittrouer et al., 2012; Schulze et al., 2005). The massive data required in hydraulic and hydrologic modeling challenges the traditional data collection methodology with the mechanical velocity or electronic/magnetic equipments. New generations of hydrodynamics instrument adopted optics, radar, acoustics and electromagnetism technology offer superior efficiency in the velocity and discharge measurement. It is replacing traditional mechanical meters both in laboratory and field conditions (Muste et al., 2008; Thandaveswara, 2011). Acoustic Doppler (current) Instrument is one of the new-emerging equipment in velocity and discharge measurement. The efficiency in data collecting with Acoustic Doppler Instrument has been proven, but the accuracy and reliability of the equipment and the measurement methodology in the field still need more research (Gunawan et al., 2010; Yorke and Oberg, 2002).

A better understanding of the velocity structure regularities in open-channel flows can provide the basic methodology for data collection, flow forecasting and the design of hydraulic engineering systems (Chiu and Tung, 2002; Rimkus, 2012; Yang and Chang, 2005). The variability of the velocity profile at the given cross section along the flow depth direction influences physical processes and have been discussed over the past decades (Singh et al., 2013). The parabola line, power and logarithmic distribution lines are mainly in use and have been proven to be efficient to describe and predict the vertical velocity profile (Bowers et al., 2012; Reniers et al., 2004). These three traditional prediction models are parameterized with the friction velocity, the real measured depth and some other observed catchment-specific values. Several studies have pointed out that the deduction methods for friction velocity were inconsistent, and to get the real measured depth is of less efficiency (Alfredsson and Örlü, 2012; Wei et al., 2005). It is plausible to expect a new velocity distribution model with some easy to determine variables.

The flow/sediment process and the related nutrients transportation within lowland eco-hydrogical systems depends on different hydraulic, chemical and biological conditions including exchange processes between streams and riparian wetlands during flood events (Rücker and Schrautzer, 2010). The evaluation of the nutrient and organic matter dynamics from a glacial river-floodplain system in the Swiss Alps (Val Roseg) indicated that the glacial melt water is the main source of the nutrients or organic matter, while the floodplain served as a major sink for particulate phosphorous and suspended sediment (Tockner et al., 2002). However, the study of river Aire and Swale, in Yorkshire, UK emphasize the potential importance of floodplain deposition as a conveyance loss. Comparison between the sediment sampled from both in-channel and on the floodplain in Aire and Swale revealed that the channel sediment storage represents less than 3% of the outlet flux (Walling et al., 2003). Due to the combination of complex geomorphology, vegetation and land use/cover condition of the floodplains, the simulation of the flow and sediment process during flood is under challenge (Rudorff et al., 2014). A detailed knowledge of flood event characteristics is in urgent need to solve the problems in nutrients migration and circulation between in-channel and floodplain system (Beechie et al., 2006; Mouri et al., 2013; Tockner et al., 2002; Walling et al., 2003).

1.2 HEC-RAS model

Hydrologic Engineering Centers River Analysis System (HEC-RAS) model (USACE, 2010) has been widely used in flow and sediment process research in the last decades. The HEC-RAS model is an integrated 1-D hydraulic model for interactive use in a multi-tasking environmental management (Brunner, 1995). The main structure and functions of the HEC-RAS model are shown in Fig. 1.1. Traditionally, the HEC-RAS model is predominantly adopted in flood forecasting, floodplain delineation and inundation assessment (Hicks and Peacock, 2005; Horritt and Bates, 2002; Yang et al., 2006). The assessments of the effects of anthropogenic river alteration, the river ice or wider river jams simulation are other important

research issues of HEC-RAS (Daly and Vuyovich, 2003; Seckin and Atabay, 2005; Sowiski, 2006).

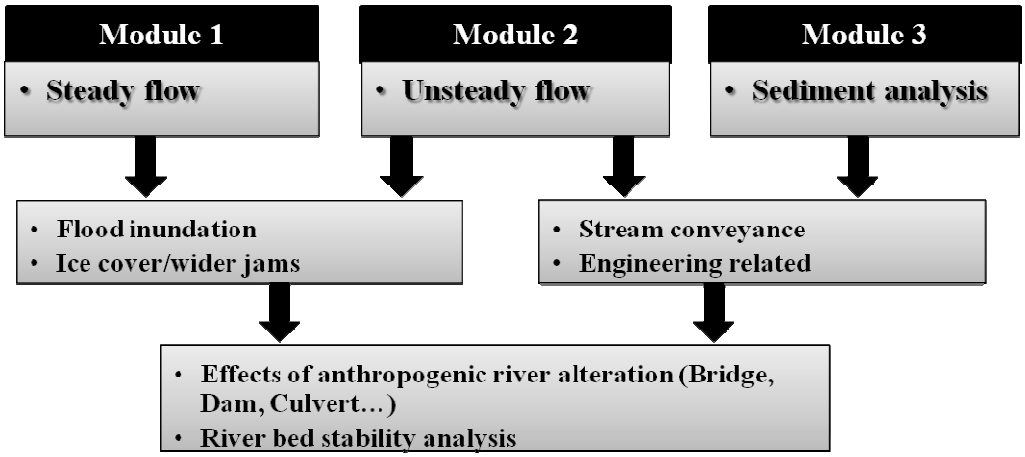

Fig. 1.1 The structure and application of the HEC-RAS model

Integrated modeling approaches aimed at linking HEC-RAS model with other models to extract the best of each individual model components have been preliminarily pursued (Fig. 1.2). Integrating HEC-RAS model with other 1-D or 2-D hydraulic models enables multi-functional assessment and simulation, such as habitat predations, aquifer/drain interaction process studies, water quality modeling etc. (Bockelmann et al., 2004; Fan et al., 2009; Rodriguez et al., 2008). The integrated HEC-RAS and DIVAST (Depth Integrated Velocity and Solute Transport model (Lin and Falconer, 1995)) modeling tool based on river Afon Morlais in United Kingdom, showed an potential increase in habitat diversity (Bockelmann et al., 2004). The combination of the HEC-RAS model and the Qual2K model (Chapra and Pelletier, 2003) enables the water quality simulation in a tidal river in Northern Taiwan, and the simulation results agree with the monitoring data from the river (Fan et al., 2009). The innovative modeling approach using integrated HEC-RAS and MODFLOW (Hsieh and Freckleton, 1993) model were applied to the groundwater/surface water system of the Choele Choel Island, Argentina. The output of the model showed smooth and realistic hydraulic profiles along drains and the backwater effects are clearly simulated (Rodriguez et al., 2008).

The SWAT model is a continuous, long-term, semi-distributed parameter model that can simulate surface and subsurface flow, soil erosion and sediment deposition, and nutrient movement through watersheds (Arnold et al., 1998). Promising results were yielded in linking sediment output of the SWAT model with the HEC-RAS model and the BIOMOD model in the bivalve habitat suitability assessment in Northern German lowland catchment (River Kielstau, Schleswig-Holstein, Germany) (Jähnig et al., 2012; Kiesel et al., 2013; Kuemmerlen et al., 2014). Another SWAT-HEC-BIOMOD integrated model was set up based on mountainous basin (Changjiang basin, Poyang Lake region, China) for the assessment of changes in the in-stream habitat conditions for benthic macroinvertebrates, which provides an important link between the

assessment of the catchment properties and the abundance and dynamics of benthic macroinvertebrate species in the river beds (Kuemmerlen et al., 2012; Schmalz et al., 2012).

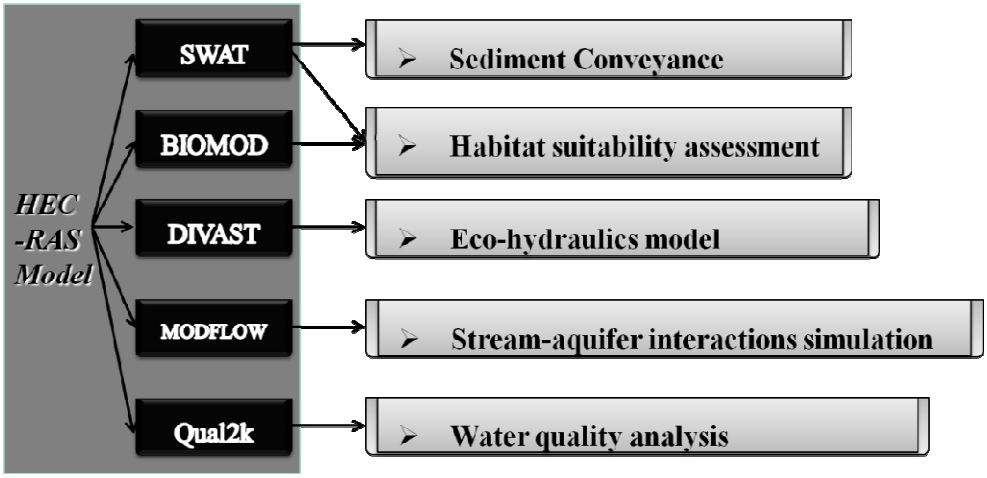

Fig. 1.2 Integrated model research of the HEC-RAS model

In this study, we combined the HEC-RAS model and the SWAT model to simulate the flow and sediment processes in-channel and on the adjacent floodplain. The continuous long-term discharge and sediment data output of the SWAT model work as the boundary condition input into the HEC-RAS model. This methodology extracts the data generation function of the SWAT model (Jain, 2010) and the geometry transform function of the HEC-RAS model.

1.3 Study area

1.3.1. Northern German lowland catchments

1.3.1.1 Catchments in Schleswig-Holstein

River Stör and Treene are located in Northern German lowland area. River Stör flows westward through the city Neumünster and joins the Elbe near Glückstadt, while River Treene is the most important tributary of the Eider river. The Upper Stör catchment, Upper Treene catchment and one of its sub-catchment Kielstau were selected as our study areas in order to exclude the tidal effect (Fig. 1.3).

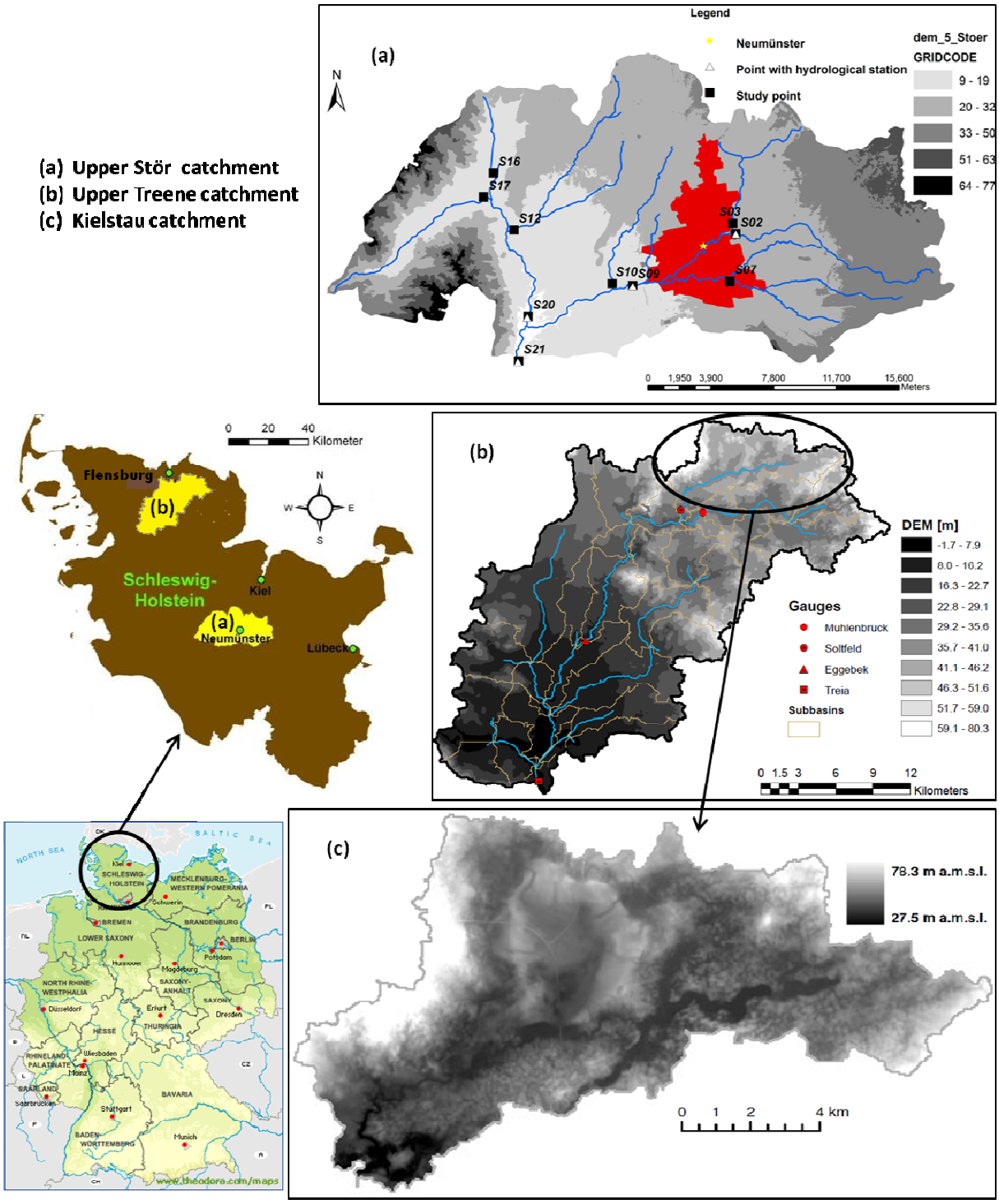

Fig. 1.3 The location of the selected catchments and the study points of the Upper Stör catchment (LVermGeoSH, 1995)

The main study area of this dissertation is the Upper Stör River catchment, which is part of the lowland area located in the middle of Schleswig-Holstein/Northern Germany (Fig. 1.3 a). With a drainage area of 468 km^2, the catchment stretches over 35 km in the east-west direction and 19 km in the north-south direction. In most of the catchment the gradients are usually smaller than 1°, except southwestern part, which has gradients of more than 3° (LVermGeoSH, 1995). Dominant soil texture classes are sands with different percentages of loam and land use is characterized by arable land (48.1%), pasture (29.5%) and forest (9.1 %) (Schmalz et al., 2008). The catchment is dominated by shallow groundwater tables and older glacial and glaciofluvial sediments. Small sand-dominated lowland rivers and small gravel-dominated lowland rivers are the two river types of this catchment (MLUR, 2004). The catchment was divided into 20 sub catchments according to the hydrological conditions of the tributaries, and ten of them were selected as study points in the model study of this thesis (Fig. 1.3 a).

Upper Treene catchment has an area of 797 km^2 and a total flow length of 82 km (MLUR, 2004) (Fig. 1.3 b). The origin of river Treene located in the lake Treßsee in the northeast of Schleswig-Holstein. River Treene flows in southwestern direction and drains into the river Eider. The main part of the catchment (79.2%) is dominated by agricultural land, including cultivated cropland, grassland and permanent pastures. The natural or near natural areas like forests, shrub land, wetland and fallow land account for an 8% of the catchment area. Construction land covers the rest of the area (Geertz, 2012). The substrates in the eastern part of the catchment are dominated by podsol and luvisol soils, and in the middle part the substrates are mainly stratified clay and sandy soils, with ombric histosols. The western part is characterized by sandy soils, changing with podsols, luvisols and gley (LANU, 2006). The altitude of the catchment varies from 0 to 97 m a.s.l. (LVermGeoSH, 1995).

Kielstau is a part of the Treene catchment, located about 10 km south-east from the city of Flensburg (Fig. 1.3 c). The river has its origin in the upper part of Lake Winderatt and drains an area of 50 km^2 with a flow length of 17 km. The catchment is dominated by loamy and peat soils. Arable land and pasture account of the 56% and 26% of the catchment area. The low surface runoff fraction and low hydraulic gradients are two main characteristics of the catchment hydrology (Kiesel et al., 2013; Schmalz et al., 2008; Wu et al., 2011) .

1.3.1.2 **Catchments in Low Saxony and Saxony-Anhalt**

One of the aims of the joint project “NaLaMa – nT” (Nachhaltiges Landmanagement im Norddeutschen Tiefland) is an innovative and sustainable land management in the North German lowlands based on changing ecological, economic and social conditions. Models were developed for sustainable water resource management in the regions Diepholz, Uelzen, Fläming and Oder-Spree (Fig. 1.4). These four regions lie on a transect line from west to east and form the natural environment, structural, economic and demographic gradients. Three of them are selected for measurements in this dissertation (NaLaMa-nt,

2014).

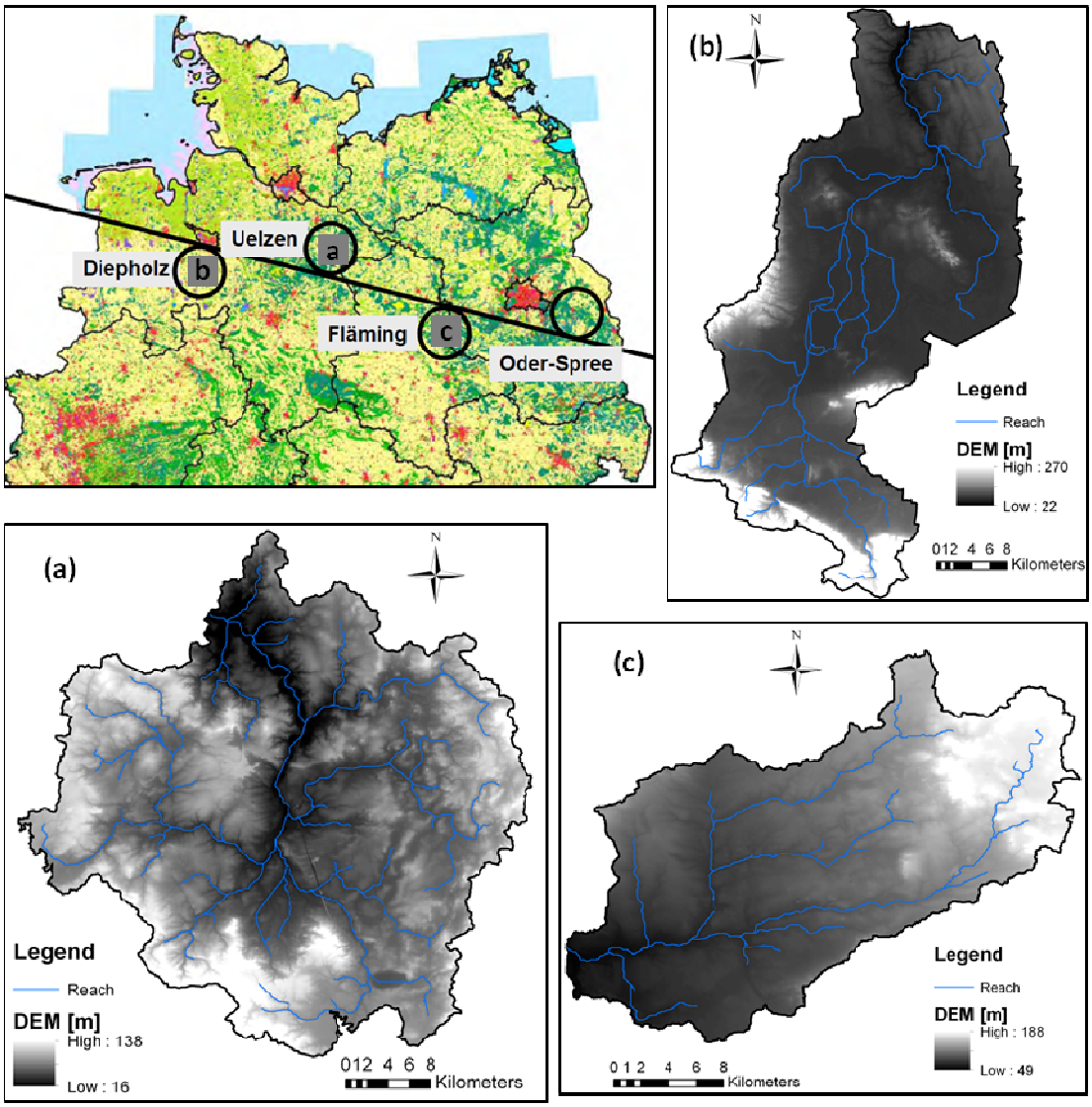

Fig. 1.4 The location of the catchments in NaLaMa-nT project, (a) Ilmenau, (b) Hunte, (c) Nuthe (ST)

Note: the DEM maps of the selected catchments based on project data from NaLaMa-nT project.

Ilmenau catchment located in the south of Hamburg is a tributary of the German river Elbe, with a drainage area of 2852 km² and a river length of 107 km. It flows through Lüneburger Heide. The catchment land use is dominated by moorland, gees land and forest (Fig. 1.4 a). River Hunte is 189 km in length and is an important tributary of river Weser, which flows into the North Sea. It is located in Northern Germany, in the south of Bremen and in the north of Osnabrück. The catchment area is around 2785 km². The river flows through the lake Dümmer (Fig. 1.4 b). Nuthe (ST) is a tributary of the river Elbe, located in the Fläming region inside the tri-city area Magdeburg-Halle (Saale)-Potsdam. The catchment is around 570 km² and the flow length is about 39 km. The agriculture land and forest cover

most part of the area (Fig. 1.4 c).

1.3.2. Low mountainous catchment

The Kinzig catchment is a low mountainous catchment located in Central Germany lying 15-80 km east of Frankfurt am Main in south-eastern Hessen. The river length of Kinzig is about 86 km and it drains an area of 1059 km². The altitude of catchment ranges from 627 m at origin, Vogelsberg mountains, down to 98 m in the Main valley (Meurer, 2012). It is classified as a mid-sized fine to coarse substrate dominated siliceous highland river (HMUELV, 2011). Average elevations are between 396 and 336 m in the north-eastern sub-basins, 240 m in the northern and 219 to 323 m in the southern center, 132 to 164 m in the western sub-basins and around 200 m in the central sub-basin along the river valley. The soil in the central part of the catchment is dominated by Cambisols (BB). From central to northern part, there occurs Cambisols (BB), Stagnosols (SS) and Luvisols (LL). Redzina (RR) and Stagnosols mainly appear in the east part. The south-west part of the catchment is mainly covered by Luvisols, while the western part is dominated by Luvisols and Gley (GG) (BGR, 2012). Forest is the main land use type in the catchment (46%). Arable land covers around 25% of the catchment, followed by pasture (20%). The remaining area is occupied by settlement (BKG, 2011).

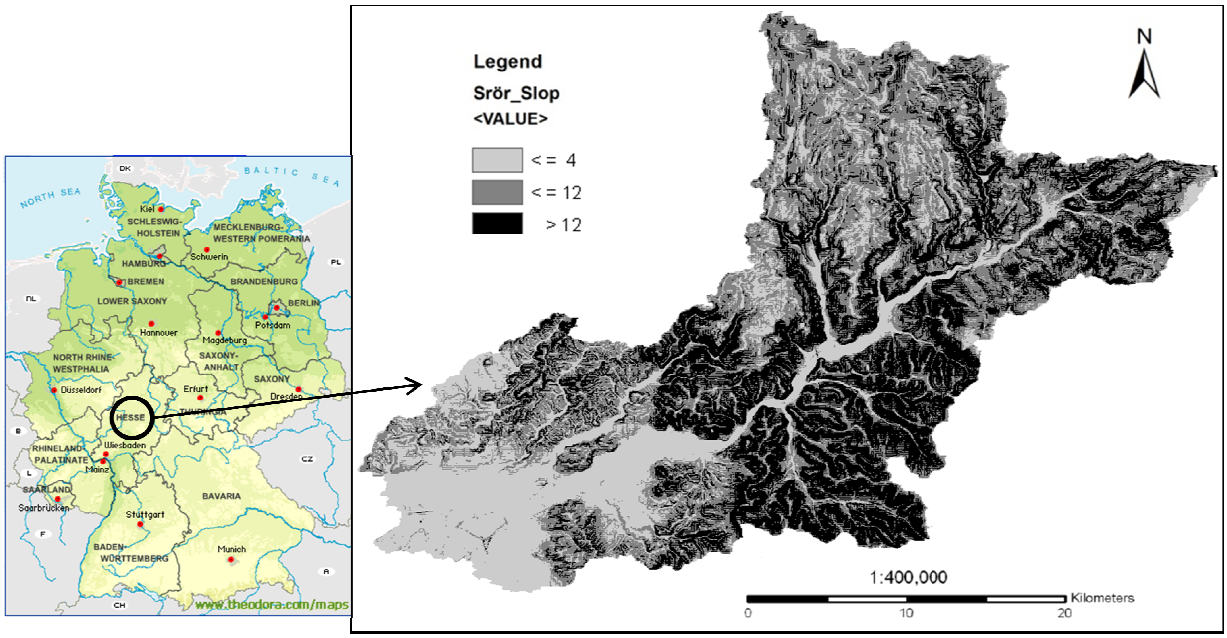

Fig. 1.5 The location and the slope map the Kinzig catchment (Meurer, 2012)

1.3.3. Mountainous catchment

The measurement carried out in this catchment is embedded in the project funded by the DFG (Deutsche

Forschungsgemeinschaft), aiming at developing the integrated modeling approach for the assessment of the impact of fast changes in the environment on aquatic ecosystems (Fohrer and Jähnig, 2009; Schmalz et al., 2012). The study area Changjiang basin is situated in the southeast of China in between Anhui and Jiangxi Province (Fig 1.6). Rapid economic development and the related large-scale land use/cover change make this zone an important research area. The main Changjiang stream drains in the Poyang Lake with a catchment area sums up to 1700 km². The landscape in the catchment is characterized by a hilly terrain with the highest peaks at the northern and northwestern catchment borders (Strehmel, 2011). The highest point of the catchment is at an altitude of 1699 m (a.s.l.) while the catchment's outlet has an altitude of 57 m a.s.l.. Most part of the catchment has a slope larger than 10 °, and in the northwestern part the slope even reach to 70°.

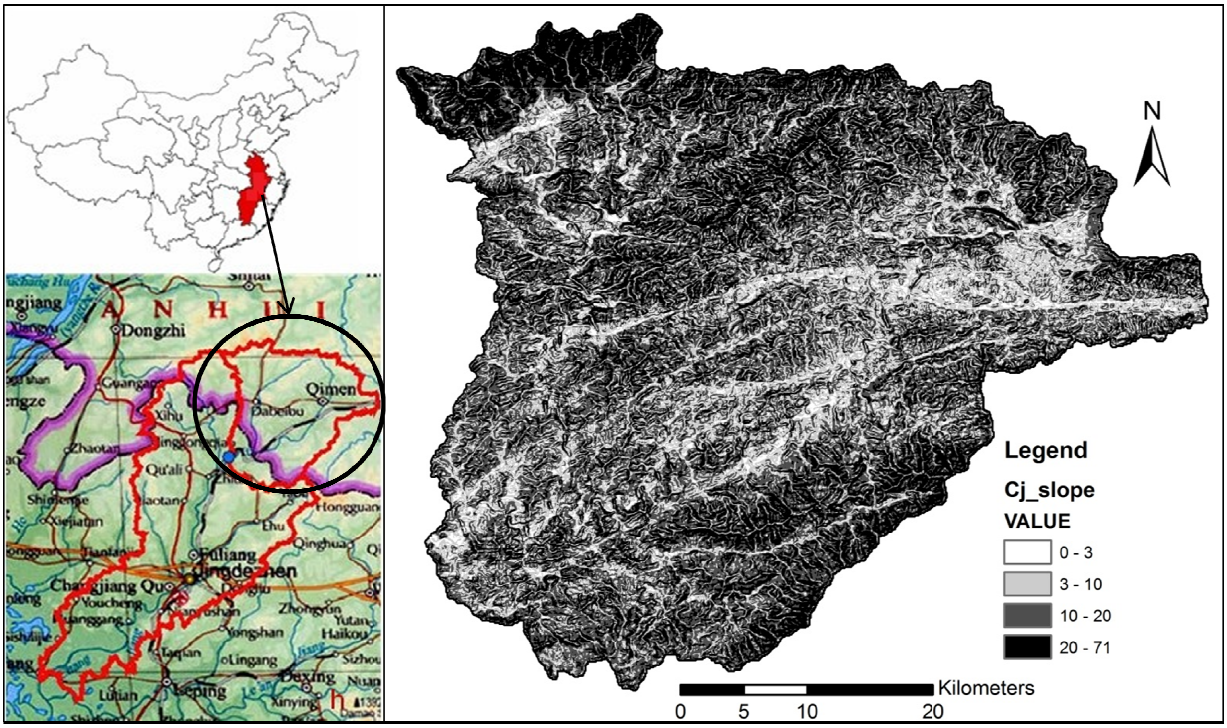

Fig. 1.6 The location and the slope map of the Changjiang catchment (ISDSP, 2013)

1.4 Data and methods

Data from catchments with a variety of hydrological or hydraulic environment is necessary in the equipment test part to exclude the local disturbance. We selected 174 sites, situated in all 8 catchments introduced in the chapter study area and collected 366 ADQ measurements from October 2010 to July 2011. The measurements covered a wide variety of spatial and temporal scales, ranging in catchment sizes from 50 to 2852 km^2, various flow conditions, dry and flood season, a large range of river geometries,

different amounts of bed load, aquatic vegetation and ecosystems. Comparison analysis was carried out between the data collected with ADQ and traditional point velocity equipment (FlowSens), as well as the repeated ADQ measurements with different inner settings.

In the vertical velocity distribution study, data from lowland area (Upper Stör catchment), low mountainous area (Kinzig catchment) and mountainous area (Changjiang catchment) were analyzed parallel to clarify the local characteristic of the flow structure. All together, 248 vertical velocity profiles measured with Acoustic Doppler Equipment and FlowSens were fitted by logarithmic, parabolic and power lines to verify the applicability of the new formulas.

A lot of hydrological and eco-hydrological studies have been carried out in the Upper Stör catchment previously (Frąckiewicz, 2010; Müller-Wohlfeil et al., 2000; Pott, 2014; Ripl and Hildmann, 2000; Schmalz et al., 2008; Venohr, 2000). All these studies provide a reliable baseline for modeling work in this catchment. The HEC-RAS models were set up based on the field measured data, 1m digital elevation model (DEM), gauged data and SWAT modeled data. Four hydrological stations from Schleswig-Holstein's government-owned company for Coastal Protection, National Parks and Ocean Protection are located in Upper Stör catchment: Brachenfeld (S02), Padenstedt (S09), Sarlhusen (S20) and Willenscharen (S21) (LKN-SH, 2012). They provide long-term hourly discharge and water elevation data series. At the points without gauged data, the SWAT modeled data is adopted. The SWAT models of the Upper Stör catchment were set up and well calibrated by the Department of Hydrology and Water Resources Management of Kiel University (Pott, 2014). The daily discharge data series correlated with each other with the coefficient of determination (R^2) of 0.86 during calibration period and 0.84 during validation period. The Nash-Sutcliffe coefficients were 0.85 and 0.83 respectively (Fig 1.7). Analysis of the calibrated daily output and real measured suspended sediment yielded the R^2 of 0.56 and the Nash-Sutcliffe coefficient (NSE) of 0.55 (Fig 1.7). The averaged R^2 and Nash-Sutcliffe coefficient produced by daily validated data were 0.61 and 0.59 respectively. The Upper Stör catchment is a suitable study area for the aims of this investigation, because the previous works provides an adequately reliable database and foundation (Pott, 2014).

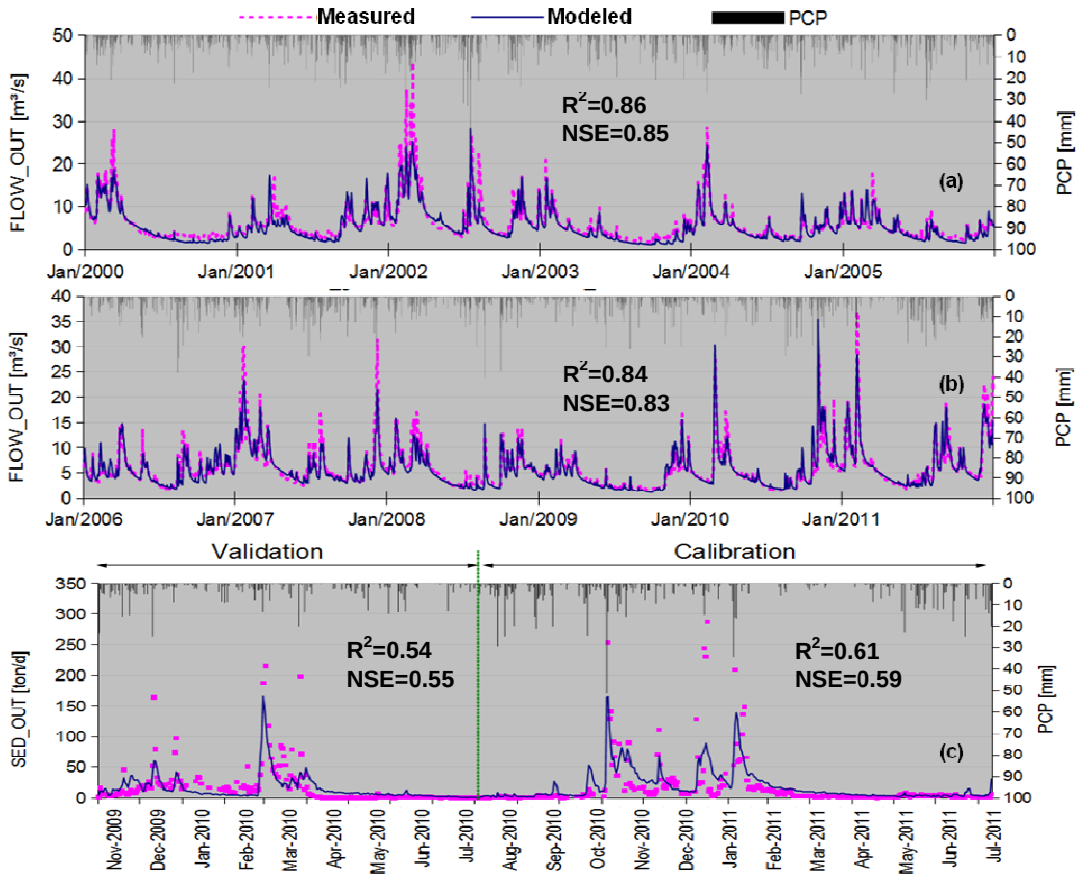

Fig. 1.7 Measured and modeled stream flow and sediment loads at the gauge Willenscharen for the calibration and validation periods (Pott, 2014)

1.5 Research questions and outline

This dissertation focuses on testing the performance of the new emerged Doppler equipment OTT Qliner (ADQ, OTT Company, Kempten/Germany) in medium sized rivers, to analyze the feasibility of simplifying the flow velocity vertical distribution law. Based on the field measurement and well calibrated HEC-RAS models, the dissertation finally studies the distribution pattern of the stream discharge, power and sediment across the cross section direction to evaluate the lowland in-stream and floodplain flow/sediment. The main objective was to model the long-term flow dynamics in the lowland catchment to evaluate the different distribution pattern of the stream discharge, power and sediment in-channel and on the floodplain, and try to find out the cause of difference in different sub catchments. The principle research questions are:

(1) Can the emerging Doppler equipment (ADQ) and the measurement we took provide accurate results compared to the traditional flow meter? Whether the accuracy of the discharge and the velocity measured with ADQ are adequately reliable for the model setup?

(2) Is it possible to use some easy-to-determine parameters to set up a simple and common

distribution model for the flow velocity in vertical direction?

(3) How do the discharge and stream power distribute in the channel and on the floodplain? What is the main cause of the different distribution among different sub-catchments?

(4) How much sediment was deposited or eroded in the study area? What are the main differences between the sediment processes in-channel and on the floodplain? Why does the sediment pattern among sub-catchments differ?

Each of the research papers correspond to chapter 2-5 of this final manuscript addressed each of the research questions. These papers composing this thesis are briefly outlined in the following part, and the structure of this thesis is shown in Fig 1.8.

Chapter 2 designs experiments to test the accuracy, reproducibility and sensitivity of the equipment (ADQ), and improves the measurement methodology for medium-sized rivers and channels. The results showed that ADQ is an efficient and reliable flow discharge and velocity sampler compared with a traditional device. Long measurement periods (50s) and appropriate cell size depth ratios (0.1-0.2) are recommended especially for shallow and slow flows.

In Chapter 3, a new structure of flow velocity vertical distribution prediction is proposed. Traditional logarithmic, power and parabolic velocity vertical distribution formulas adopt friction velocity (u*) and the depth (y) of the measurement point in prediction. The new formulas we proposed use relative flow velocity based on mean vertical velocity ($u/\bar{u}$) and dimensionless relative water depth (y/H). Analysis of the 248 measured vertical water profiles from a Northern German lowland catchment, a German low mountain catchment and a mountainous catchment in China proved that this substitution were reliable and applicable. The parabolic curve works best in describing the vertical flow velocity distribution best. There is no uniform prediction formula within the same catchments, but the catchment slope is related to the coefficients and constants.

The main aim of Chapter 4 is to evaluate the stream discharge and power distribution in cross section direction during flood. The HEC-RAS flow models were set up for ten river sections in the Upper Stör catchment, based on a 1 m digital elevation model, field data and long term daily SWAT modeled discharge series. Model performance is evaluated using the common statistical criteria and visual comparison. The distribution patterns were given and the causes of the different distribution pattern in different catchments were then discussed in detail. In addition, Chapter 4 is the prerequisite of Chapter 5, because the sediment model is based on the flow model.

Chapter 5 evaluates the sediment processes in the Upper Stör catchment from 2001 to 2010. The sedimentation depth, sedimentation rate and the granularity of the sediment in-channel and on the floodplain were computed and analyzed. The results yielded by the combination of HEC-RAS and SWAT model are comparable to the traditional radioactive dating or sediment trapping method in the similar and nearby catchments.

In Chapter 6 the discussion of the key findings and the important results of this study are given. At the end, an overall conclusions and outlook is presented, which provides the future research issue based on the results of the current research.

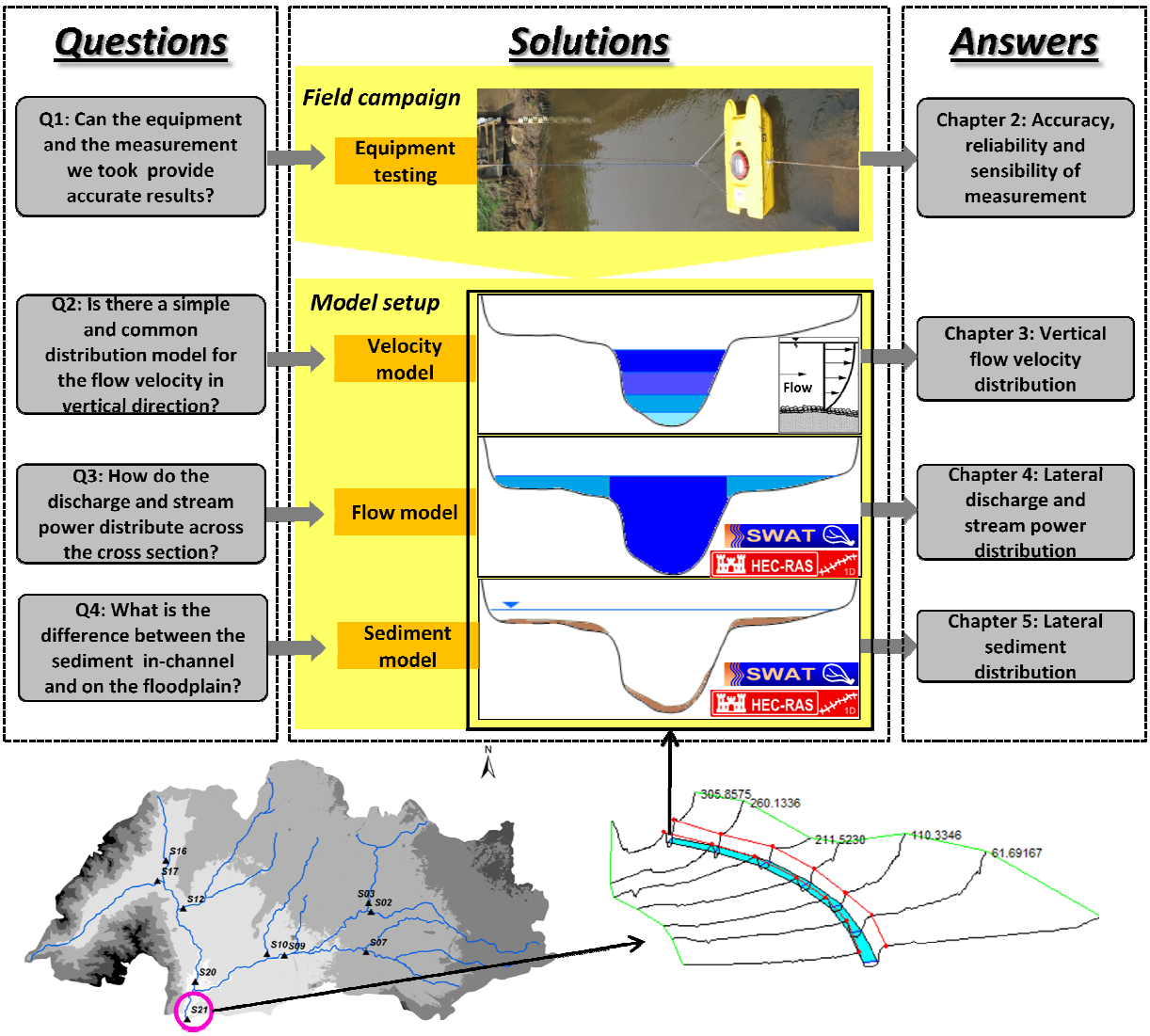

Fig. 1.8 The structure of this thesis

Chapter 2. Accuracy, reproducibility and sensitivity of discharge measurements in medium-size rivers with Acoustic Doppler Technology

S. Song, B. Schmalz, G. Hörmann, N. Fohrer
Hydrological Sciences Journal, 57(8) 2012: 1626–1641.
Submitted, 1 January 2012; Accepted, 27 March 2012

Abstract: With increased interest and requirements in surface water quality and hydrodynamics, additional information is needed about water flow in streams. The mobile OTT Qliner with acoustic Doppler technology (ADQ) provides a highly efficient and accurate way to collect this information. For this paper we completed 366 measurements for flow velocity, water depth and discharge with ADQ from Sep 2010 to Jun 2011 at 174 cross sections in 8 catchments of different sizes located in Northern Germany, Central Germany and Southeastern China. The measurements were used to study the accuracy, reproducibility and sensitivity of the device, and to improve the hydrodynamic sampling for medium-sized rivers and channels by hinting at their internal parameters. The observations reported in this paper clearly show that the results of flow average, profile, layer and point values of ADQ compare very well with electromagnetic or ultrasonic devices. Generally speaking, the flow average velocity represents the highest agreement. Vertical velocity has a better quality than the layer velocity, which indicates a greater precision in the horizontal than in the perpendicular direction. Point velocity, the composite of vertical velocity and layer velocity, has intermediate precision. Inner setting tests revealed that the measurement is more sensitive to cell size than to time interval setting. The cell size depth ratio between 0.1 and 0.2 meters produced the highest reliability. A measurement period of 30 s is needed for velocities faster than 0.3 m/s, for shallow and slow flowing rivers, an interval of 50 s or even a longer time interval is recommended. The nearer the measured points to the river bank or bed, the larger the measurement error might be. River bed can also influence the measurement more distinctly than the river bank.
Keywords: discharge measurement, ADQ application analysis, acoustic Doppler technology, medium-size rivers

2.1 Introduction

Recent research has recognized the importance of river flow analysis and the need to understand the interaction with the river bed (Jähnig et al., 2008; Jowett, 1998; Smith and Pavelsky, 2008) and the ecosystem (Kiesel et al., 2009a; Yuan et al., 2010). More accurate information about river flow and its

components is important to analyze the effects of human activities on river systems, including water pollution, hydraulic construction, water quality distribution and prediction, river resource management, flood estimation and flood damage prevention, etc. (Gunawan et al., 2010; Kawahara and Umetsu, 1986; Lozano and Mateos, 2009; Stacey et al., 1999).

One of the most widespread methods to calculate river discharge is the velocity–area method, where the depth-averaged velocity is determined at different verticals along the width of a river. The result is multiplied by the area of each depth-averaged velocity to get the total flow discharge (Rantz, 1982). This means that flow velocity measurement is the first and most basic step to determine river discharge. During the last century, flow velocity measurements mainly relied on mechanical propeller velocity meters (Muste et al., 2008). With the fast progress in computing power and improved electric batteries, the use of electronics in velocity instruments to map river hydrodynamics has gained more popularity in the last few decades, because of their higher efficiency, easier operation and lower cost (Muste et al., 2012; Pasquale et al., 2011). The progress in optics, radar, acoustics and electromagnetism has led to a new generation of flow measurement devices, which can offer superior efficiency, performance and reproducibility for velocity and discharge measurement (Muste et al., 2008; Thandaveswara, 2011). One of the replacements for the mechanical propeller is the electromagnetic velocity meter, which provides the convenience for use in open channels with fouling, weeds or sewage. Characterized by high accuracy point velocity result, the electromagnetic velocity meter is widely accepted in small-scale catchments, especially in hydro-ecology related research (Rücker and Schrautzer, 2010; Wu et al., 2011). The use of an acoustic method meets the increasing demand for more precise flow velocity and discharge measurement, and ADC (Acoustic Digital Current meter), ADV (Acoustic Doppler Velocimeter), ADCP (Acoustic Doppler Current Profiler) and ADQ (Acoustic Doppler Qliner) are the representatives of acoustic-based current equipment. A vast amount of literature describing the underlying principles, configuration and operational aspects of acoustic based equipment is available (Instruments R. D., 1996; SonTek, 2000). ADC and ADV are point acoustic velocity meters and have been verified in various water environments and catchment sizes (Gomani et al., 2010; Zhang et al., 2006). United States Geological Survey (USGS) use ADCP and other point acoustic velocity meter for water velocity and discharge measuring at 33% of their gauging stations (Muste et al., 2012). Because it is the latest acoustic product, only some ADQ tests measurement have been carried out in a laboratory flume (Frizell and Vermeyen, 2007) and in a field experiment at one cross section in the Charles Hansen Feeder Canal (Craig et al., 2009) so far. They discovered that ADQ measurements show only low deviations compared either with ADV in the lab experiment or with the Price AA current meter in the field. If the sampling time is too short, the results are relatively noisy. The findings seem to be promising, but they only report singular conditions. Further experiments are therefore needed for different flow conditions to evaluate the performance of the device. Field research revealed that, compared with point velocity meters (including electromagnetic velocity meter ADC and ADV acoustic), vertical velocity

meters such as the ADQ and ADCP profoundly changed the collection of hydraulic data due to the replacement of point technology for vertical measurement technology. Generally speaking, ADC and ADV are velocity meters which give results for a certain point, but ADCP and ADQ provides velocity profiles over the depth. The technologically differences make ADCP and ADQ depends more on the available water depth and cannot be used in slope zones. These instruments can also determine flow velocity in less time and with fewer costs. The other new emerging velocity equipment is based on image or radar technology. The key advantage of radar technology is that it simultaneously and remotely measures flow velocities over the entire imaged flow surface, but these instruments have yet to be validated in the field for the same range of discharge measurement conditions as acoustic-based equipment. Particle Image Velocimetry (PIV) and Particle Tracking Velocimetry (PTV) are based on image technology and have been widely used in hydro-science. This new non-intrusive technique was applied successfully in water body velocity distribution analysis and measurements at the water surface, using an appropriate camera and natural or artificial seeding tracers (Muste et al., 2011; Nezu and Sanjou, 2011; Weitbrecht et al., 2011). PIV and PTV have been proved to be powerful and efficient velocity meter, however, the complication and weakness base on PIV/PTV algorithms are the main arguments of scientists and engineers (Cameron, 2011).

Generally speaking, the acoustic-, radar- and image-based electronic velocity meters are revolutionizing the hydrodynamic mapping process and creating the possibility for larger spatial scales and higher spatial resolution sampling. They are also less time consuming and more economical. Currently, the most widely used technology for velocity sampling is acoustic-based equipment. According to literature research, the following measurement techniques are frequently applied today: in small rivers, mechanical, electronic, electromagnetic and acoustic point-velocity meters are fixed to a wading rod or sampling platform to sample flow velocity and discharge (Yorke and Oberg, 2002). In large rivers, the ADCPs (Acoustic Doppler Current Profiler), which was originally designed for ocean environments, are reliable and efficient (Lu and Lueck, 1999; Stone and Hotchkiss, 2007). However, a medium-size river is too deep to enter but too shallow to use ADCPs. Thus both the step-into-river technique and ADCPs technique mentioned above cannot be used (Mc Gahey et al., 2008). Stone tried to measure in a medium-size river with improved ADCPs in 2007. Although the vertical profile and depth-averaged velocity seemed acceptable compared to an Acoustic Doppler Velocity meter (ADV), excessive noise during the experiment reduced the effectiveness of the ADCPs velocity measurements. These technical limitations have slowed down the hydrodynamic research in medium size rivers in recent years. These problems can be solved by the new emerging Doppler Effect device called ADQ, which is designed especially for medium size rivers. The proper use of this new instrument requires a good understanding of the underlying measurement principles and a careful evaluation of the instruments' capabilities in various sampling environments.

The objectives of this research were to investigate the accuracy, reproducibility and sensitivity of the ADQ for velocity and discharge measurements in medium-size rivers, to evaluate the sensitivity of different parameter settings in different catchments, to study the influence of the local conditions on the results, to optimize device settings and to improve hydrodynamic sampling technique and methodology for medium-size rivers. The accuracy of a measurement system is the degree of closeness between a measured quantity value and the actual quantity (JCGM, 2008). In our study, it considered to be the capability of providing a correct reading or measurement under the ADQ methodology. Reproducibility is the ability of an experiment or study to be accurately reproduced or replicated, and it can be evaluated by the measurement precision of repeated measurement (JCGM, 2008). The variation (uncertainty) of the output of a statistical model or measurement system can be attributed to the difference in input variables, known as "sensitivity" in statistics, which is the third target of our study.

2.2 Principle of operation

2.2.1. Characteristics of the devices

A common method to evaluate new instruments is to compare the results with other well-calibrated instruments (Oberg, 2002). For this comparison we selected a direct reading electromagnetic velocity meter (FlowSens) and a portable Acoustic Digital Current Meter (ADC) as control devices. Both of them are point velocity meters and have been verified to be suitable for all typical river flow regimes (Instruments R. D., 1996; Rücker and Schrautzer, 2010; SonTek, 2000; Wu et al., 2011). The characteristics of the three instruments are shown in Fig. 2.1.

2.2.1.1 **Electromagnetic velocity meter (FlowSens)**

The measurement principle of FlowSens (SEBA, Hydrometrie, Germany). The coil equipped in the sensor of FlowSens can produce a magnetic field, and a corresponding voltage will result when the flowing conductor existing in the flow moves through the magnetic field. According to the voltage intensity, the velocity is calculated and then displayed on the digital control unit. Because FlowSens can only give a direct value of flow velocity for each measured point, the user must estimate the depth according to the scale marked on the rod, or sample with another hard texture ruler such as wood or mental for the sake of accuracy when sample with FlowSens. Another measuring tape is also needed for river width measurement and vertical profile mark (Fig. 2.1). Additional to equipment, more office work for hydraulic calculation is essential to get the discharge, velocity and some other parameters. FlowSens can measure the velocity very close to the bed (2 cm) and calculates average and standard deviation of point velocity for a time interval of up to 30 s (FlowSens 2010). The key advantage of this instrument lies in its ability to measure in a range of fluids including fresh water, waste water, salt water, water with vegetation and

suspending sediment.

2.2.1.2 **ADC**

ADC (OTT Company, Kempten/Germany) is designed for point velocity measurement in natural streams, rivers, creeks and open channels based on acoustic technology. Measured depth, velocity and discharge are displayed on the graphical handheld display. Water depth is measured with a built-in pressure sensor. Water point velocity is measured based on pulse-coherent technology in which the phase difference ($\Delta\Phi$) and lag time (τ) of different transmitted acoustic pulses are calculated and the water velocity is then calculated with the formulation $v=k*\Delta\Phi/\tau$ (OTT, 2008, 2011). ADC provides digital reading of water depth, measured depth and point velocity at the same time. During measurement only measuring tape for width and vertical mark is necessary (Figure 2.1). The PDA of ADC will finish the basic hydraulic calculation after each cross section sample and no more office work need except download the data to computer.

Device	**FlowSens**	**ADC**	**ADQ**
Sensor & display unit	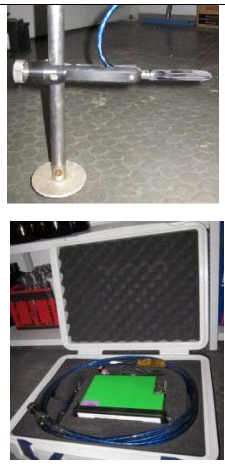		
Principle	Faraday's Law	Acoustic Pulse-coherent Technology	Acoustic Doppler Effect
Measurem-ents			

Fig. 2.1 Equipment compared in this study

2.2.1.3 **Acoustic Doppler Qliner (ADQ)**

Acoustic Doppler Qliner (ADQ, OTT Company, Kempten/Germany) is the latest acoustic device to determine water velocity, water depth and discharge in medium-size natural or artificial rivers and other open water areas. It contains four sensors situated underneath the fiberglass catamaran. The ADQ communicates via Bluetooth with a PDA, where a program displays velocity, discharge, depth, signal amplitude for each vertical profile measurement and finally river discharge and flow velocity distribution. Four main progresses are made by ADQ compared to the other flow measurement techniques: 1) the Bluetooth design excludes the need to step into the water; 2) the use of a PDA with direct calculation of the results cut the time cost prominently; 3) compared with point by point measurement process applied in FlowSens and ADC, ADQ measures velocities vertical by vertical, and vertical mean velocity and each point velocity is stored immediately; 4) the fully enclosed fiberglass catamaran has no moving or sensitive parts which are easily blocked or damaged and it is very stable even in turbulent or high velocity currents. It is also suitable for narrow waterways with steep side walls (OTT, 2010); 5) downloaded ADQ data contains more specific hydraulic parameters compared with downloaded ADC data.

2.2.2. Instrument requirements

2.2.2.1 **FlowSens and ADC**

During measurement, special rules must be taken into account for FlowSens and ADC, which work in the typical point by point way. Common requirements have to be met for FlowSens and ADC to fulfill a reliable measurement:

The right position of the sensor: both sensors have to be positioned against the flow direction to measure velocity properly, and because they are attached on the scale iron rod to determine the depth of measured point, the rod must be perpendicular to the water surface.

The minimum external turbulence: users have to step into the river at a point without a bridge in order to operate the equipment, which might perturb the flow movement. Staying as far as possible away from the sensor in downstream direction can essentially lower the turbulence.

Find exactly the same vertical: working in a point by point way, finding exactly the same vertical for different depths is another target to cut down the uncertainty of the measurement.

2.2.2.2 **ADQ**

Compared with FlowSens and ADC, more complicated boundary conditions must be met for ADQ to get a reliable and accurate measurement results:

Bluetooth signal range: The maximum distance to transmit wireless data between ADQ and PDA is 50-70

m in the horizontal and 100-200 m in vertical direction. The distances will decrease in case of low battery, moisture at the ADQ surface and interference with other Bluetooth signals nearby, etc.

The stability of the ADQ: The measurements can be taken from a bridge/cableway or from the river bank. When a bridge/cableway is selected, wires have to be attached to the front eyes on both sides of the ADQ with shackles. An extra weight at the cable keeps the fiberglass catamaran stable, in particular at high flow velocities or at high bridges. For measurements from the river bank, two wires have to be attached at the long side of the ADQ with shackles. The instrument is moved with a pulley in a narrow river or with the help of a second person.

Measurement range: The sensor of the ADQ works with 2MHz transducers; the measuring range is illustrated in Table 2.1. The specific settings vary according to the river size.

Tab. 2.1 Technical parameters of the ADQ used in this study (OTT 2010)

Sensor Frequency	Cell size (m)	Water depth range (m)	Minimum Blanking distance (m)	Maximum Nr. Of cells	Velocity Range (m/s)	Operating Temperature (°C)
2MHz	0.1-2	0.35-10	0.05	40	±10	-5-35

2.3 Methods and data collection

2.3.1. Sampling sites

Several criteria for the field site selection should be clarified in advance for a successful measurement. First, the water depth has to be >0.35 m and the sites should cover a broad range of cell sizes for ADQ and hydrological conditions. The site should be as complex as possible, but turbulence caused by large obstacles, dams or waterfalls must be avoided. Secondly, the place must be suitable for a measurement with ADQ either from a bridge or from the river bank. For measurements from the river bank, both banks should be accessible. Based on those criteria, 174 sites were chosen, situated in 7 catchments within Germany and 1 catchment in southern China. From October 2010 to July 2011, 366 ADQ measurements were completed (Table 2.2 and Appendix 1), covering a broad spatial and temporal scale, ranging in catchment sizes from 50-1760 km^2, including different flow conditions, dry and flood season, a large range of river geometries, different amounts of bed load, aquatic vegetation and ecosystems. Thus we covered a wide variety of hydrological conditions.

Tab. 2.2 Evaluation sites and number of measurements with the ADQ

Catchment	Location	Size (km^2)	Landscape type	Width: (m)	Depth: (m)	No [1]	No[2]
Kielstau	Schleswig-Holstein, Germany	50	Lowland	4	0.5-1	12	15
Upper Stör	Schleswig-Holstein, Germany	468[3]	Lowland	10-15	1.5-2.5	1	18
Nuthe	Saxony-Anhalt, Germany	509	Lowland	6-10	0.5-1	8	40
Upper Treene	Schleswig-Holstein, Germany	517	Lowland	8-16	0.5-1.5	25	40
Hunte	Lower Saxony, Germany	1318	Lowland	10-20	0.5-1.5	18	90
Ilmenau	Lower Saxony, Germany	1434	Lowland	15-25	0.5-1	12	60
Kinzig	Hessen, Germany	1170	Low mountain area	15-25	1-2	77	77
Changjiang	Anhui Province, China	1760	Mountainous area	60	1-1.5	21	26

Note: [1] Number of cross sections. [2] Number of measurements (at some cross sections several repeated measurement were made). [3] (Schmalz et al. 2008)

2.3.2. Experimental design

2.3.2.1 **Comparison measurements**

The comparison measurements outlined below are designed to test the accuracy of ADQ, namely two devices common comparison measurements and three devices point-to-point comparison measurements.

Two devices common comparison between ADQ and FlowSens was conducted to evaluate the river mean parameters and mean vertical profile parameters obtained by ADQ from eight approximately rectangular and smooth cross-sections in the catchments Kielstau, Nuthe, Upper Treene, Upper Stör, which are without interference of aquatic plants, stones or high amounts of sediment, etc. Measurements with both instruments were finished within one hour at the same cross section. ADQ displays mean river discharge, water depth and flow velocity directly in the field. The analysis and calculation of the FlowSens results was done in the office with EN ISO 748 or so called mid-section method. Due to the different working principle, the distribution of measured points within the same cross section is shown in Figure 2.2 (a).

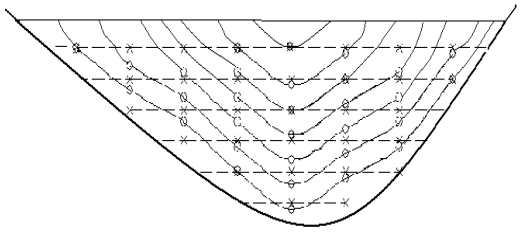

(a) Two devices Common comparison

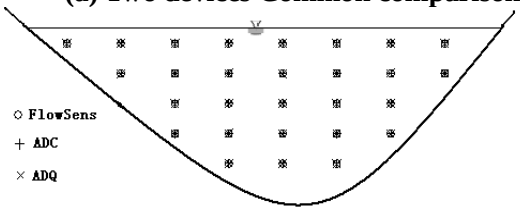

(b) Three devices point-to-point comparison

Fig. 2.2 The distribution of measured points

Three devices point-to-point comparison measurements were collected between ADQ, FlowSens and ADC. The measurements were aimed at the appraisal of mean layer velocity (velocity at different depth) and

each point velocity. The measurements were made in nearly rectangular smooth cross sections in river Treene. The distribution of measured points is in Figure 2.2 (b).

2.3.2.2 **Repeated measurements**

The turbulence in any river or channel affects the measured discharge, depth and velocity values, which is a challenge for the measurement stability (Hauet et al., 2008; Stacey et al., 1999). To analyse this stability repeated measurements were designed. Five repeated measurements at the same cross sections were carried out with the same equipment settings and methodology in 39 cross sections selected from all the catchments.

In addition, another 52 measurements located in 5 rivers give evidence for the reproducibility of ADQ at different cross sections in the same river. All measurements were completed within the same day without precipitation. Discharge result was standardized by the mean discharge at all cross sections of the same river to make the data more comparable, and then the coefficient of variation (Craig et al., 2009) of the cross section discharge was analyzed as the representative indicator of the equipment stability.

2.3.2.3 **Test of operational settings**

The ADQ user manual contains some basic instructions and site criteria for different river conditions (OTT 2011), but it deals mostly with instrument specifications. More experiments are needed to test the operational settings and the effects of external factors in more complicated field environment to find the appropriate measurement techniques for specific site and flow conditions. Cell size and time interval are assumed to be the most influential inner aspects. Cell size is the distance between adjacent measurement points at the same profile and time interval is the measuring time for each single profile. The external factors that might affect the accurate measurement of flow characteristics include river bed and bank. Because the depth values are much less variable, we focused on discharge and velocity, which are more sensitive to changing boundary conditions and are probably the main source of measurement variance.

Data collected from eight cross sections with depth ranging from 0.6 m to 2 m focus on the impact of different cell sizes. Five repetitions were carried out using cell sizes of 0.1 m, 0.2 m, 0.3 m, 0.4 m and 0.5 m at each cross section. The time interval was set to 30 s except locations h15, h31 and h34, where we used 50 s to compensate the low flow velocity. Time interval experiments mainly relied on the data sampled at time settings of 10 s, 20 s, 30 s, 40 s and 50 s at 25 cross sections in northern Germany and Southern China with water depths from 0.6 m to 1.3 m and flow velocities between 0.044 m/s and 0.51 m/s. A constant cell size of 0.1 m was used for all cross sections to eliminate the effect of different cell sizes. The discharge and flow velocity were standardized to the mean value of the five cell sizes in the time and cell size tests to make the data more comparable.

Ultra sound is sensitive to obstacles both floating and stationary in the river. Therefore, the influence of

the river bank and bed should be taken into consideration. For a better understanding of these impacts, ADQ and FlowSens results obtained in 3 devices point-to-point comparison were analysed again, and the correlation between the result difference and standard distance to obstacles reflect the influence of river bed and bank. The flow chart of the experiment is shown in Figure 2.3.

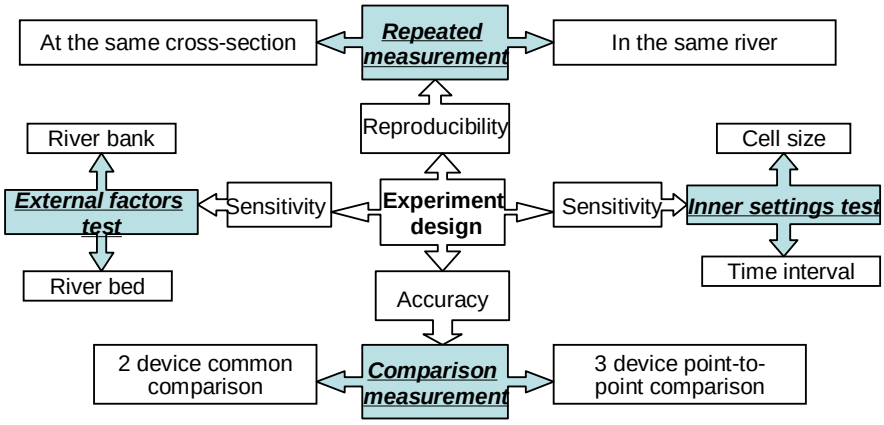

Fig. 2.3 Flow chart of experiment design

2.4 Data analysis

2.4.1. Accuracy analysis

2.4.1.1 **Two devices common comparison**

2.4.1.1.1 River mean parameter

As shown in Figure 2.4, ADQ and FlowSens measurements are strongly correlated and close to ideal correlation. The regression coefficients of discharge, depth and velocity measurement are 1.01, 0.99 and 0.96 with R^2 of 0.998, 0.999 and 0.84 respectively. This indicates the good comparability of both FlowSense and ADQ in river mean level. The discharge and depth differences are acceptable at 99% and the velocity is of 96% accuracy level in comparison with the FlowSens.

The discharge correlation seems to suggest that in small rivers with low flow velocity and a discharge of less than $1m^3/s$, FlowSens tends to indicate larger discharge, while in large rivers or rivers with high flow velocity, ADQ results are higher than FlowSens. The discharge and depth measurements by different instruments fit very well with an R^2 greater than 0.99. For mean river velocity, the slope and R^2 are a little lower, but still the two measurements show good agreement. The relatively large velocity differences might be caused by the proximity of the river bank and bed. This will be discussed in the section about external factors.

The conclusion is comparable to the comparison measurements made in the Charles Hansen Feeder Canal (Frizell and Vermeyen, 2007). The results measured by ADQ are also very similar to the official water

gauge value of 2.757 m^3/s at Colnrade in the Hunte catchment on May 24th 2011 (NLWKN, 2011). The ADQ results from two cross sections upstream of the official station of NLWKN (2011) at noon of the same day were 2.761 m^3/s and 2.832 m^3/s independently.

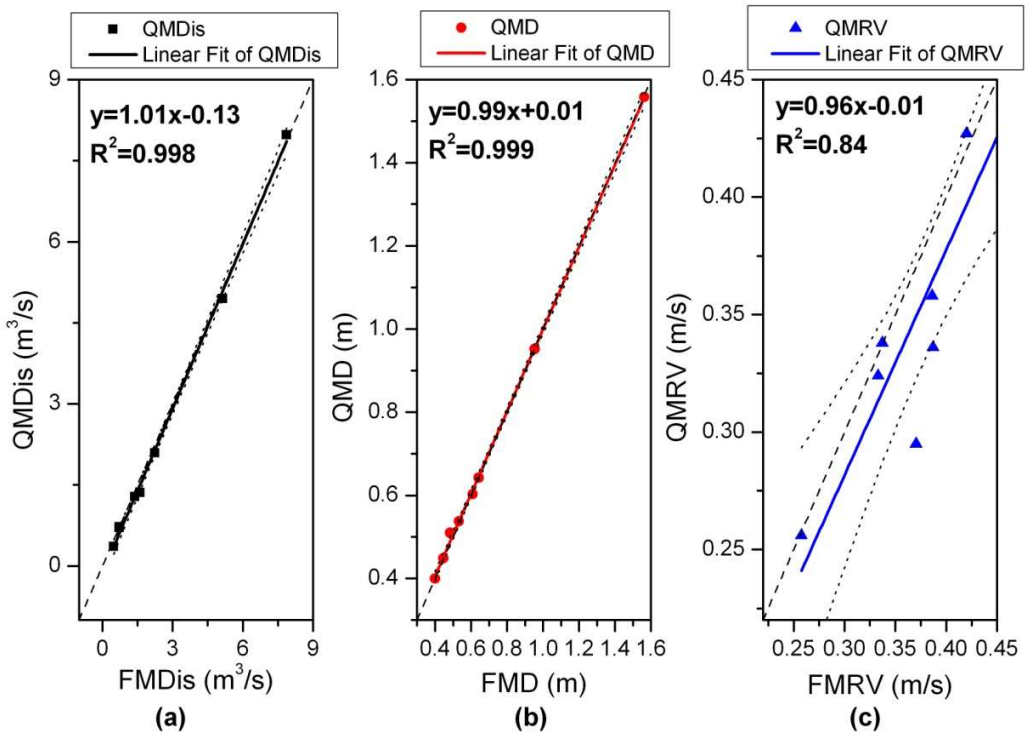

Fig. 2.4 Correlation between ADQ and FlowSens measurements in river mean parameters, discharge (a), depth (b) and velocity (c)

QMDis: mean river discharge measured by ADQ; FMDis: mean river discharge measured by FlowSens; QMD: mean river depth measured by ADQ; FMD: mean river depth measured by FlowSens; QMRV: mean river velocity measured by ADQ; FMRV: mean river velocity measured by FlowSens. Dashed lines are the ideal lines. Dotted lines indicate the 95% confidence level.

2.4.1.1.2 Vertical profile parameter

In addition to the mean values of the whole cross section, single vertical profiles parameters from different equipment were collected to evaluate the performance of ADQ at different positions across the river. Similar to river mean parameters, the mean vertical profile parameters reflect satisfactory fitting (Figure 2.5). The slope of vertical discharge, depth and velocity are 1.07, 0.99 and 0.92 respectively, with determination coefficients of 0.97, 0.99 and 0.82. Compared to the river mean parameters, there is only a slight decline in the slope and R^2 for discharge and depth, while the fitting quality for velocity decreases by a relatively lower extent, reflecting ADQ's better ability in river mean velocity than in vertical profile velocity.

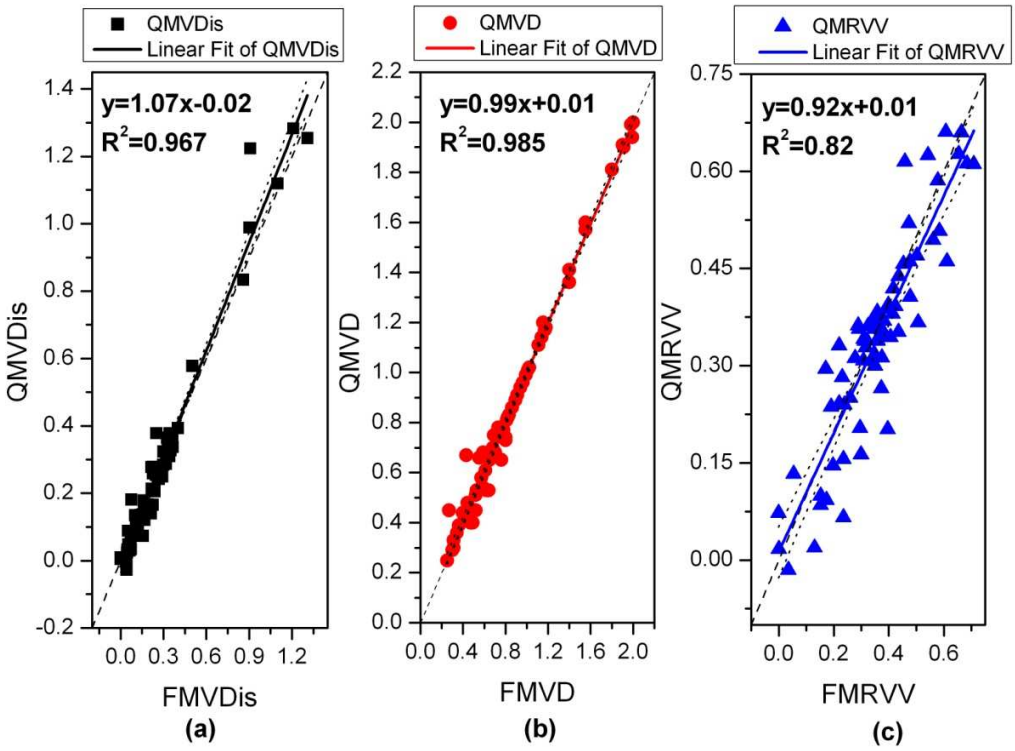

Fig. 2.5 Correlation between ADQ and FlowSens measurements in vertical mean discharge (a), depth (b) and velocity (c)

QMVDis: mean vertical discharge measured with ADQ; FMVDis: mean vertical discharge measured by FlowSens; QMVD: mean vertical depth measured by ADQ; FMVD: mean vertical depth measured by FlowSens; QMRVV: mean vertical velocity measured by ADQ; FMRVV: mean vertical velocity measured by FlowSens. Dashed lines are the ideal lines. Dotted lines indicate the 95% confidence level.

2.4.1.2 **Three devices point-to-point comparison**

Regression analysis between mean vertical velocity, mean layer velocity and point velocity measurements by ADQ, ADC and FlowSens with a fixed intercept of 0, reveals higher agreement of all variables between FlowSens and ADC, and comparatively lower agreement between ADQ and FlowSens except in mean vertical velocity (Figure 2.6). For mean vertical velocity, all devices are in accordance with each other. The correlation between point velocity of ADQ and FlowSens is higher than for mean layer velocity, but weaker than mean vertical velocity.

Generally speaking, FlowSens and ADC fit very well for all three variables. ADQ and FlowSens fit well for vertical velocity, lower for point velocity and lowest for mean layer velocity. These observations suggest that ADQ is well suited for vertical velocity measurement, but less suitable for layer velocity measurement. Being affected by both vertical and layer velocity, ADQ point velocity accuracy is in between mean profile velocity and mean layer velocity.

There might be some practical reasons for the lower accuracy of point velocity, such as the direction and the swing of the equipment, the disturbance caused by persons standing or wading in the river, the

perpendicular fixture of the stick or ruler, etc. Another reason for the difference in velocity is that it was difficult to find exactly the same position for all 3 instruments. The ADQ samples automatically and continuously. For FlowSens and ADC, users have to identify the sampling point manually. These unavoidable errors may lead to the poorer fitting and scattered distribution reflected on the linear regression curve.

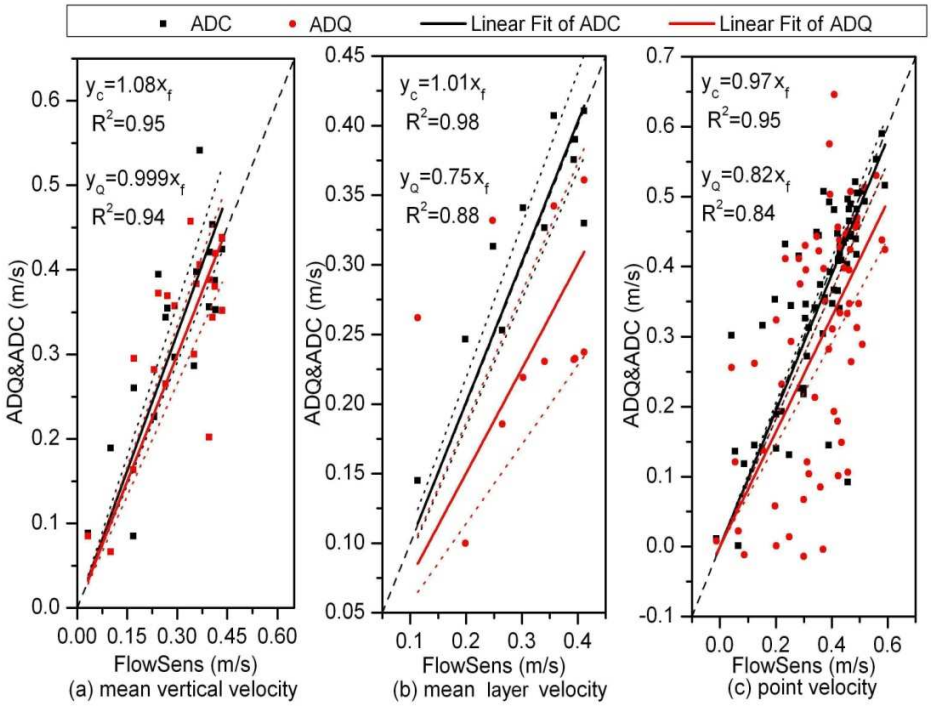

Fig. 2.6 The relationships between mean vertical velocity (a), mean layer velocity (b) and point velocity (c) measured by FlowSens, ADC and ADQ

Dashed lines are the lines with slope=1. Dotted lines indicate the 95% confidence level; y_C, the regression equation for ADC; y_Q , the regression equation for ADQ; x_f, the measured results of FlowSens.

2.4.2. Reproducibility analysis

2.4.2.1 **Repetitions at same cross section**

As is shown in Figure 2.7, the centralized distribution of CV values below 0.1 demonstrates the high repeatability of ADQ measurement at the same cross section. Interestingly, while the CV of mean depth varies only between 0 and 0.085, CV of mean discharge and velocity display a 3 times wider variation amplitude. The statistical conclusion revealed that the depth measurement is more repeatable than the velocity and discharge measurement, in accordance with accuracy comparison conclusion.

On the other hand, all three CVs decrease with the increasing real value of discharge, depth and velocity, and the Log3P1 type shows strong correlation coefficients for all curves.

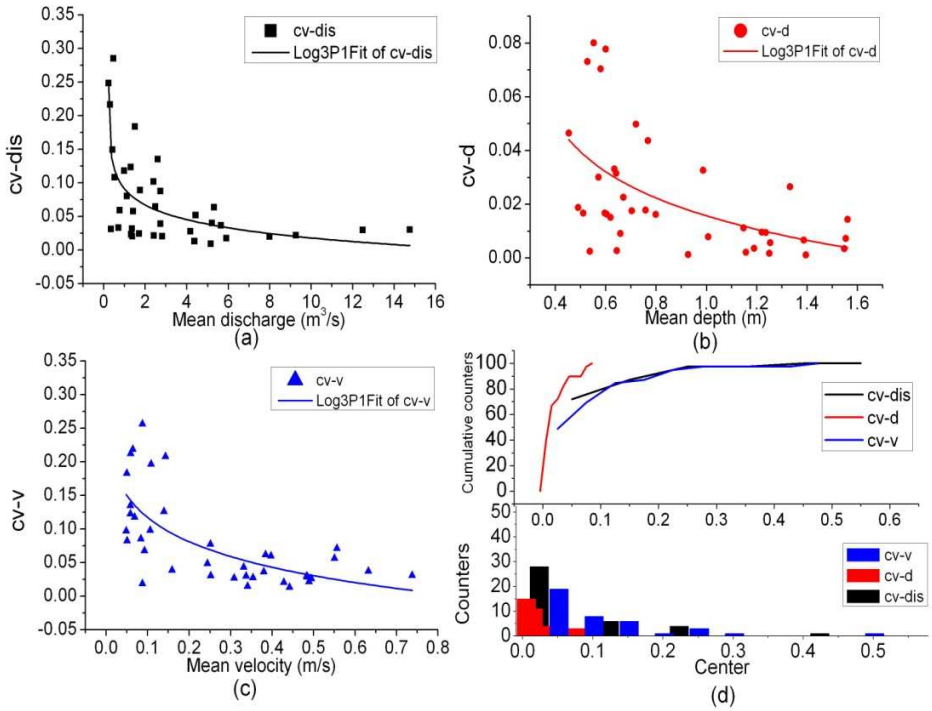

Fig. 2.7 CV of discharge (a), depth (b), velocity (c) and counters and cumulative counters chart (d) in the repeated measurements

2.4.2.2 **Repetitions in the same river**

Due to the variability of depth and width at different cross sections along the river section, only the discharge results are comparable for different measurements in the repetitions experiment in the same river. Figure 2.8 reports that most of the measurement variations are within ±10% except the Kielstau River, which is relatively shallower and slower than other four rivers. A similar trend as the repeated measurements at the same cross sections was observed here, the larger the mean discharge, the narrower the variance will be.

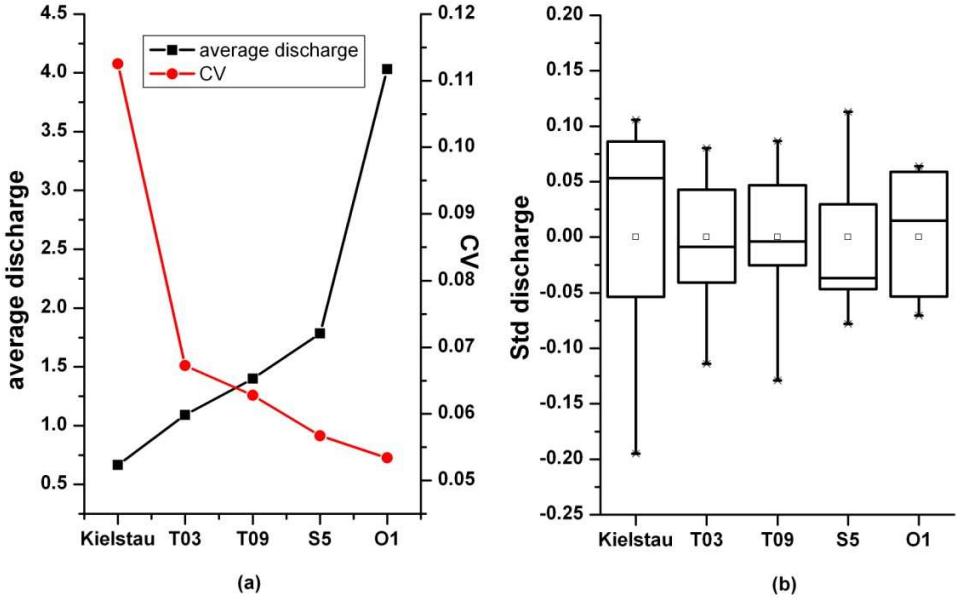

Fig. 2.8 Standard discharge, mean discharge and the CV of cross section discharge

2.4.3. Sensitivity analysis

2.4.3.1 **Equipment inner parameter settings**

2.4.3.1.1 Cell size

According to Figure 2.9 (a) and (b), discharge and flow velocity display nearly the same trend. They first increase and then decrease with increasing cell size, with a maximum at a cell size of 0.3 m. For a given river depth, the larger the cell size, the deeper the location of the first measurement is. With a cell size of 0.1 or 0.2 m, the measurement starts close to the water surface and ends near river bed. The cross section is divided into a "dense net" with small grid elements, which will fully reflect the influence of river bed and bank on the flow. For a cell size between 0.4 m and 0.5 m, we only had two or three measurements near the center of the river, which decreased the mean velocity and discharge. Thus the 0.3 m cell size setting led to the highest results in flow velocity and discharge.

Figure 2.9 (a) and (b) also demonstrate that all results are accurate at a high level, and most of them were within a range of ±10%. In addition, the smooth distribution lines are normally from deep and high velocity points, such as point s070111, s130111 and t060111 (Appendix 1), with the mean depth of 1.35 m and mean velocity of 0.4 m/s. Their measured values varied within ±5% range compared with mean values. The lines made from points h15, h31 and h34, with the mean depth less than 1m and the mean velocity less than 0.1 m/s, are very steep and precipitous, with a variation of ±15%.

A comparison between ADQ and FlowSens was made for 3 of the 8 cross sections. The 0.1 m cell size setting for point ks100111 and t060111, and 0.2 m cell size for point s070111, provided the closest

discharge and velocity values compared to FlowSens results (Tab. 2.3). This seems to suggest that the ratio between cell size and mean water depth should be within 0.1-0.2 to assure a high quality sampling.

Tab. 2.3 Discharge and velocity comparison between FlowSens and ADQ with different cell size

Equipment & settings / Point name		ADQ					Flow-Sens	Selected cell size/depth
		0.1 m	0.2 m	0.3 m	0.4 m	0.5 m		
ks100111	Discharge (m³/s)	**1.281**	1.455	1.477	1.475	1.403	**1.319**	0.15
	Velocity (m/s)	**0.499**	0.566	0.571	0.573	0.544	**0.513**	
t060111	Discharge (m³/s)	**4.943**	5.076	5.226	5.53	5.775	**4.768**	0.11
	Velocity (m/s)	**0.324**	0.334	0.324	0.342	0.358	**0.313**	
s070111	Discharge (m³/s)	7.976	**7.751**	8.169	7.914	8.082	**7.518**	0.13
	Velocity (m/s)	0.427	**0.414**	0.438	0.430	0.432	**0.404**	

2.4.3.1.2 Time interval

The variability is indirectly proportional to the increase in flow velocity, which is shown in Figure 2.9 (c) and (d), which suggests that the measurement duration has little influence on the measurement results for higher flow velocities, while for low flow velocities the effect of the time setting is distinct. The discharge lines for different velocity groups appear to be less steep than the velocity line in general due to the lower sensitivity of discharge measurements to the time interval. A similar phenomenon appears in the comparison measurements, where the discharge regression always displays better agreement than the flow velocity regression.

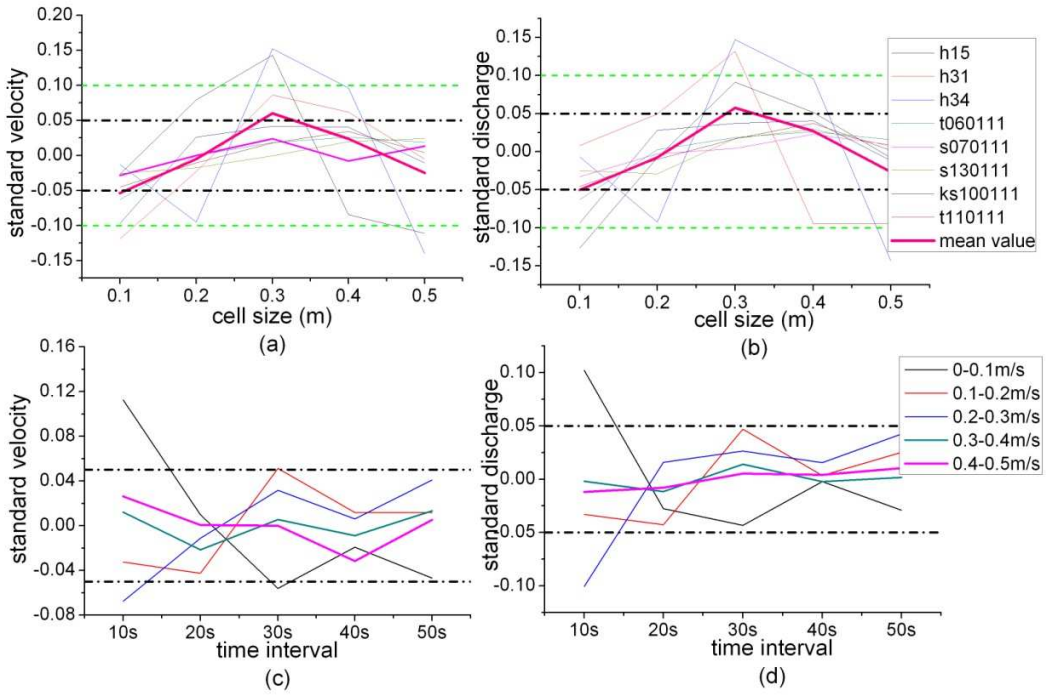

Fig. 2.9 Distribution of standard discharge and velocity under different cell sizes and time intervals
Dotted lines indicate the 95% confidence level and green dashed lines are 90% confidence level.

Comparisons in Figure 2.9 between (a) and (c), (b) and (d), lead to the conclusion that the cell size setting produces higher variations than the time interval settings. The performance of ADQ is more sensitive to the cell size setting than to the time interval setting.

Additional comparison results displayed in Table 2.4 suggest that a minimum of 30 s are needed for the higher velocity groups to achieve the reliable result. For the river group with velocities below 0.3 m/s, 50 s or even longer time intervals are essential to assure an accurate measurement.

Tab. 2.4 Comparison between FlowSens and ADQ with different time settings

Equipment & settings / Point name		ADQ					FlowSens
		10 s	20 s	30 s	40 s	50 s	
n23	Discharge (m^3/s)	0.343	0.335	0.333	0.352	**0.358**	**0.402**
	Velocity (m/s)	0.251	0.239	0.257	0.257	**0.256**	**0.266**
n24	Discharge (m^3/s)	0.67	0.698	**0.735**	0.701	0.712	**0.725**
	Velocity (m/s)	0.328	0.337	**0.353**	0.329	0.338	**0.341**

2.4.3.2 **The effect of external factors**

The distance from the bank and bed to the sample point is standardized by the following formula:

$$Dh_i = \begin{cases} P_i / W & P_i < W/2 \\ 1 - P_i / W & P_i > W/2 \end{cases} \qquad i = 1,2,3\cdots n \qquad (1)$$

$$Dv_j = 1 - \frac{\sum_{i=1}^{n} Md_{ij} / D_i}{n} \qquad j = 1,2,3\cdots m \qquad (2)$$

where i is the vertical number and j is the measured depth number; n is total vertical numbers and m is total measured points at each vertical. Dh_i is the standard distance from the river bank (%), P_i is the vertical position (m); W is the river width (m); Dv_j is the standard distance from the river bed (%); Md_{ij} is the measured depth at vertical i (m); D_i is the depth of vertical i (m).

2.4.3.2.1 River bank

The distances from the bank are negatively correlated with the profile mean parameter error, which is found for all three variables. The depth has the weakest correlation, with an error of less than 0.2 at most points, while the mean discharge and velocity had a similar regression with a standard error ranging from 0 to 0.5 and up to 0.7 at some points (Figure 2.10).

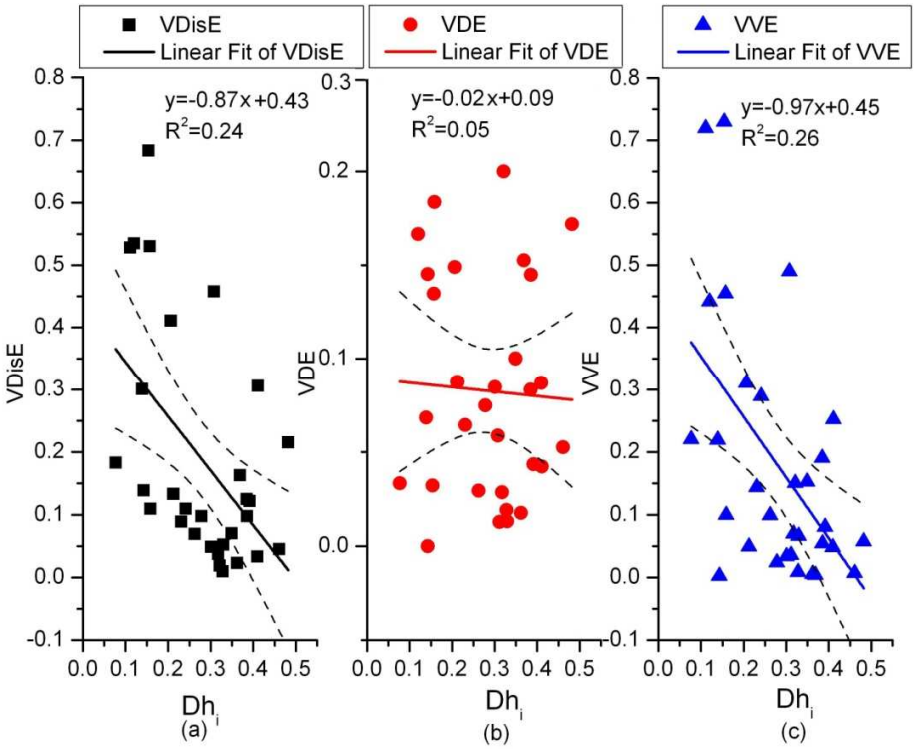

Fig. 2.10 Correlation between vertical parameter error and the standard distance from the bank
VDisE is vertical discharge error, VDE is vertical depth error, VVE is vertical velocity error, Dh_i is the standard distance from river bank. Dotted lines indicate the 95% confidence level

2.4.3.2.2 River bed

A negative correlation is also found between mean layer velocity and the standard distance from the bed, with the correlation coefficients higher than that of the profile mean velocity error (Figure 2.11). This indicates the higher unreliability and instability of ADQ velocity measurements along vertical direction.

In summary, river bank and bed can affect the performance of ADQ to varying extents; the nearer the measured point to the bank or bed, the larger the measurement error will be. River bed appears to have a larger influence than river bank.

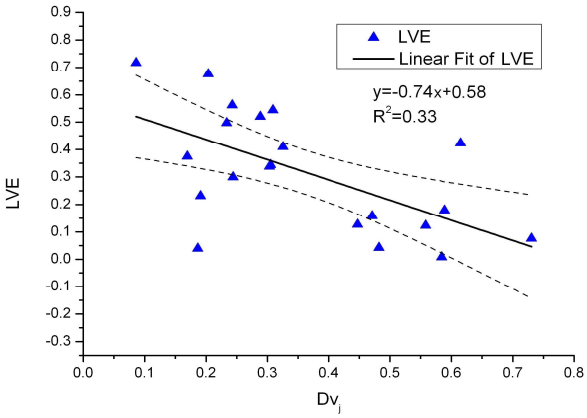

Fig. 2.11 Correlation between mean layer velocity error and the standard distance from the bed
LVE is the layer velocity error; Dv_j is the standard distance from the river bed. Dotted lines indicate the 95% confidence level

2.5 Conclusion and discussion

In this paper we analyzed the accuracy, stability and sensitivity of velocity, depth and discharge measurements from an ADQ device for 366 measurements at 174 cross sections located in 8 catchments of different sizes with various flow. Two devices common comparison measurements between FlowSens and ADQ, three devices point-to-point comparison measurements between FlowSens, ADC and ADQ, repeated measurements, inner setting and external factors test experiments were designed to evaluate the accuracy, reproducibility and sensitivity of the application of ADQ in medium size river. The observations reported in this paper clearly show that,

Compared with the electromagnetic device FlowSens, ADQ produced comparable results for depth, velocity and discharge. Depth measurement appears to have the best quality and highest consistency in all comparisons. River mean discharge measurements from different instruments agree better than vertical profile discharge measurements. For flow velocity measurements, a strong agreement between measurements with all three instruments was observed in river mean velocity, vertical mean velocity, layer averaged and point velocity. Among them, river mean velocity measurement expressed the highest unity, followed by vertical velocity and point velocity measurements. Mean layer velocity measurement has the worst regression quality.

Repeated measurement at the same cross section and within the same river sections demonstrate the high reproducibility of the ADQ measurements. The CVs of the measured river mean depth, velocity and discharge reveal stable and reliable ADQ performance. The larger the mean measured value, the narrower the variance will be.

A test of different settings for cell size and time interval of ADQ revealed that the measurement is more sensitive to cell size setting than time interval setting. The ratio between cell size and depth within 0.1-0.2 is recommended for a reliable measurement. Higher variability was discovered for measurements at the same cross section in shallow and low flow conditions with a different time interval. The longer the time interval, the smaller the deviation between different measurements is. As a result we recommend longer time intervals of 40-50 s in relative shallow rivers or low flow conditions. For channels with high velocity, a shorter measurement time interval of 20-30 s is sufficient.

Statistical analysis suggests that ADQ measurement error of profile and mean layer parameter is negatively correlated with the distance from river bank and bed, and river bed seems to influence the measurement more severely than river bank.

The ADQ is an efficient device for medium-size flow measurement. With the database of the field campaign, the accuracy and reproducibility of the equipment was tested, and suggestions for optimal parameter settings were given for freshwater areas in Northern Germany as well as in China for similar hydrologic conditions. External influences were also checked which might be a good resource for similar research in the future.

Chapter 3. Improved Estimation of Vertical Flow Velocity Distribution in Natural Rivers based on Mean Vertical Profile Velocity and Relative Water Depth

S. Song, B. Schmalz, J. X. Zhang, N. Fohrer
Water Resource Research
Submitted, 07 March 2014

Abstract: Vertical flow velocity distribution in natural rivers has been well studied in the last decades. Logarithmic, power and parabolic distribution laws were proven to be efficient for the prediction of the vertical velocity distribution. Traditionally the distribution formulas involve the friction velocity (u_*) and the depth (y) of the measurement point. The low availability of friction velocity and limitation of real water depth data hindered the promotion and comparison of the available flow velocity formulas. In this paper, we proposed a new structure of three prediction formulas adopting a relative flow velocity based on mean vertical velocity ($u/\bar{u}$) and dimensionless relative water depth (y/H). The formulas were applied to 248 measured vertical water profiles sampled from a northern German lowland catchment, a German low mountain catchment and a mountainous catchment in China, and the variation of fitted coefficients and constants were analyzed. In addition, the accuracy of the synthetic flow velocity at different relative depths was examined and the variation of the formula coefficients and constants among different catchments were discussed. The observations clearly showed that: 1) all three resulting curves worked well in the vertical velocity distribution prediction. This proved the substitution of u_* and y with the $u/\bar{u}$ and y/H were reliable and applicable; 2) the parabolic curve described the vertical flow velocity distribution best with an error of 7%, but the scatter of parabolically fitted coefficients was extremely large. The prediction accuracy of the logarithmic curve is slightly higher than that of the power curve and the logarithmic and power error were 10% and 11%, respectively; 3) in water depth direction, the predicted results of the middle depth of the vertical profiles tend to be more reliable and precise. The highest estimated error appeared in the area near the water surface, and high deviations were then found in the river bed region; 4) higher catchment slope resulted in larger coefficients and constants in logarithmic and power fitting.

Keywords: Vertical flow velocity distribution, logarithmic formula, power formula, parabolic formula, dimensionless flow velocity, dimensionless water depth, natural rivers

3.1 Introduction

A recurring problem in hydraulic or hydrological research and engineering is the estimation of vertical flow velocity distribution in open channels under varying conditions (Samani and Mazaheri, 2010). Many attempts have been made to express the flow velocity distribution mathematically and distribution functions have been proposed to describe velocity under different hydraulic conditions (Wang et al., 1995; Wiberg and Smith, 1991; Zhu and Li, 2009). According to the analysis, parabola line, power and logarithmic distribution lines are usually used to describe the vertical flow velocity profile. Previous studies suggested that a vertical profile from laminar flow fits the parabola line better, while vertical profiles from turbulent flow fit the logarithmic distribution law more frequently. In wide and shallow rivers the vertical velocity tends to show an exponential or logarithmical distribution (Bergstrom et al., 2001; Chen et al., 1999). Because of the complexity of natural river bed and river cross section conditions, measured vertical velocity profiles frequently shows mixed characteristics of two or three distribution laws.

The logarithmic distribution law or so called law of the wall was proposed by von Kármán (1931). He stated that the average velocity of a turbulent flow at a certain point is proportional to the logarithm of the distance from that point to the river bed or bank (von Kármán, 1931). This well-known logarithmic law for flow velocity distribution was considered to be a good approximation for the entire flow velocity profile of natural rivers and has been used widely in various turbulent shear flows over a solid surface, such as boundary layer flows, pipe flows, and open-channel flows (Cheng and Chiew, 1998).

While there are several manifestations of the law of the wall, the most succinct one is as follows,

$$U^+ = \frac{1}{\mathrm{k}} \ln \mathrm{y}^+ + \mathrm{B_i} \qquad (1)$$

where $U^+ = u/\mathrm{u}_*$, $y^+ = y\mathrm{u}_*/\nu$, u is the mean point velocity, y is the distance between measured point and river bed; ν is the kinematic viscosity; u_* is the friction velocity defined from the wall skin friction through its relationship with the stress at the bottom (τ_b), $\mathrm{u}_* = \sqrt{\tau_b/\rho}$ (ρ is the density of the flow); k is the so-called von Kármán constant and $\mathrm{B_i}$ is another constant.

During the last 80 years the logarithmic distribution law has been extensively studied by engineers and researchers and a systematical theory was achieved. Literature review shows that k is considered to cover the range of 0.35-0.45 (He and Wang, 2003; Zagarola and Smits, 1998; Zanoun et al., 2003). The constant $\mathrm{B_i}$ was believed to be universal, but recent researches showed that it covers a wider range from 4 to 10 (George, 2007; Perlin et al., 2005).

Most of the k and $\mathrm{B_i}$ discussed in literature are based on the laboratory experiments or pipe flow data. Natural rivers have not been extensively analyzed yet. One of the reasons is the difficulty of friction velocity u_* determination in non-uniform flow in the field because of the complexity of natural flow

conditions (Alfredsson and Örlü, 2012; Wei et al., 2005).

According to the principle of dimensional analysis, the power law was presented to be an alternative model to represent the vertical distribution of velocity in open channel flows in 1930's (Zhang and Dong, 1998). It can be expressed in general as follows,

$$U^+ = c(y^+)^n \qquad (2)$$

C is the constant and n is the index, the other variables are the same as in the logarithm law (eq. 1). The applicability of different power functions were analyzed by (González et al., 1996). Both c and n are empirical constants that are determined by the specific hydraulic condition. The variation and complexity of the open flow lead to the lack of the universality of the constants. The combination of c=8.74 and n=1/7 is far more common compared with other conditions (Zhang, 2008). Based on the theoretical considerations, the perfect agreement between the power law and the logarithmic law requires that the product of k, c and n should be equal to 1/e (e is the base of natural logarithms) (Chen, 1991). Experimental research showed that for low Reynolds numbers in open channels, the power law seems to describe the velocity distribution better than the logarithm law in the boundary layer and the power law provides a better estimation for u_* (Bergstrom et al., 2001).

The existence of the parabolic nature of flow velocity distribution of turbulence in open channels has been mentioned by earlier investigators (Blench, 1966; Coleman, 1973). Based on cross-sectional flow velocity data, experimental scientists put forward an additional water profile distribution law, a parabolic law (Sarma et al., 1983), which can be explained as:

$$\frac{u_m - u}{u_*} = c\left(1 - \frac{y}{H}\right)^2 \qquad (3)$$

Here u_m is the maximum point velocity along the vertical profile, c is a pending constant, y is the depth of the measured point from the bottom and H is the real water depth of the profile. Observations later showed that the boundary between the inner and outer regions of the vertical flow profile which is marked by y/H, is independent of the Reynolds number of flow (Vedula and Achanta, 1985). New expressions of the parabolic distribution based on formula (3) were established and certificated in a recent research (Zhang, 2008).

In addition to these three main flow velocity distribution laws discussed above, more vertical profile description formulas were established based on theoretical assumptions, such as the quadratic polynomial distribution law and rectangular cross-sectional binary velocity distribution formulas (Coleman, 1973; Guo, 0). Being expressed by the deduced parameters in a complex form, these new formulas are inefficient in wide application range because of the theoretical argument.

The logarithmic (L), power (P1) and parabolic (P2) vertical velocity distribution laws mentioned in this

paper involve u_*, which is difficult to measure directly. Calculated values of u_* based on different deduction methods were proven to be of less consistency (Zhang, 2008). The absolute depths of the measured points in logarithm law and power law makes the comparative analysis of the distribution law between different lab experiments and open flow data even more difficult. A uniform formula which involves only easy-to-determine parameters would be a good solution to the velocity estimation and the comparison between sites. In this paper we take u/ū (ū is the mean profile velocity) and relative depth (y/H) as the dimensionless flow velocity and depth to search for a new distribution formula for vertical flow velocity profiles. To maintain the uniformity of the variables, instead of formula (3), formula (6) was taken to express the parabolic velocity distribution. Formula (6) was derived based on formula (3) and was proven to be applicable in lab experiments (Yan et al., 2005). The three distribution laws were consequently deformed into the following forms:

$$\frac{u}{\bar{u}} = k_1 \ln\left(\frac{y}{H}\right) + b_1 \quad (4)$$

$$\frac{u}{\bar{u}} = k_2 \left(\frac{y}{H}\right)^n \quad (5)$$

$$\frac{u}{\bar{u}} = k_3 \left(\frac{y}{H}\right)^2 + k_4 \left(\frac{y}{H}\right) + b_2 \quad (6)$$

Here k_1, k_2, k_3 and k_4 are coefficients; n, b_1 and b_2 are constants, the remaining symbols are the same as mentioned above.

The objectives of this study are to analyze the vertical velocity distribution formula in natural rivers in various catchments based on the relative flow velocity and relative depth, to evaluate the applicability of the three prediction curves by fitting the synthetic velocity values against the real measured values from the field, and to analyze the accuracy of the formulas at different relative depths. A third aim is to identify the best distribution law and to compare and investigate the formulas in different catchments with different slopes.

3.2 Methodology

3.2.1. Equipment and measurement principle

Mechanical propellers or electromagnetic velocity meters are widely accepted in hydro-related research (Muste et al., 2008; Wu et al., 2011). FlowSens (SEBA Hydrometrie, Germany) is a widespread electromagnetic velocity meter based on the Faraday's Law (Wu et al. 2010). It is an intrusive instrument and works in the classic point-by-point way (Fig. 3.1 a). ADC (Acoustic Digital Current Meter, OTT Company, Kempten/Germany) is another point velocity meter, which measures depth, velocity and discharge with acoustic signal. The depth is measured with a built-in pressure sensor and the point

velocity is measured based on pulse-coherent technology (Fig. 3.1 b). The key advantage of these instruments lies in their ability to measure in a range of fluids including fresh water, waste water, salt water and water with heavy vegetation or suspended sediment (OTT, 2008; SEBA, 2010). FlowSens is able to offer the single measured point velocity directly in the field and additional office work is needed for mean velocity or discharge calculation. The PDA of ADC finishes the basic hydraulic calculation after each cross section sampling and no more office work is needed except downloading the data to a computer. Characterized by faster measurements and higher data accuracy, the use of acoustic methods in hydrodynamic sample meets the increasing demand for more precise flow velocity and discharge measurements. Acoustic Doppler Qliner (ADQ, OTT Company, Kempten/Germany) is a representative of acoustic-based hydraulic measurement equipment which is designed especially for the medium-sized rivers and channels and has been proven to be a reliable and accurate sampling equipment (Song et al., 2012).

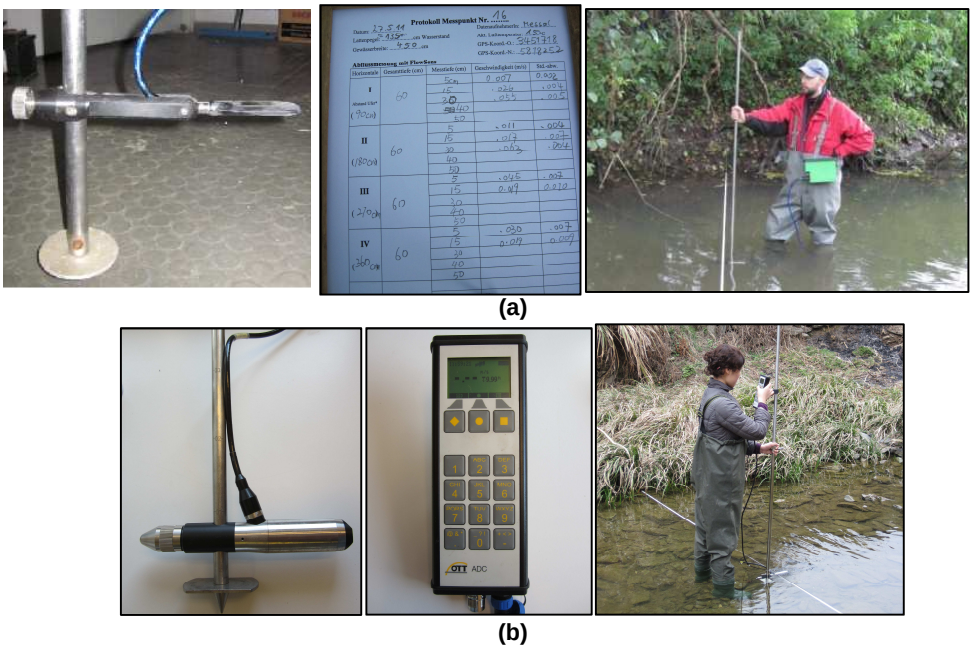

Fig. 3.1 Point velocity meters. (a). FlowSens; (b). ADC.

ADQ samples water depth, velocity and discharge for each water profile simultaneously. The water velocity is calculated based on the Doppler Effect and the water depth is estimated by the transmission time between the signal transmitted and reflected by the river bottom to the sensors (Fig. 3.2 a). Bluetooth communication between the additional PDA and the four sensors suited underneath the fiberglass catamaran excludes man from stepping into the water (Fig. 3.2 b). The transportation of ADQ from one vertical to the next can be done with the ropes and ironic wires (Fig. 3.2 c). The built-in program in PDA instantly provides the direct-reading velocity, discharge, depth, signal amplitude for each vertical profile measurement and finally river discharge and flow velocity distribution (OTT, 2010). Compared with

traditional equipment, ADQ is an innovation that automatically provides complete velocity profiles with both point velocity and the average profile velocity based on integration calculation, together with water depth and measured depth of each point. These advantages make ADQ a suitable instrument for the sampling and analyses of u/ū and y/H.

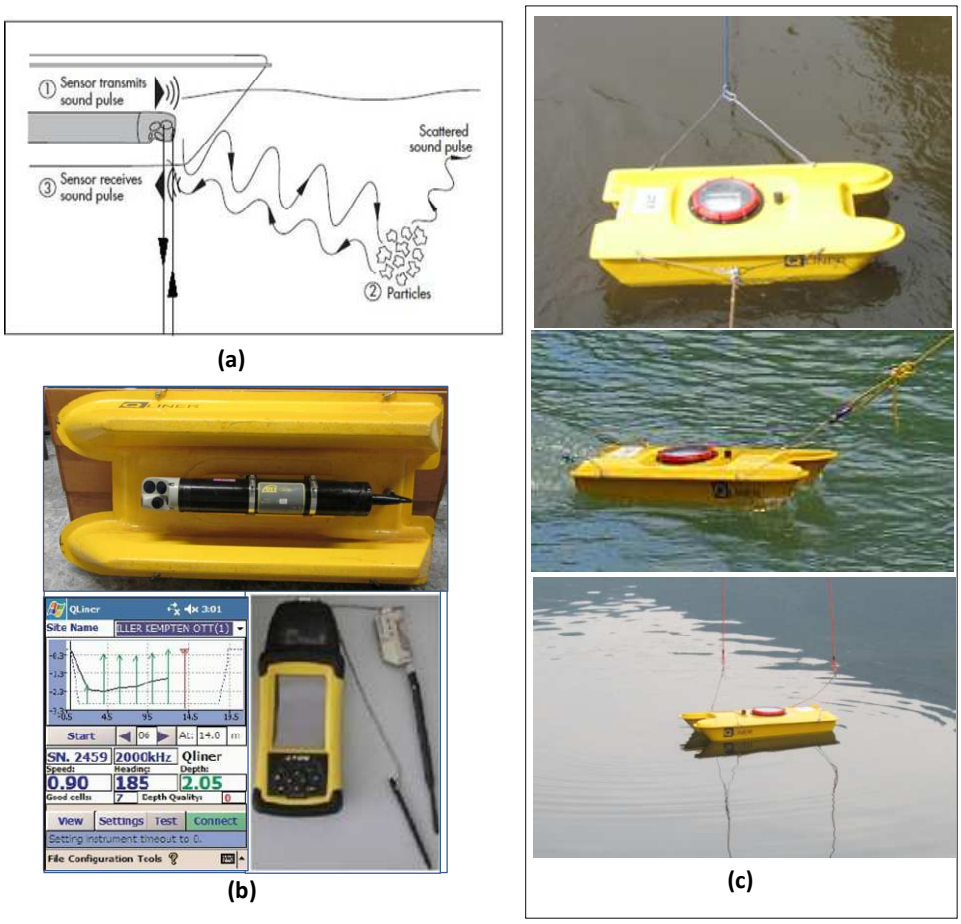

Fig. 3.2 (a). ADQ measurement principle for water velocity and depth (OTT 2010); (b). ADQ, PDA and the display system; (c). ADQ during measurements.

3.2.2. Measurements of the Water Profiles

The FlowSens and ADQ introduced above were used complementary to each other in the field. The FlowSens was applied in the narrow shallow rivers or streams with heavy vegetation where the ADQ was not suitable, while the ADQ was preferred for the deep and fast flowing steams. All the velocity profiles in the Chinese Changjiang catchment were measured with ADC. Field campaigns were accomplished from 2010 October to 2011 December in the Upper Stör (Northern Germany), Kinzig (West-Central Germany) and Changjiang catchment (China) to record the water vertical profiles. Finally, 248 water profiles were measured in order to setup and verify our assumptions in equations (4), (5) and (6).The

characteristics of all three catchments are shown in Fig. 3.3 and Tab. 3.1.

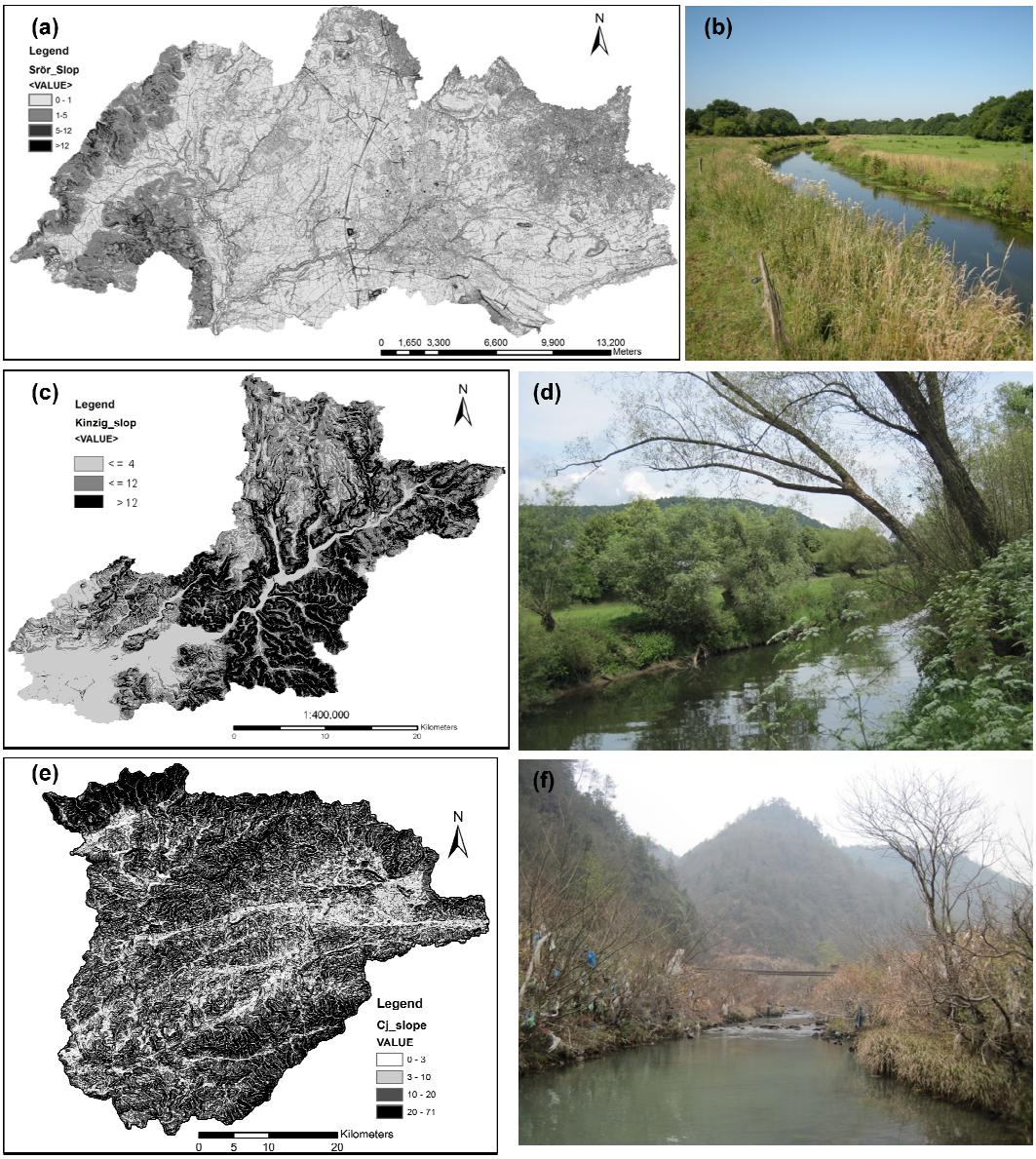

Fig. 3.3 The slope maps and landscape photos of the studied catchments, (a) and (b), Upper Stör catchment (LVermGeoSH, 1995); (c) and (d), Kinzig catchment (HVBG, 2011); (e) and (f) Changjiang catchment (ISDSP, 2013).

The upper Stör catchment is located in the middle of Schleswig-Holstein/Northern (Fig. 3.3 a, b, Tab. 3.1). The area is dominated by shallow groundwater tables and glacial and glaciofluvial sediments, and the landscape is mainly covered by arable land (48.1%), pasture (29.5%) and forest (9.1 %) (Müller-Wohlfeil et al., 2000; Schmalz and Fohrer, 2009; Schmalz et al., 2008). Stör catchment is part of Northern German lowland area and in most of the catchment the slope gradients are usually smaller than 1° in most part of

the catchment, except southwestern part which has gradients of more than 3° (LVA, 1995).

The Kinzig catchment lies 15-80 km east of Frankfurt am Main in south-eastern Hessen, Germany. The main river is 86 km long and drains a catchment of 1059 km² (Fig. 3.3 c, d, Tab. 3.1). The altitude of catchment ranges from 627 m at origin down to 98 m in the Main valley (Meurer, 2012). It is classified as a mid-sized fine to coarse substrate dominated siliceous highland river (HMUELV, 2011).

The Changjiang basin is situated in the southeast of China (Fig 3.3 e, f, Tab. 3.1). The catchment area sums up to 1700 km² and the main Changjiang stream drains in the Poyang Lake. The landscape in the catchment is characterized by a hilly terrain with the highest peaks at the northern and northwestern catchment borders (Strehmel, 2011). The highest point of the catchment is at an altitude of 1699 m (a.s.l.) while the catchment's outlet has an altitude of 57 m a.s.l..

Tab. 3.1 Evaluation sites and the number of measurements

Catchment	Location	Size (km^2)	Landscape type	Main river slope(%)	Width(m)	Depth(m)	No.[1]
Upper Stör	S-H[2], Germany	468	Lowland	0.22	10-15	1.5-2.5	140
Kinzig	Hessen, Germany	1059	Low mountain area	0.62	15-25	1-2	48
Changjiang	Anhui Province, China	1700	Mountainous area	1.93	60	1-1.5	60

Note: [1] number of the water vertical profile measurements; [2] S-H: Schleswig-Holstein

3.3 Statistical Analysis

3.3.1. Fitting analysis of synthetic values against measured velocities

The logarithmic, power and parabolic synthetic velocities were fitted against the measured velocity of all three catchments. Coefficient of determination (R^2) and residual sum of square (RSS) are representative indexes of regression quality. The cumulative probability distributions of R^2 of every vertical profile and the relative error of every single point were adopted to test the accuracy of the predication formulas. Finally, the comparison analysis was made between the coefficients and constants derived from each catchment to examine the complexity of the predication formula.

3.3.1.1 **Fitting results**

Analysis of fitting results for logarithmic fitting (L), power curve (P1) and parabolic curve (P2) resulted in R^2 higher than 0.75 and the RSS less than 0.18. This demonstrates that all three curves can describe the vertical distribution in a satisfying way (Tab. 3.2).

The averaged R^2 of the 248 verticals fitting with formulas (4), (5) and (6) tends to be convincing, although the RSS and the coefficient of variation (CV) of these fitted vertical profiles showed high variability. The R^2 and RSS of the fittings showed the highest accuracy of the parabolic prediction and the relatively

higher accuracy of the logarithmic fitting than that of power fitting. Higher variability of parabolic formula parameters were reported by the higher value CV of k_3, k_4 and b_2.

Tab. 3.2 Averaged values of the results of logarithmic, power and parabolic fittings

	Logarithmic	Averaged	CV	Power	Averaged	CV	Parabolic	Averaged	CV
R^2	R^2-L	0.77	0.28	R^2-P1	0.75	0.29	R^2-P2	0.78	0.33
RSS	RSS-L	0.18	1.09	RSS-P1	0.14	1.29	RSS-P2	0.11	1.35
Coefficient	K_1	0.50	0.55	K_2	1.47	0.33	K_3	-1.91	-1.10
							K_4	3.12	0.70
Constant	b_1	1.28	0.24	n	0.71	0.63	b_2	-0.11	-5.25

3.3.1.2 **Correlation of fitted coefficients and constants**

Fitting analysis revealed the high positive correlation between k_1 and b_1, and k_2 and n, while k_3 is strongly negative correlated with k_4 (Tab 3.3). The correlation coefficients were 0.76, 0.73 and -0.94 respectively. The strong correlations provided the possibility of expressing constants with coefficients in formula (4), (5) and (6).

Tab. 3.3 Correlation coefficients of fitted parameters

Correlation coefficient	k_1	b_1	k_2	n	k_3	k_4	b_2
k_1	1.00						
b_1	***0.76***	1.00					
k_2	0.73	0.70	1.00				
n	0.61	0.16	***0.73***	1.00			
k_3	-0.22	-0.28	0.20	0.35	1.00		
k_4	0.51	0.49	0.09	-0.09	***-0.94***	1.00	
b_2	-0.73	-0.40	-0.29	-0.35	***0.69***	***-0.86***	1.00

The linear fitting between fitted coefficients and constants were made to explain their algebraic relationship (Fig. 3.4 a, b and c). The $R^2$of the fitting were 0.89, 0.84 and 0.90, respectively. The regression formulas demonstrated that b, n and k_4 can be approximately expressed as $2.25k_1$, $0.47k_2$ and $-1.26k_3$.

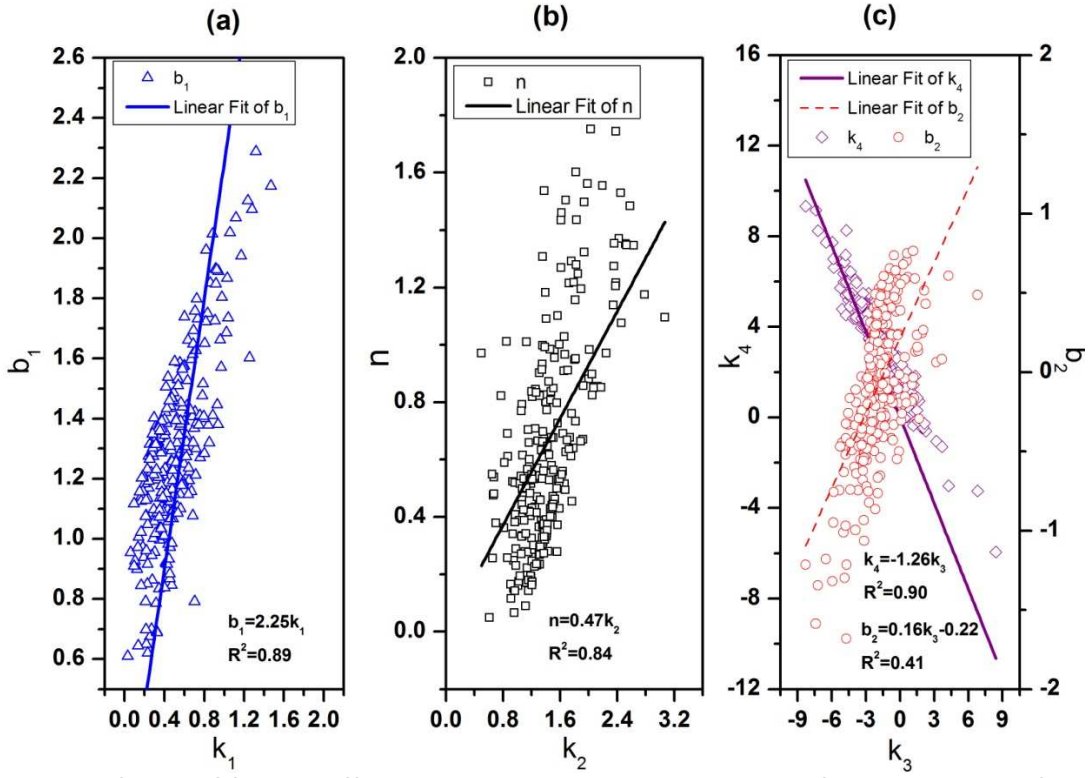

Fig. 3.4 Linear fitting of fitted coefficients and constants, (a) logarithmic fitting; (b) power fitting; (c) parabolic fitting.

3.3.2. Accuracy of the predication at different measured water depths

3.3.2.1 **Relative error of the single points at different depths**

As it is shown in Fig. 3.5, the highest error of the logarithmic prediction formula was at the water surface area, where the real measured velocity was higher than the fitted velocity by 15%. Near the river bottom the error was between ±5-10%. In the middle parts the deviations of the fitted values from the measured values were within a range of ±5%, which reveals high quality of the logarithmic prediction especially in the middle part of the verticals.

Fig. 3.5 also clearly shows that the errors of the power fitting were as high as -20% near the river surface and bottom. The power synthetic velocity from the river bed to around 2/3 of the water depths was about 10% lower than the real measured values. A similar phenomenon was observed near the water surface area. The measured values were higher than the fitted velocities by around 5%in the middle part of the profiles. Generally speaking, the synthetic velocity was smaller in the lower and upper water layers, while in the middle layer the fitted velocities were higher than the observations.

Although the averaged error suggested that the parabolic curve estimated the vertical velocity with the highest quality, the high estimated error at the water surface area was still as high as -10%. Apart from that,

the prediction agreed well with the measured field data in the other parts of the profile.

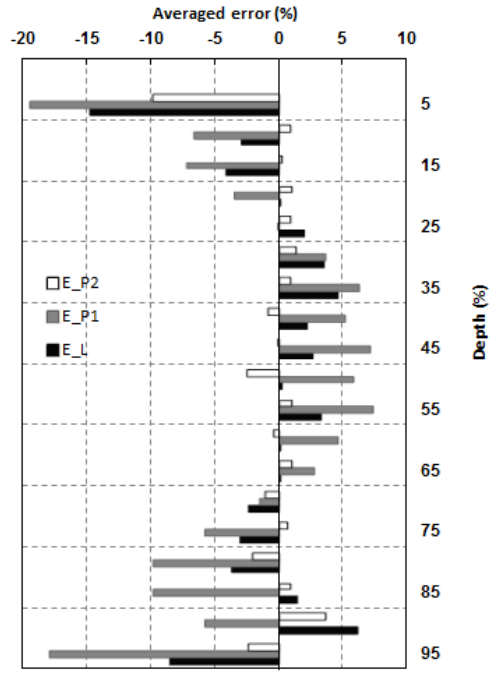

Fig. 3.5 Averaged error of every single point velocity at different relative depth

Note: E_L is the error of logarithmic curve; E_P1 and E_P2represent the error of power and parabolic fitting respectively.

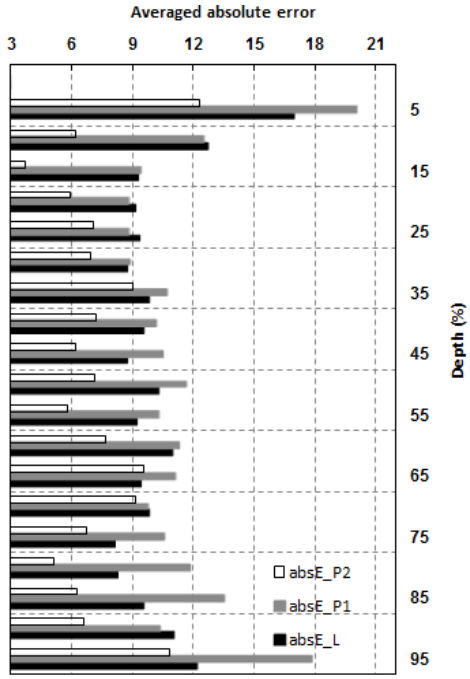

Fig. 3.6 Averaged absolute error of every single point velocity at different relative depth

Note: absE_L is the absolute logarithmic error; absE_P1 and absE_P2represent that of power and parabolic fitting respectively.

3.3.2.2 **Averaged absolute relative error of single points at different depths**

Fig. 3.6 displays the averaged absolute error of the synthetic point velocity to the measured point velocity at every measured point in water depth direction. The higher deviation trend in the water surface and bottom area was shown by the histogram. All the averaged absolute errors were smaller than 20%, which means that the three curves performed well in the whole profile. The averaged absolute errors were 10%, 11% and 7% for logarithmic, power and parabolic fitting, respectively. In accordance with the results of the averaged error analysis, the highest deviation from the measured velocity appeared at the area near the water surface. The errors reached 17%, 20% and 13% in the logarithmic, power and parabolic prediction respectively. Close to the river bed absolute error of the power function was as high as 18%, and the absolute errors of logarithmic and parabolic formulas were around 10%. In the middle part of the profile, the absolute error of the logarithmic fitting ranged from 4% to 10%, while the power and parabolic fitting results deviated more than 10% of the real measured data.

3.3.3. Variability of fitted parameters in different catchments

3.3.3.1 **Logarithmic fitting**

Logarithmic fitting analysis indicated that the coefficient k_1 ranged from 0.25 to 1.5, and constants b varied from 0.5 to 2.5 from all the fitting profiles. The box plots of k_1 and b in Fig. 3.7 revealed a similar degree of dispersion, but different value ranges in Stör, Kinzig and Changjiang catchment. In the catchment Stör, k_1 varied from -0.4 to 1.3 with an average value of 0.37, while the k_1 value in the Kinzig catchment increased overall and reached an average value of 0.63.Compared with the condition in the Kinzig catchment, the k_1 value range of the Changjiang catchment increased and the averaged value was as high as 0.75. This implied that the vertical velocity in Changjiang catchments tend to increase faster from the bottom to the water surface.

The constant b_1 of the three catchments showed similar trends. The Changjiang catchment provided the highest value range with the average value of 1.50. The averaged b_1-Kinzig and b_1-Stör are 1.28 and 1.19, respectively. This demonstrated the higher surface velocity in the craggy catchment.

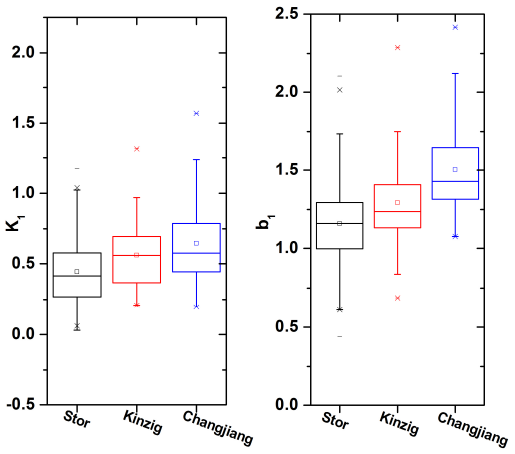

Fig. 3.7 Box plots of k_1 and b in different catchments

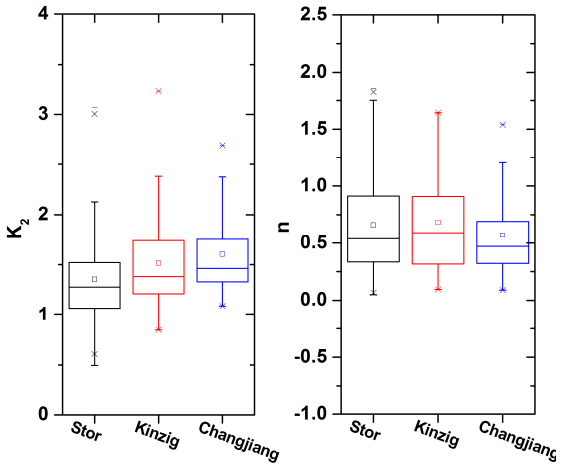

Fig. 3.8 Box plots of the coefficient k_2 and index n in different catchments

3.3.3.2 **Power fitting**

Fig. 3.8 presented the box plots of the power fitted coefficients and indices. The coefficient k_2 ranged from 0.4 to 3.4, while the index n varied from -0.6 to 1.8, which implies the similar variability as that of the logarithmic parameters. The figure also displays that the distributions of k_2 and n in the Changjiang catchment were relatively more centralized compared with those of the other two catchments. Apart from that, the increasing tendency of k_2 with the increase of the catchment slope was revealed. No noticeable difference of n was discovered except its lower dispersion in the Changjiang catchment. The averaged n values in the three catchments were around 0.52 and very close to each other. The higher coefficients in the steeper catchment gain manifested the higher surface velocity and steeper vertical velocity profiles.

3.3.3.3 **Parabolic fitting**

The box plot of the parabolic parameters in Fig. 3.9 shows that there is considerable scatter in the coefficients k_3 and k_4. However, in spite of this scatter, it is also readily apparent that the parameters from Kinzig catchment had the widest value ranges, while the Changjiang catchment parameters displayed the lowest dispersion. In addition to the individual parameters, the sum of k_3, k_4 and b_2 was further explored based on the fact that this sum is the ratio of the surface velocity to the profile averaged velocity. The increase of this sum value in Kinzig and Changjiang catchments clarifies the higher ratio between surface velocity and profile averaged velocity in mountainous catchments. This is consistent with the results of the logarithmic and power fittings.

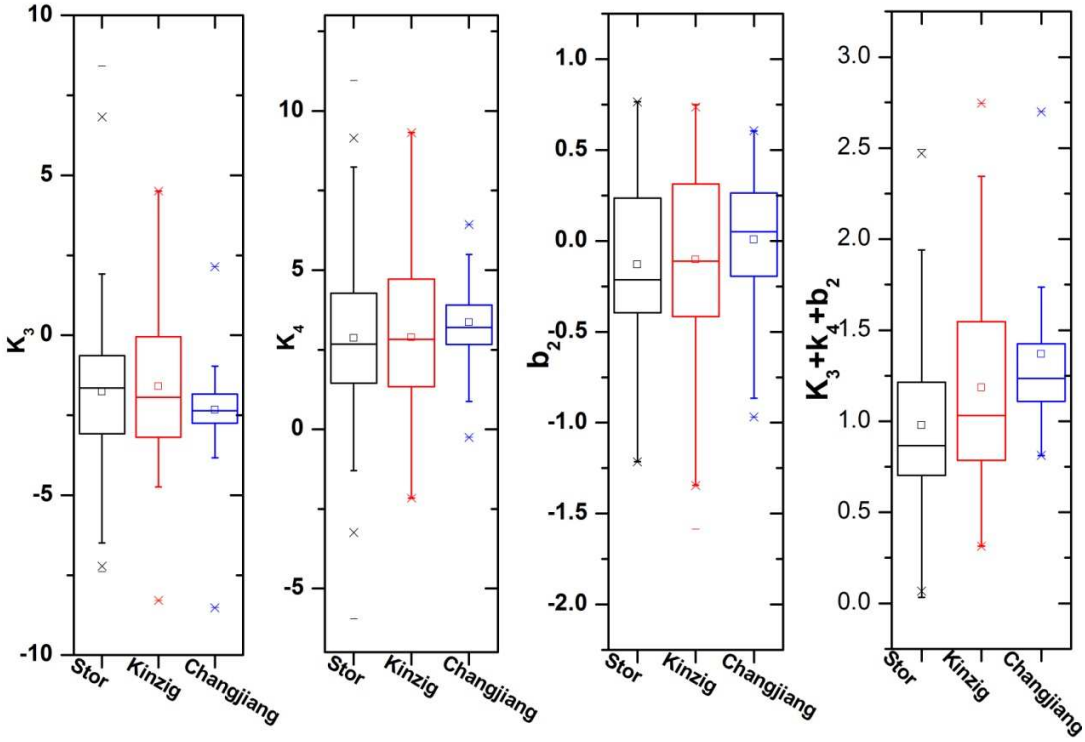

Fig. 3.9 Box plots of the parabolic parameters in different catchments

3.4 Discussion

3.4.1. Formula parameters

Parabolic fitting leads to the highest regression quality between measured and fitted data with the highest R^2 and lowest RSS. But higher CV of k_3, k_4 and b_2 suggest that they are sensitive to the channel hydrological conditions, such as roughness, width/depth ratio, river slope etc.. Logarithm formula and power formula provided similar fitting quality but the higher index variability in power fitting made the logarithmic formula relatively superior. It is difficult to find the unique coefficients and constant which are

applicable for natural rivers within the same catchment or among the different catchments.

This is consistent with the fact that the vertical water profiles in the natural rivers demonstrate logarithmic, power and parabolic characteristics simultaneously (Afzal, 2001). Because of the complexity of geometry, boundary resistance and other hydraulic or hydrological factors, the idea of a universal law for flows is not supported by either the theory or the data (George, 2007). However, the high correlation between the fitted coefficients and constants provided the opportunity to establish the simplified but relatively rough formulas.

3.4.2. Predication and relative depth

All three prediction formulas worked well in the whole water profile with averaged error around ±10%. The averaged error and the averaged absolute error of the profile at the different relative depths of the profile proved that the parabolic fitting provides best quality in describing the vertical velocity distribution, while the power fitting lead to the highest prediction errors. The quality of the logarithmic prediction was in between the power and parabolic fitting at nearly all relative depths. Earlier researchers also pointed out that parabolic fitting was most appropriate for describing the vertical water profile in natural rivers or channels (Sarma et al., 1983; Zhang, 2008). In addition, previous studies mentioned that the verticals in wide and shallow rivers with larger width/depth ratio tended to display exponential or logarithmical characteristics (Bergstrom et al., 2001; Chen, 1991). But the rivers in our study were with relatively low width/depth ratio, which might explain the higher efficiency of the parabolic prediction.

3.4.3. Predication in different catchments

The fitted coefficients and constants varied in a wide range both within the same catchment and among the different catchments, which leads to the inefficiency in the setup of the uniform formula. Generally speaking, the increase of the logarithmic coefficient (k_1) and constant (b_1) with the rise of the river slope represents the steeper water vertical profiles. Although the index (n) valued around 0.52 and varied slightly among different catchments, the power coefficient (k_3) rises apparently from lowland area to mountainous catchment.

Despite the considerable scatter of the parabolic coefficients (k_3 and k_4), the sum of the parabolic coefficients and constants (b_2) explained the greater increase rate of velocity from bottom to the surface of the mountainous water vertical profiles. Coincidently, the variability of parabolic fitted coefficients and constants between different rivers were even higher according to previous literature (Sun et al., 2004).

3.5 Conclusion

Based on the dimensionless relative flow velocity and relative water depth, the three vertical velocity distribution predicting formulas were set up. Empirical analysis with the 248 vertical water profiles

measured from a German lowland catchment, a low mountain catchment in Germany and a mountainous catchment from China reached following results.

(1) The logarithmic, power and parabolic formulas described the vertical distribution at a precise level. The substitution of U^+ and y^+ in the old formulas with the relative flow velocity u/ū and relative depth y/H were proven to be reliable and applicable.

(2) The parabolic formula provided the best prediction of the vertical flow velocity profile, while the logarithmic formula tended to be slightly superior to the power formula. The averaged absolute logarithmic, power and parabolic errors were around 10%, 11% and 7% respectively.

(3) In the vertical direction, all three prediction formulas showed highest deviation in the area near the water surface. Apart from that the predicted errors in the region near the river bed were also very high. The prediction for the middle part of the profile tended to be more reliable and precise.

(4) The variation of the formula coefficients and constants leads to the inefficiency in the setup of a uniform formula. The increases of the k_1, b_1, k_3 and the sum of the parabolic parameters ($k_3+k_4+b_2$) with the increase of the catchment slope represent the greater velocity increase rate from the river bottom to the surface in steeper catchments. Despite the highest fitting quality of parabolic formula, the scatter of fitted coefficients and constants was extremely large.

The logarithmic, power and parabolic formulas discussed in this study proved a high reliability of substitutionu_* with ū in vertical profiles prediction. It then provides the opportunity of predicting the whole vertical profiles with only ū and the water depth. Combined with the mean profile velocity horizontal distribution prediction research, the point velocity distribution model for the whole cross section can be established and the needed input for the model will be the geometry of the cross section and the experienced coefficients of the river section, which would be easily estimated with some real measured data. This model will prominently improve the data accessibility.

Chapter 4. Simulation and Comparison of stream power In-channel and on the Floodplain in a German Lowland Area

S. Song, B. Schmalz, N. Fohrer
Journal of Hydrology and Hydromechanics
Submitted, 18 October 2013; Accepted, 28 February 2014

Abstract: Extensive lowland floodplains cover substantial parts of the glacially formed landscape of Northern Germany. Stream power is recognized as a force of formation and development of the river morphology and an interaction system between channel and floodplain. In order to understand the effects of the river power and flood power, HEC-RAS models were set up for ten river sections in the Upper Stör catchment, based on a 1 m digital elevation model and field data, sampled during a moderate water level period (September, 2011), flood season (January, 2012) and dry season (April, 2012). The models were proven to be highly efficient and accurate through the seasonal roughness modification. The coefficients of determination (R^2) of the calibrated models were 0.90, 0.90, 0.93 and 0.95 respectively**.** Combined with the continuous and long-term data support from SWAT model, the stream power both in-channel and on the floodplain was analysed. Results show that the 10-year-averaged discharge and unit stream power were around 1/3 of bankfull discharge and unit power, and the 10-year-peak discharge and unit power were nearly 1.6 times the bankfull conditions. Unit stream power was proportional to the increase of stream discharge, while the increase rate of unit in-channel power was 3 times higher than that of unit flow power on the floodplain. Finally, the distribution of the hydraulic parameters under 10-years-peak discharge conditions was shown, indicating that only 1-10% of flow power was generated by floodplain flow, but 40-75% volume of water was located on the floodplain. The variation of the increasing rate of the flow power was dominated by the local roughness height, while the flow power distributed on the floodplain mainly depended on the local slope of the .

Keywords: HEC-RAS model, in-channel flow, floodplain flow, unit stream power, inundation area

4.1 Introduction

Recent studies have recognized the importance of river flow analysis and the need to understand the interaction with the river bed and the ecosystem (Sponseller et al., 2010; Wu et al., 2010). More accurate information about river flow and floodplain flow is important for analyzing the alluvial and hydrological effects of the river systems, including water pollutants diffusion, hydraulic construction, water quality

distribution and prediction, river resource management, flood estimation and flood damage prevention, etc. (Brocca et al., 2011; Christian et al., 2013; Lau and Ghani, 2012; Posey, 2009). The driving force of these flow behaviors is commonly expressed as stream power (Jain et al., 2006). Stream power is defined as the time rate of expenditure of potential energy (or supply) when the water travels downstream (Rhoads, 1987). The stream power of the high-magnitude flood is more powerful to cause the major, abrupt morphological change in channel and on the floodplain (Vocal Ferencevic and Ashmore, 2012). Total stream power per unit channel length, or so called unit stream power (Ω, W/m) is mathematically defined as,

$$\Omega = \gamma Q S_e$$

Here, γ is the specific weight of water (N), Q is discharge (m^3/s) and S_e is energy slope, which can be approximated by the water surface slope (Barker et al., 2009; Knighton, 1999).

Europe has been under arising threat of floods, especially high-magnitude floods in the last years (Marchi et al., 2010b). Analysis of the gauged data from 145 stations across Germany suggest an increasing flood hazard during the last five decades, and these observed flood behavior trends are proven to be mainly climate-driven (Petrow and Merz, 2009). Most notable increases in flood losses across the different climate future scenarios are projected for countries in Western Europe (Dankers and Feyen, 2009). The assessment of river risk based on climate scenarios in parts of Germany estimated that the small and medium flood discharge will increase by around 40–50% while the 100-year floods is going to increase by 15% in 2050 (Kundzewicz et al., 2010).

Bankfull discharge is the maximum flow volume the channel can carry and is identified as an important parameter for studying river morphology, flood dynamics and their ecological impacts (Navratil et al., 2006). Discharge above this split value leads to the interaction process between in-channel and floodplain flow and triggers the additional energy losses due to the expansion and friction change of the overbank flow (Knight and Shiono, 1996). The flood magnitude determined the flood wave propagation and attenuation during the overbank flow process (Archer, 1989). Although the flow energy variation with discharge gained very little attention according to the literature review, quantifying the bankfull stream power and the variation of stream power with discharge would provide significant insights into the stream and flood events development (Vocal Ferencevic and Ashmore, 2012).

Considering the increasing flood risk and the important role of stream power in the function of fluvial systems, the spatial flow and flood energy expenditure deserve to be extended by experimental or modeling approaches (Horritt and Bates, 2002; Knighton, 1999). Earlier studies have paid attention to estimate the longitudinal distribution of the stream power from both point-location cross section studies and continuous profile studies (Barker et al., 2009; Jain et al., 2006; Knighton, 1999). The reconstruction of stream peak discharge and flood power at different cross sections along the main stream provide the longitudinal distribution of stream power on basin scale (Marchi et al., 2010a). Modeling approaches have

been adopted in exploring the downstream distribution of the stream power and pointed out that the variability of stream power in headwater reaches is explained by discharge variability, while the variability in midstream and downstream reaches governed by the high variability of channel gradient (Evans et al., 2009). It has been revealed in the literature that the latitudinal distribution of flow and flood were relatively less studied in the last decades. Traditionally stream power data measured from limited cross sections is not sufficiently enough to describe the energy distribution of the flow in-channel and on the floodplain (Barker et al., 2009). Modeling approaches would be a highly efficient supplement in quantifying the latitudinal discharge and energy expenditure.

In this study, we show a combined model approach to evaluate latitudinal stream power distribution. The high precise 1D-hydraulic models in the Upper Stör catchment in Northern German lowland were established, 1) to quantify the variation of stream power both in channel and on the floodplain; 2) to exam the latitudinal distributions of the stream power in channel and on the floodplain, and 3) try to investigate the cause of the different distribution patterns among the sub-catchments.

4.2 Study area and Methodology

4.2.1. Study area

The Upper Stör River catchment is part of the lowland area located in the middle of Schleswig-Holstein/Northern Germany. The catchment stretches over 35 km in the east-west direction and 19 km in the north-south direction covering a drainage area of 468 km^2 (Fig. 4.1, Tab. 4.1). In most of the catchment the gradients are usually smaller than 1°, except southwestern part, which has gradients of more than 3° (LVermGeoSH, 1995).

The catchment was divided into 21 sub-catchments covered every tributary, but only ten of them were selected in our study (Fig. 4.1). The 300m river sections at the outlet of the selected sub-catchments were measured. A criterion for river section selection was that the sites diversity had to be sufficiently enough to reveal the catchment conditions, while some major disturbances or obstacles need to be avoided. The sites had to be easily accessible and suitable to measure with a flow meter. According to such criteria, the sub-catchments we chose sized from 32 km^2 to 461 km^2, and the adjacent floodplains were covered by pasture, forest, arable land and construction land. The slope, area and the roughness of the adjacent floodplain at each river section was given in Tab. 4.1. The slope varied from -0.2% to 0.55% on the floodplain, and ranged from -0.05% to 0.43% in the channel. At most river sections, the floodplain roughness height is higher than the in-channel roughness.

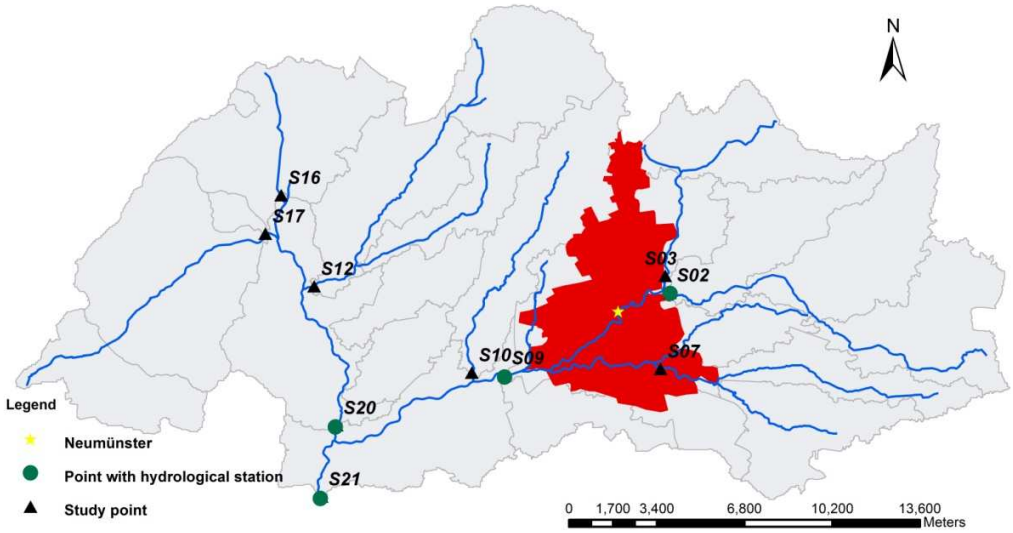

Fig. 4.1 The location of Upper Stör catchment and study river sections

Tab. 4.1 Characteristics of the selected ten sub-catchments

Site No.	Catchment size [km^2]	Slope (%)			Land use & (Roughness Height)			Area (m^2)	
		LOB	CH	ROB	LOB	CH	ROB	LOB	ROB
S02	70.09	0.40	0.21	0.55	C (0.10)	0.05	P (0.07)	187.40	144.20
S03	30.98	0.33	0.20	0.33	F (0.12)	0.04	F (0.12)	1.00	64.67
S07	33.29	0.40	0.09	0.50	C (0.10)	0.06	F (0.10)	30.67	149.17
S09	196.05	0.20	0.43	0.10	C (0.09)	0.06	P (0.07)	1.17	256.33
S10	32.34	0.33	0.10	0.40	P (0.07)	0.04	C (0.09)	24.83	16.50
S12	60.63	0.33	0.25	0.17	C (0.08)	0.05	P (0.09)	0.00	278.50
S16	32.33	0.27	0.09	0.10	A (0.07)	0.05	A (0.07)	0.00	0.00
S17	56.92	-0.01	0.05	0.10	P (0.07)	0.04	P (0.07)	209.83	73.67
S20	203.02	0.10	0.19	0.13	P (0.08)	0.06	A (0.08)	256.33	750.33
S21	461.74	0.17	0.10	-0.2	P (0.08)	0.06	P (0.08)	231.83	479.00

Note: LOB is the left bank of the channel; CH is the channel; ROB is the right bank of the channel. The area refers to the submerged area in the 10year-peak flood; C refers to the construction land use; F means Forest; P is pasture land; A is arable land.

4.2.2. Model Cascade and Data Transfer

4.2.2.1 **SWAT and HEC-RAS Model description**

The SWAT model is a continuous, long-term, semi-distributed parameter model that can simulate surface and subsurface flow, soil erosion and sediment deposition, and nutrient movement through watersheds (Arnold et al., 1998). The soil water balance equation is the basis of hydrological modeling. The land phase of the hydrological cycle and the routing of runoff through the river network is the major framework of the SWAT model. The simulated processes include surface runoff, infiltration, evaporation, plant water uptake, lateral flow, and percolation to shallow and deep aquifers (Coffey et al., 2010; Luo et al., 2012). Discharge is one of the outputs of the flow routing, and has proven to be successfully linked to other

models (e.g., MODFLOW) to provide background data for the model development (Johnston et al., 2011; Kiesel et al., 2013; Zhang, 2011).

Hydrologic Engineering Centers River Analysis System (HEC- RAS) developed by the US Army Corps of Engineers is an integrated 1-D hydraulic model for interactive use in a multi-tasking environmental management (Brunner, 1995). Although the main function of this model is to simulate steady/unsteady river dynamics, sediment transportation and water quality dynamics (Hicks and Peacock, 2005; Horritt and Bates, 2002; Yang et al., 2006), it is also adopted as an effective stream power estimation tool (Vocal Ferencevic and Ashmore, 2012). The boundary condition in forms of flow series, normal depth, stage series or rating curve is the essential input during the steady and unsteady flow analysis process. The steady and unsteady flow analysis calculation base on the fundamental hydraulic equations, including the continuity equation, energy equation, and flow resistance equation (Kasper, 2005). The adoption of resistance equation in HEC-RAS model is criticized as being the overly sensitive factor in many researches (Pappenberger et al., 2005; Parhi, 2013; Parhi et al., 2012). The uncertainty in flow characteristics modeling is not only caused by the calibration process of the roughness parameter, but also because of the difficulty in selecting the 'correct' roughness in practical application (Pappenberger et al., 2005; Parhi, 2013; Parhi et al., 2012).

The suitability and accuracy of the HEC-RAS model have been proven to be comparable to other 1D (Hicks and Peacock, 2005; Knebl et al., 2005) and 2D hydrological models (Bates and De Roo, 2000; Hervouet, 2000; Horritt and Bates, 2002). Besides the single model approach, the integrated model approaches aimed at linking the HEC-RAS model with other models to extract the best of each individual model component have been primarily pursued. Promising results were yielded in integrating sediment output of the SWAT model (Soil and Water Assessment Tool) (Arnold et al., 1998) to HEC-RAS model and BIOMOD (Thuiller, 2003) model (Jähnig et al., 2012; Kuemmerlen et al., 2012; Schmalz et al., 2012; Strehmel, 2011).

4.2.2.2 **Data Transfer**

We integrated the distributed eco-hydrological model with the 1-D hydraulic model to simulate the variation of the unit stream power in the Upper Stör catchment. The SWAT model is an adequate supplement to the HEC-RAS model in hydraulic dynamic modeling, providing basic discharge input. The long-term continuous daily flow output from SWAT model of every was adopted as the boundary condition input in HEC-RAS model. The SWAT model for the study area has been setup and well calibrated until 2010 (Pott, 2014). Preliminary calibration and validation of the SWAT daily simulations yielded an averaged Nash-Sutcliffe of 0.83 and an averaged coefficient of determination (R^2) of 0.88 at the outlet of the Upper Stör catchment (Fig. 4.2). This proved the efficient performance of the SWAT model and it's suitability to work as the HEC-RAS input data.

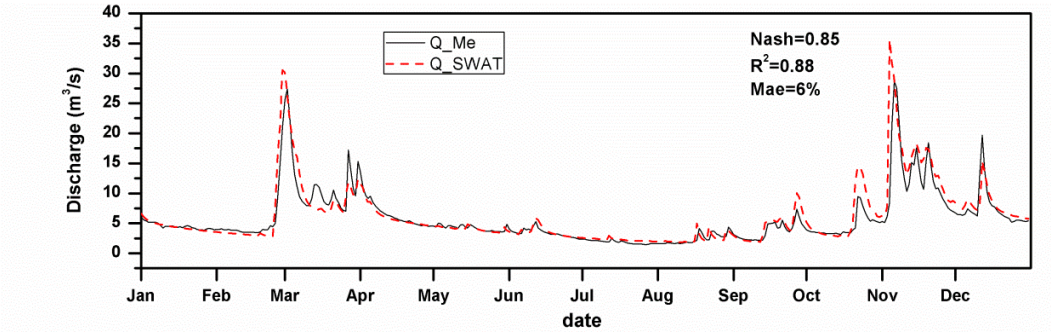

Fig. 4.2 The measured and SWAT-modeled discharge at the catchment outlet (S21) in 2010
Note: Mae means absolute error of the water surface elevation; Nash, Nash-Sutcliffe efficiency.

4.2.3. Data collection

Cross-sectional profiles of water surface width, depth, velocity and discharge for seven cross sections evenly distributed along the 300 m river sections at the outlet of the ten selected sub-catchments were collected. Field campaigns were carried out during the moderate water level period (September, 2011), and surveys were then repeated at the same cross sections during flood season (January, 2012) and dry season (April, 2012) respectively at the ten selected river sections of the Upper Stör River (Fig. 1). The river depth, velocity and discharge were measured with the FlowSens device (SEBA Hydrometrie, Germany) during dry season and an Acoustic Doppler device called Qliner (ADQ, OTT Company, Kempten/Germany) during moderate water leve1 period and flood season. The accuracy and applicability of both equipment has been proven in a previous study (Song et al., 2012). Additionally bank elevation, bank vegetation and sediment condition were mapped in the first field campaign in September 2011 in order to set up the 1-D hydraulic HEC-RAS model. Bank elevation together with cross-sectional depth determined the geometry of every cross section. Bank vegetation and channel sediment were then transformed into roughness height according to the conversion relationship (Chow, 1959).

4.2.4. The Setup of HEC-RAS Model

Stream channel cross sections were obtained from the Laboratory's computer-based geographic information system (ArcGIS 9.3) in addition to field survey data basis (Fig. 4.3). Topographic data of floodplains were automatically extracted from the Digital Elevation Model (DEM) with 1 m resolution using HEC–geoRAS, an ArcView extensive capability developed by the USACE–HEC. These cross-sectional features containing the geo-referenced information were then exported to the HEC–RAS model, in order to set up the main river geometry system. The HEC-RAS models for each river section were first produced, and then the roughness factor and the edited river bed geometry were imported. The complete procedure is shown in Fig.4. 3.

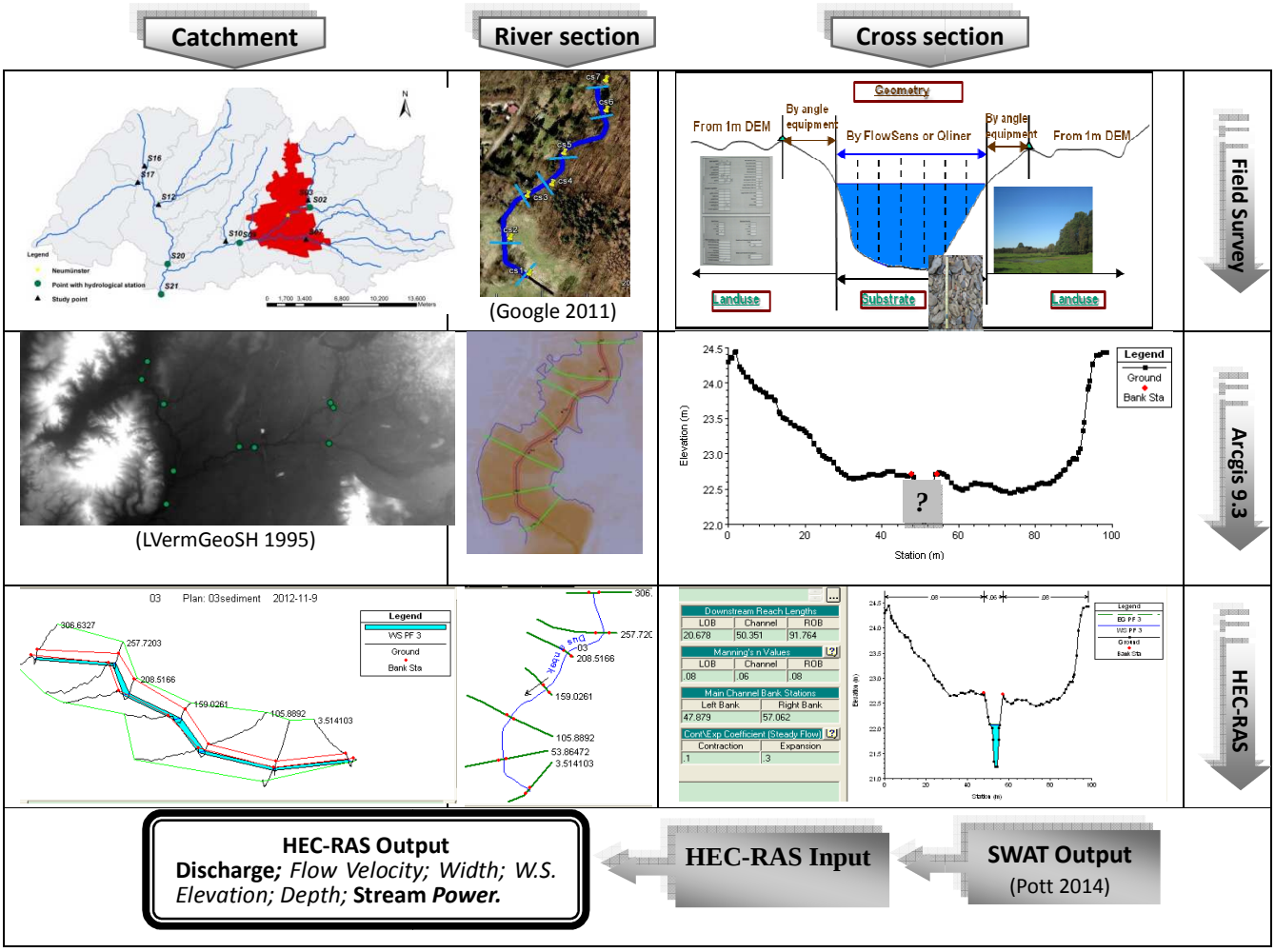

Fig. 4.3 Flow chart of HEC-RAS model setup

4.3 Model calibration and validation

Model calibration and validation are necessary and critical steps in the model application for parameter evaluation and refinement. In our calibration and validation procedure, in addition to the surveyed data from the three field campaigns, measured hourly water surface elevation data and the calculated discharge data from 1991 to 2010 were collected from Schleswig-Holstein's government-owned company for Coastal Protection, National Parks and Ocean Protection (LKN-SH 2012). The data were available at four hydrological stations: Brachenfeld (S02), Padenstedt (S09), Sarlhusen (S20) and Willenscharen (S21). Consequently, the steady flow calibration procedure involved all ten models, but the unsteady flow validation is only available for the four river sections mentioned before.

4.3.1. Seasonal roughness coefficient

The roughness of the river beds, banks and floodplains have been evaluated in the field and calibrated in the steady flow simulation. However the roughness conditions in the unsteady flow simulation cannot be rigorously represented based on continuous daily or hourly data due to vegetation and fluvial seasonal variations. The errors between simulated water level and real measured water level were calculated to reveal the effect of seasonal vegetation based on the daily data from 2010. As shown in Fig. 4.4, the model errors were much lower after the seasonal adjustment of the roughness factors.

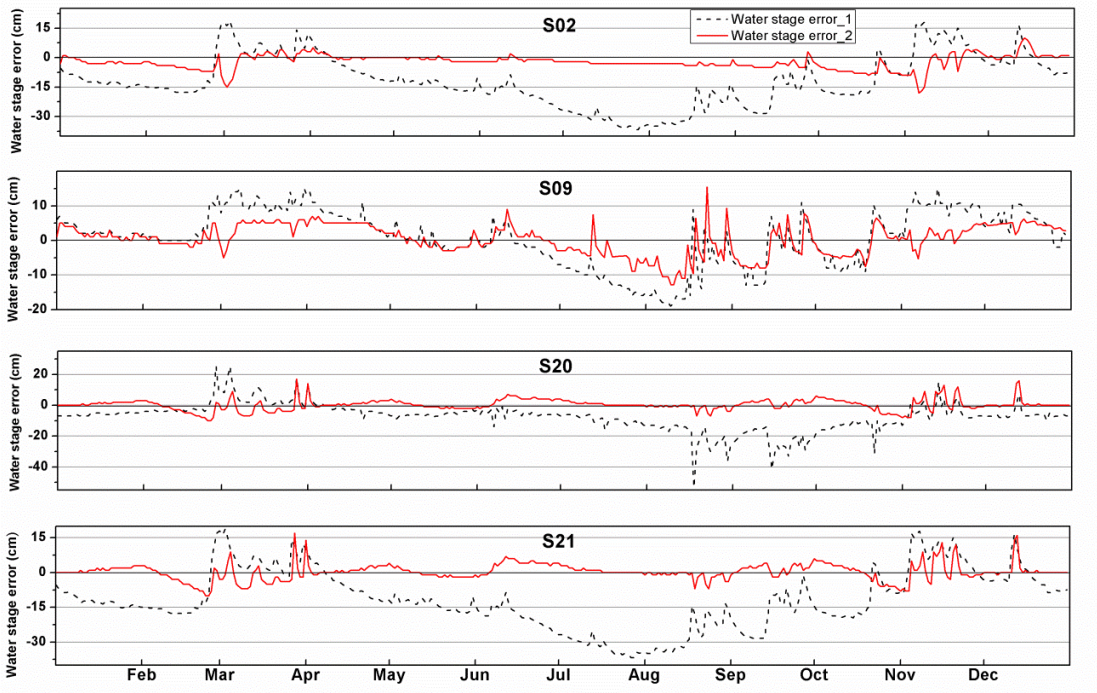

Fig. 4.4 Model errors under different roughness conditions

Note: Water stage error_1 – error under general mean roughness condition; Water stage error_2 – error under seasonal roughness conditions.

The seasonal roughness factors were increased when the modeled water surface elevation was lower than the real data, and were decreased while the real measured data was lower. Several rounds of calibration were completed, in order to get the most satisfying factor for minimization of the disparity (Fig. 4.5 and Tab. 4.2). The trends of the four seasonal roughness factor sets are similar. The roughness in March, April, November and December is lower than the general roughness by approximately 40%. While in July, August, September and October the roughness is higher than the general roughness height.

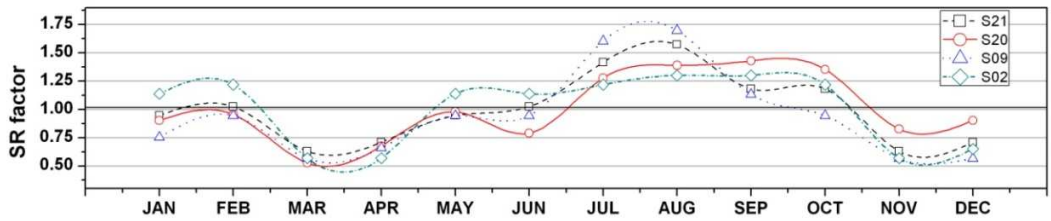

Fig. 4.5 Seasonal roughness factors of calibration points

Tab. 4.2 Seasonal roughness factors of the models

	JAN	FEB	MAR	APR	MAY	JUN	JUL	AUG	SEP	OCT	NOV	DEC
S02	1.14	1.22	0.57	0.57	1.14	1.14	1.22	1.30	1.30	1.22	0.57	0.65
S09	0.75	0.94	0.57	0.66	0.94	0.94	1.60	1.70	1.13	0.94	0.57	0.57
S20	0.90	0.95	0.53	0.68	0.98	0.79	1.28	1.39	1.43	1.35	0.83	0.90
S21	0.94	1.02	0.63	0.71	0.94	1.02	1.42	1.57	1.18	1.18	0.63	0.71
Mean	**0.94**	**1.04**	**0.57**	**0.65**	**1.00**	**0.97**	**1.38**	**1.49**	**1.26**	**1.17**	**0.65**	**0.71**

4.3.2. Model calibration

Main attention was paid to gradient and roughness calibration, due to the difficulty of determining a representative Manning's n value and the lack of river bed elevation data in the DEM model. The steady flow simulations were run for every cross section, based on the three seasonal measured data series. Strong positive correlations between HEC-RAS output and velocity, top width, maximum depth and hydraulic depth surveyed in the field were found. All the correlation coefficients were higher than 0.9. Mean absolute relative error of velocity, top width, maximum depth and hydraulic depth of each cross section were averaged in the steady models under different water levels to evaluate the accuracy and precision of the model. The mean absolute measured errors in dry season were higher and deviated roughly 9%-16% from the real measured value. Relative errors in flood season varied from 3.3% to 8.9%, which indicated a better model performance in flood conditions than in low water level. The best calibration results lay in moderate level season, where relative errors were less than 5%.

Theoretically, unsteady flow calibration should also involve the gradient and roughness height as in the steady flow calibration. However, this gradient information was not available and cannot be estimated or simulated. Consequently, no more reliable and credible adjustment of this factor can be realized and roughness temporal variation is the only key adjustment in this part. Only 2010 daily data were used in unsteady roughness calibration in order to exclude the impact of the gradient variation.

4.3.3. Model validation

Next modeling efforts were made for validation of the measured water surface elevation. Long-term (1991-2010) daily simulations were carried out and the results are shown in Fig. 4.6. The modeled water surface elevation reflected the real measured data in general (Fig. 4.6). The coefficients of determination

(R^2) for the four models were 0.91, 0.92, 0.95 and 0.99 respectively, which reflected a very high correlation between the modeled and measured data sets. The Nash-Sutcliffe efficiency varied from 0.74 to 0.82. The mean absolute errors were around 7 cm in S02 and S09, and as high as 15 cm in the other two models. The main inconsistency occurred during dry season, where the measured data was higher than the modeled data (Fig. 4.6). During flood season in particular the peak flow simulations are not consistent with the observed data. The simulated elevation was lower than the measured elevation in S02 and S20, while the opposite situation was revealed in S09 and S21.

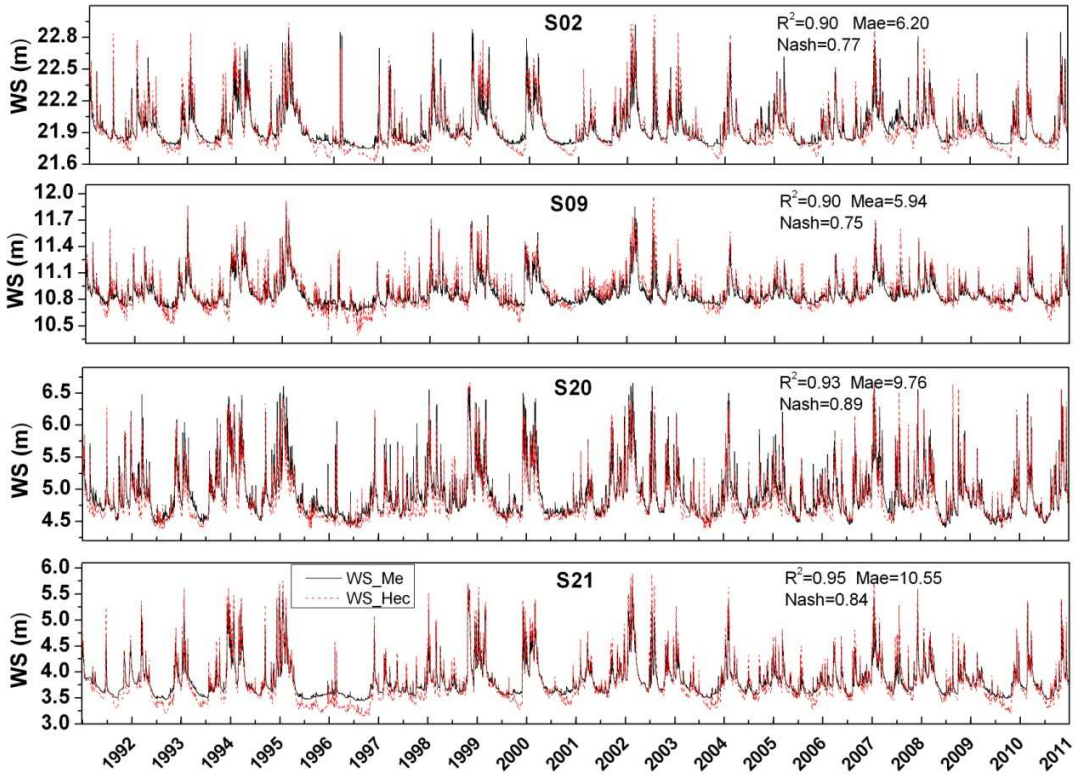

Fig. 4.6 Daily measured and HEC-RAS output water surface elevation from 1991 to 2010.
Note: Mae means absolute error of the water surface elevation; Nash, Nash-Sutcliffe efficiency.

The quality of the validated model outputs under different water levels were shown in the Tab. 4.3. The Nash- Sutcliffe efficiency was highest during bankfull condition, but lowest during moderate conditions. During flood condition the Nash-Sutcliffe efficiency was as high as 0.81. These efficiencies reflected the well performance of the model at all flow conditions.

Tab. 4.3 Nash-Sutcliffe efficiencies under different flow conditions

Flow conditions	Moderate	Bankfull	Flood
Nash-Sutcliffe efficiencies	0.76	0.87	0.81

4.4 Model results

4.4.1. Temporal distribution of discharge and unit stream power

4.4.1.1 Flow power under moderate, bankfull and peak discharge conditions

The importance of the bankfull hydraulics has been recognized in prior research (Vocal Ferencevic and Ashmore 2012). The 10-year-averaged mean value of the river discharge and power reflect the moderate conditions of selected river conditions, while the discharge and the unit stream power under 10-year-peak flow represent the hydraulic environment under high level flood conditions. In this part of our research, the discharge and unit stream power were standardized against bankfull values to examine the variation of river under representative conditions. The highest daily discharge of each during 2000 - 2010 was picked up as 10-year-peak discharge, and the results are shown in Fig. 4.7. The variations of stream discharge and unit power have similar trends. Stream discharge and unit power under 10-year-averaged conditions were around 1/3 of that under bankfull discharge conditions, and the 10-year-peak discharge and unit power were nearly 1.6 times higher than that of the corresponding bankfull variables.

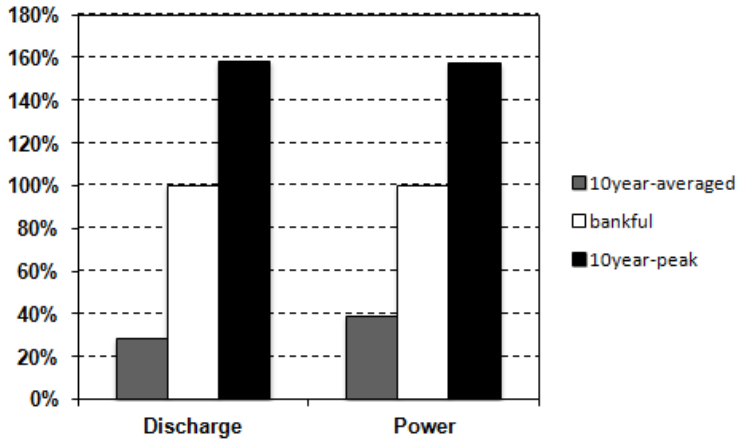

Fig. 4.7 Standardized hydraulic variables under representative flow conditions

4.4.1.2 Increase rate of the in-channel and floodplain unit stream power

As shown in Fig. 4.8 (a) and (b), the in-channel unit stream power is proportional to the increase of the flow discharge. All the power/discharge plots from 10 reaches can be described by exponential or logarithmic fitting curves with R^2 higher than 0.85.

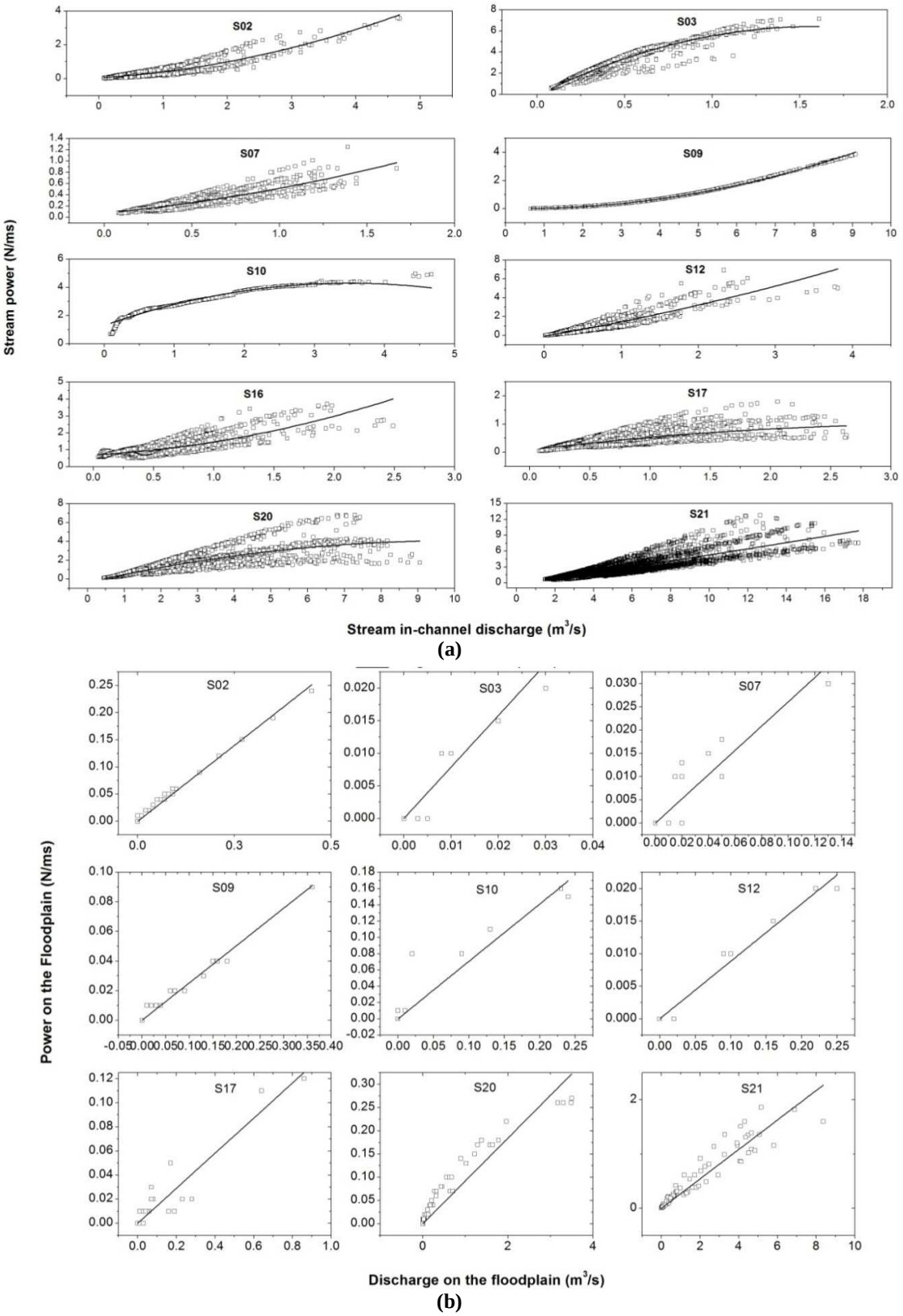

Fig. 4.8 Flow power plotted against flow discharge, (a) in-channel; (b) on the floodplain.
Note: The solid line is the trend line of the stream power with the increase of the discharge

The averaged unit power increasing rate of in-channel flow is 1.29 N/ms per unit discharge, as shown in Tab 4.4. There were no flood events on reach S16 during the simulation period. The unit flow power on the floodplain from the other 9 reaches seems to linear correlated to the flood discharge. Linear fitting analysis provided an increasing rate of the power on the floodplain (Tab 4.4). The mean values show that the in-channel power grows 3 times more than the flood flow power with the same increase of discharge.

Tab. 4.4 Mean power increase rate of the in-channel flow and flood flow

	S02	**S03**	**S07**	**S09**	**S10**	**S12**	**S16**	**S17**	**S20**	**S21**	**Mean**
In-channel flow	0.76	4.4	0.55	0.42	2.3	1	1.83	0.53	0.44	0.7	1.29
Flood flow	0.55	0.66	0.24	0.25	0.75	0.09	—	0.14	0.09	0.27	0.34

4.4.2. The lateral distribution of unit stream power

The section-averaged in-channel unit stream power is 4.34 N/ms with a discharge of 7.95 m^3/s, while the overbank flow generated 0.18 N/ms with a discharge of 2.6 m^3/s. The stacked column in Fig. 4.9 shows the distribution of the hydraulic discharge and energy on the floodplain and in the channel. Fig. 4.9 (a) clearly shows that the flood energy accounts for 1% - 10% of the total stream energy. The flood energy percentage is the highest at the outlet at river section S21.

According to Fig. 4.9 (b), despite the very low energy the flood produced, around 40% of the total cross-sectional discharge distributed on the floodplain. On average, 95% of the power is concentrated in the main channel, and 5% of the power distributed on broadly on the floodplain.

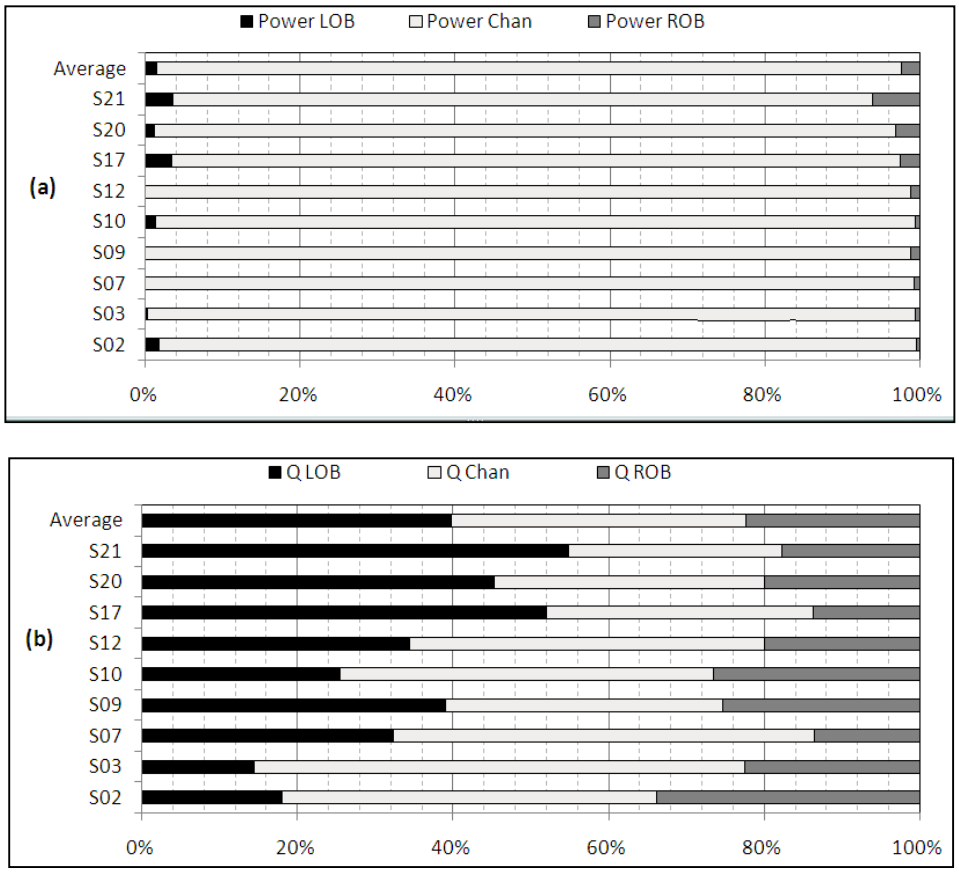

Fig. 4.9 Lateral stream power (a) and discharge (b) distribution of 10year peak flood
Note: LOB is the left bank of the channel; ROB is the right bank of the channel.

4.5 Discussion

4.5.1. Model calibration and validation

The smallest deviation between measured data and modeled data was revealed in the steady flow calibration part, during the medium water level season. One possible reason for this phenomenon is that the systematic field work was carried out in the moderate water level season. Although the hydraulic measurements were repeated in 2012, errors were inevitable, due to the vegetation alteration and inaccuracies in identifying precisely the same cross section in the field.

After the calibration and validation, the simulated results generally fit the measured data. The simulation errors varied from -50 cm to 30 cm, but 90% of the errors were distributed within ±15 cm. Simulated output lower than measured data was identified under low water level conditions. The errors during flood seasons were lower than that during dry seasons. Similar results were found from a model set up for the NyI river in Africa, where the disparity between modeled and measured data appeared mostly in dry season (Birkhead, James, and Kleynhans 2007). Another case study in India revealed the highest

estimation quality during flood modeling, as the computed errors were only around 5.42% (Parhi 2013). The measured water surface elevation was about 30-50 cm higher and 20-50 cm lower than the modeled data during the dry season and flood season respectively. The model worked best for estimation during high water level season.

4.5.2. Annual variation of roughness

The variability in roughness values attribute to differences in aquatic plant growth and the water depth (O'Hare et al. 2010; Shih and Rahi 1982). The study in marsh area suggested that the manning roughness increased was proportional to the vegetation density and inversely proportional to the water depth (Shih and Rahi 1982). Research in England and Scotland pointed out that the manning roughness values varied ±30% from the annually mean values in summer and winter (O'Hare et al. 2010). A study from River Test, Hampshire (USACE) utilize the continuous stage records of 25 years yielded maximum roughness in August and September and then declined to its minimum value in winter months (Gurnell and Midgley 1994). In our study, the maximum roughness values occurred during the autumn season when the biomass was at its highest amount and the water surface kept at low level. The roughness coefficient declined to minimum in flood season in March and April, because of the combination of low biomass and high water level. Weather statistic from Schleswig-Holstein showed that the averaged minimum temperature in January and February was -2 °C and -1.7 °C respectively (Climatemps 2013). It is reasonable that the roughness increased because of the increase of the viscosity of the water body when it started to freeze.

4.5.3. Bankfull discharge hydraulics

Stream power and shear stress are the key variables for the formation and evolution of fluvial systems. Stream hydraulics under bankfull discharge are considered to be even more significant, because it makes the homogeneous comparisons between different river sections available (Marchi et al. 2010a). In the Upper Stör catchment, the unit stream power under bankfull discharge of each river section varied from 0.4 N/ms to 5.85 N/ms. A series of researches studies carried out in gravel-bed rivers in Belgian Ardenne catchment, which has a similar catchment size with the Upper Stör catchment produced much higher bankfull unit stream power, from 17 N/ms to 126 N/ms (Petit et al. 2005). The quite marked slope in the Ardenne catchment varying from 5% for head water streams to around 0.2% for large downstream rivers assumes to be the proper explanation for the much higher unit stream power. Through bankfull condition comparison, it is clear that the rivers in the Upper Stör catchment yield very low power because of the flat and broad lowland characteristic.

The prior studies about hydraulic characteristics of in-channel flow mainly focus on downstream variation in spatial scale. Earlier studies predicted that the position of the maximum stream power turns out at intermediate positions, and the exact position depends on the ratio of discharge change and slope change

in the downstream part of the catchment (Knighton 1999). Very little literature has been found about the variation of the unit stream power with the channel discharge variation.

4.5.4. The in-channel flow and the cross section geometry

The different increasing pattern of the in-channel flow in different sub-catchments was mainly caused by cross section conditions. As we can see from Fig. 4.8 (a), the plots of S09 and S10 showed more distinct relationship than that from the other sites due to the regular geometry of the artificial constructed cross sections. The cross section from S09 was trapezium shaped with big stone, while the cross section from S10 was in rectangle shape and constructed with concrete. No seasonal vegetation interference the flow condition at both cross sections.

The plots from S03, S10, S17 and S20 obviously showed the logarithmic trend, while the rest can be descript in exponential fitting lines as shown in Fig 4.8 (a). This was mainly caused by the shape of the cross sections in different sites. The cross sections from S03, S10, S17 and S20 were in rectangle shape, while the cross sections from the other sires were in trapezium shape.

4.5.5. The different flow patterns among the sub-catchments

The roughness coefficient and slope both in-channel and on the floodplain of our studied sub-catchments covered a wide range (Tab. 4.1). The variation of the in-channel roughness coefficient mainly depended on the sediment size and the density of plantation, while the floodplain roughness was governed by the land use pattern. The local channel and floodplain slope ware calculated in the 1 m DEM. The combination of the local roughness heights and slope determined the hydrological conditions.

The correlation analysis was carried out between the flow power and the characteristics to find out the influencing factors of the stream power patterns among different sub-catchments. The results were shown in Tab. 4.5 and Fig. 4.10. The increase rate of the in-channel flow power was highly inversely correlated with the channel roughness, with a correlation coefficient valued at 0.84. At the same time the highly positive correlation between the increase rate of flood flow and floodplain roughness was detected. On the other hand, the slope differences of the river sections and floodplains weakly correlated with the increase rate of the flow power (Tab. 4.5). This suggested that variation of the flow increasing rate were mainly caused by the different channel and floodplain roughness.

Tab. 4.5 The correlation results of the flow power with the slope and roughness

Correlation coefficient	Increase rate		Flood flow power (%)
	In-channel	Floodplain	
Slope	-0.09	0.57	***-0.77***
Roughness	***-0.84***	***0.8***	-0.51

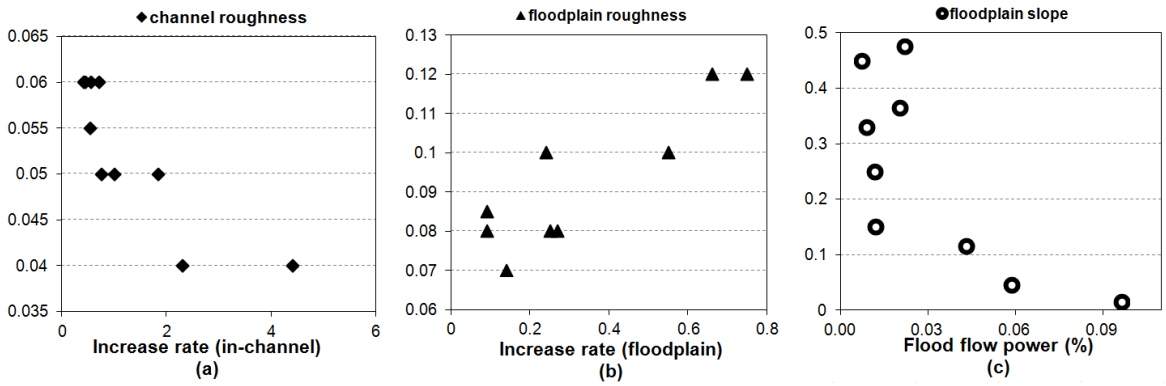

Fig. 4.10 Plots of the flow power against slope and roughness in , (a) increase rate of in-channel stream power and the channel roughness; (b) increase rate of the flood flow power and the floodplain roughness; (c) the percentage of flood flow power plot against floodplain slope.

According to Tab. 4.1, both the roughness height and the slope varied in a wider range on the floodplain than in the channel. Negative correlation between the flood power percentage and the floodplain slope were found, and the correlation coefficient was as high as 0.77 (Tab. 4.5). This demonstrated that the diversity of the slope among all the sub-catchments mainly affected the percentage of the flow power located on the floodplain. Relatively less stream power were located on the steeper floodplain.

4.6 Conclusion and outlook

In this paper HEC-RAS models for ten selected river sections in the Upper Stör catchment were set up and calibrated with a seasonal roughness coefficient. Combined with the SWAT model output database, we evaluated the flow power both in-channel and on the floodplain. The findings are a significant reference for the sediment transportation, nutrient migration and habitat shift in lowland river system. The results clearly show that,

(1) stream discharge and unit stream power varied by a larger extent under bankfull condition, 10-year-averaged mean flow condition and 10-year-peak flow condition compared with the other hydraulic parameters. The 10-year-averaged discharge and unit power were around 1/3 of bankfull discharge and unit power, and the 10-year-peak discharge and unit power were nearly 1.6 times of the corresponding bankfull parameters.

(2) unit stream power was proportional to the increase of the stream discharge, while the in-channel power grew 3 times faster than the floodplain power. The dominating factor of the different increasing rate was the local roughness factor.

(3) during 10year-peak flood, the floodplain flow can generate 40-75% of the total discharge but only 1-10% of the stream power was produced. A relatively higher percentage of stream power was located on the floodplain with lower slope.

HEC-RAS has proven to be an efficient and accurate hydraulic model, which makes a thorough examination of the channel and floodplain possible. The seasonal roughness factor adopted in our catchment minimized the model error compared with the measured data. The continuous and long-term data source advantage of the eco-hydrological SWAT model and the hydraulic modeling advantage of HEC-RAS model were integrated in our research. The findings of this study on floodplain and main channel might be a good basis for further ecologic, sedimentologic or river dynamics research. The comparison of the in-channel and floodplain hydraulic behavior of this study would provide proof for erosion and deposition processes, as well as the associated nutrient and containment transportation of the river system.

Chapter 5. Simulation, Quantification and Comparison of Channelized and Floodplain Sediment Processes in a German Lowland Area

S. Song, B. Schmalz, N. Fohrer
Earth Surface Processes and Landforms
Submitted, 06 March 2014

Abstract: Erosion and sedimentation processes within the channel and on the floodplain indicate the catchment hydrodynamic procedure, the associated nutrient and contaminant transportation. In this paper, we implemented the sediment series from the eco-hydrological SWAT model into the hydraulic HEC-RAS model to setup the sediment model for 10 river sections in the Upper Stör catchment and simulated the sediment processes from 2001 to 2010. Based on the HEC-RAS output the quantification and comparison of channelized and floodplain sediment process was conducted. The results indicate that, (1) with an average sedimentation depth of 2.85 cm, the deposition process dominated the Upper Stör catchment in the decadal time scale, and the land use/cover condition result in the different sedimentation amount in different sub-catchments. (2) The mean deposition rate was 1.75 g/m^2/d in the channel and 1.69 g/m^2/d on the floodplain respectively, and the floodplain deposition accounted for only 1 % of the total sedimentation amount. This was mainly because of the stream power distribution in channel and on the floodplain. (3) The granularity of the channelized sedimentation was dominated by the altitude of the river section, while the granularity of the floodplain sedimentation positively correlated with the stream power of the flood. The D50 of the channelized and floodplain sediment was 0.92 mm and 0.16 mm respectively, while the D90 of the sediment was 4.2 mm in the channel and 0.32 mm on the floodplain. The results yielded by the combination of HEC-RAS and SWAT model are comparable to the traditional radioactive dating or sediment trapping method in the similar and nearby catchments.
Keywords: HEC-RAS model, channelized sediment process, floodplain sediment process, lowland area.

5.1 Introduction

Growing awareness of the environmental significance of channel and flood conveyance have been witnessed in recent years (Nicholas et al., 2006). Erosion and suspended sediment transport occur primarily during flood periods, and the sediment deposits in the channel bed and floodplains normally in dry seasons and moderate water level conditions (Wilson et al., 2004). These perplexing erosion, transportation and deposition processes in the fluvial system are dominated by the catchment topography

and hydrological characteristics. The storage, constitution and distribution of the sediments, which are determined by the soil texture and land cover/land use of the catchment, frequently represent the dissemination of the associated nutrients and contamination (Hoffmann et al., 2009).

Channel-bed sedimentation warrants investigation for the environmental, eco-hydrological and engineering reasons (Fromin et al., 2010; López-Tarazón et al., 2011; Wellman et al., 2000). Studies related land use impacts on sediment yields in coastal British Columbia revealed that geologically young landscapes caused loss of in-stream wood and erosion acceleration (Lisle, 1989; Rosenfeld et al., 2010).Temporal and spatial variation in sedimentation in California streams suggests that individual storms of moderate size pose a threat to eggs in many but not all areas selected by fish for spawning (Lisle, 1989). A climate-related study reported the increase of fine sediment (material<6mm), which can fill pool sand decrease bed stability (Lisle et al., 2000; Wohl and Cenderelli, 2000). A recent observation from central Idaho suggests that the basin-scale sediment yields within the next few years to decades could be greater than the long-term average rate of 146 T km^{-2} $year^{-1}$, which will likely affects downstream reservoirs designed under historically sediment yielding rate (Goode et al., 2012).

Floodplains are normally intensively cultivated due to the hypertrophy and homogenous topography but sensitive to hydrological extremes and fluctuations, especially the lowland river-floodplain. The combination of the sensitivity and land use value leads to the scientific significance of the sedimentation process in this area (Baldwin and Mitchell, 2000; Lewin, 2013). Floodplain hydrology has been known as the major factor that determines the functions and structures of the floodplain ecosystems (Ward and Stanford, 1995). The hydrological connectivity of floodplains to streams or rivers dominates the exchange process of chemicals and organisms between them (Mitsch and Gosselink, 2007; Tockner et al., 2000). During flooding the flow slows down when the water flows onto the floodplain due to the shallow water depth and increased surface roughness caused by the floodplain vegetation. The transport capacity of the flood flow then decreases because of the lower velocity and consequently different sized suspended sediments deposit in the floodplain at the various settling velocities (Walling and He, 1998). Fine grain is usually transported and deposited distantly on the floodplain, and coarse sand is normally deposited close to the channel during traction as bed load (Middelkoop and Asselman, 1998). Overbank sedimentation is driven by the mechanism such as traction, convection and diffusion (James, 1985; Pizzuto, 1987). The different transportation mechanism is one of the factors that determine the overbank sedimentation pattern. The diffusion mechanism dominants the sediment transportation in the steady flood flow and on the flat floodplain, while the sediments are transported primarily by convection and diffusion on the floodplains with non-uniformed topography (James, 1985; Marriott, 1992; Pizzuto, 1987). Based on the transportation mechanism, empirical overbank sediment transportation and deposition formulas were developed in the last century and provided roughly estimation for the sedimentation process. However, these formulas failed to describe more complex sedimentation pattern caused by the variation of local topography and

hydraulic conditions at different stages of inundation (Lewin and Hughes, 1980). The ecological effects of the floodplain sedimentation have gained considerable investigation, especially the ecological effects caused by contaminant migration and transformation during the sedimentation process (Walling and Owens, 2003). Recent ecological research in Austria pointed out that the release of phosphorus from the sediments affect the dominating primary producers, biodiversity, the degree of floodplain aggradations and thus the potential life span of aquatic habitats (Kiesel et al., 2009a; Reckendorfer et al., 2013).

Previous researches have also focused on the quantity, process and spatial variability of the sediment on the floodplain under long-term scale (Macklin et al., 2003; Walling and He, 1998). A wide applied method for long-term historical period deposition rates estimation both channelized and floodplain sediment is dating specific levels or horizons with fallout radionuclide such as ^{137}Cs (Caesium-137) or ^{210}Pb (lead-210) (Goodbred Jr and Kuehl, 1998; Xiang et al., 2002; Yeager and Santschi, 2003). Event scale sediment accumulation can be estimated by the measurement of conveyance loss (Estrany et al., 2012; Middelkoop and Asselman, 1998). Reconnaissance surveys carried out following single sufficiently large flood events can also indicate the local variability in sediment accumulation to a large extent (Darwish, 2010; Johnson et al., 2010; Zorn and Wills, 2012). Sediment traps were adopted to capture the patterns of sediment accumulation when the flood and deposition were low (Lambert and Walling, 1987; Schulz et al., 2003; Storlazzi et al., 2011). An earlier study has already demonstrated that the sediment traps made of artificial grass perform well in documenting the spatial pattern of sediment deposition during flood events (Asselman and Middelkoop, 1995). In decadal time scale, the regular observed bed elevation data or sediment load series provided reliable support to the sediment process research. A group of systematically developed models were widely adopted as the supplement in the area lack of real measured data (Chang, 2008; Simões and Yang, 2008; Zeng and Beck, 2003). The main difference of these models lies in the model structure, the solving equations and the phenomenon progress (Markowska et al., 2012).

The significance of in-channel and overbank sediment processes in a wide range of environmental settings, and the close inter-connection between sediment and the total suspended sediment in-channel have been realized in the last decades. Literature review found that more attention was paid on the overbank sedimentation process (Goodbred Jr and Kuehl, 1998; Hoffmann et al., 2009; Zorn and Wills, 2012) and the long-term in-channel erosion or deposition process especially at the delta or estuary (Dickhudt et al., 2009; Yang et al., 2011). Relatively less literature focused on the in-channel sediment process, and comparatively little research has been conducted to quantify the difference of the overbank and the channelized sediment process.

The aims of this study were setting up and calibrating the sediment transportation model for the ten sub-basins in Upper Stör catchment with the HEC-RAS model based on SWAT model results transfer, to examine the comprehensive sediment transportation and accumulation process in the selected river channel over the decadal time scale, including the sedimentation quantity, granularity constitution and its

relationship with sediment loads, and finally to conclude the difference between the channelized deposition and overbank deposition both qualitatively and quantitatively among different sub-catchment.

5.2 Methods and material

5.2.1. Study area

The Upper Stör catchment is located in the center of Schleswig-Holstein/Northern Germany with a drainage area of 468 km^2, which is part of the extensive glacially formed lowland area of Northern Europe (Fig. 5.1). The width of the main river varies from 0.5 m at the origin in Willingrade to 18 m at the outlet in Willenscharen. The discharge gauged at the outlet ranges from 1.26 m^3/s to 44 m^3/s (LKN-SH, 2012). Four gauge stations Brachenfeld (S02), Padenstedt (S09), Sarlhusen (S20) and Willenscharen (S21) are located respectively in the area. The small sand-dominated and small gravel-dominated lowland river is widely distributed in the catchment. The channel bed and banks are locally covered by fine sand and sandy silt, along which the boulder size clasts are discontinuously exposed. As is shown in Fig. 1, the gley-podsol and podsol-gley soils appear mainly in the western part of the catchment. Soils in the eastern part primarily involve sediments formed after the Weichsel ice age, while the central part is mainly build of brown soils (BGR, 1999). The land in the Upper Stör catchment is mainly used by agriculture purpose (48.1%). Pasture, grassland and forest account for 41% of the catchment area (DLR, 1995; EEA, 2000).The elevation of this area falls from 90m and 60m in the western and eastern parts, respectively, to 2 m a.s.l. at the outlet. In most of the catchment the gradients are usually smaller than 1°, except the southwestern part, which has gradients of more than 3° (LVermA, 1995).

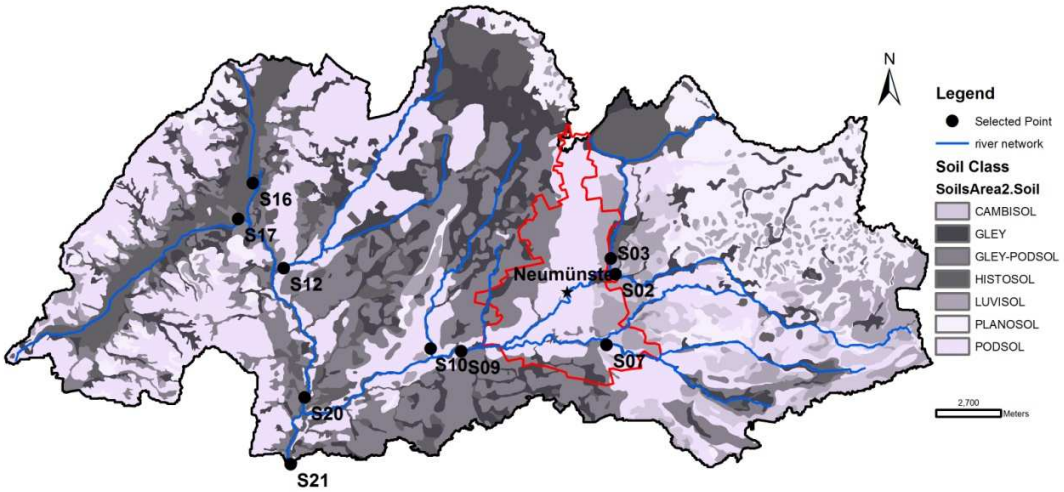

Fig. 5.1 The location and soil classes of Upper Stör catchment and study river sections (BGR, 1999)

5.2.2. Models and data source

5.2.2.1 **Model cascade**

The Soil and Water Assessment Tool (SWAT) model is a continuous, long-term, semi-distributed parameter model that can simulate surface and subsurface flow, soil erosion and sediment deposition, and nutrient movement through watersheds (Arnold et al., 1998). As a comprehensive process-based model, SWAT was adopted in the sediment load estimation. Previous studies showed that SWAT can be successfully used for modeling eco-hydrological processes in lowland areas (Schmalz et al., 2008). SWAT is capable of modeling the ungauged catchment or the prediction of the impacts of scenarios, which provides a reliable procedure to fill in the missing data (Jain, 2010). Application analysis has found out that the SWAT model yields reasonable results and provides accurate model parameterizations and well sediment model performance (Talebizadeh et al., 2009). Comparisons with the other models, SWAT indicates higher model efficiency and acceptable uncertainty (Parajuli et al., 2009; Talebizadeh et al., 2009).

The hydrologic Engineering Centers River Analysis System (HEC- RAS) is an integrated model for interactive use in a multi-tasking environmental management, mainly focusing on the steady/unsteady river flow, sediment transportation and water quality dynamics analysis, which was developed by US Army Corps of Engineers and first released in 1995 (USACE, 2010). According to recent research, the simplified approach used in the HEC-RAS model could perfectly work in a real-time operational model used for estimating watercourse channel geometry changes (Fleming et al., 2010; Markowska et al., 2012). The combination of SWAT model and HEC-RAS model in flow and sediment simulation was applied in several catchments and the methodology has been well described in earlier research (Kiesel et al., 2013; Schmalz et al., 2012; Song et al., 2014). In this study, the flow and sediment output from the SWAT models works as the data base of the HEC-RAS model. The new integrated model approach merged the data generation capability of the SWAT model and the geometry variation simulating capability of the HEC-RAS model, enabled the simulation of the decadal time scale sedimentation process in the open channel catchment. The sediment model of the Upper Stör catchment was setup in HEC-RAS based on the SWAT output and the field campaigns from 2011 September to 2012 June. Fig. 5.2 shows the technical procedures of the models combination and simulation.

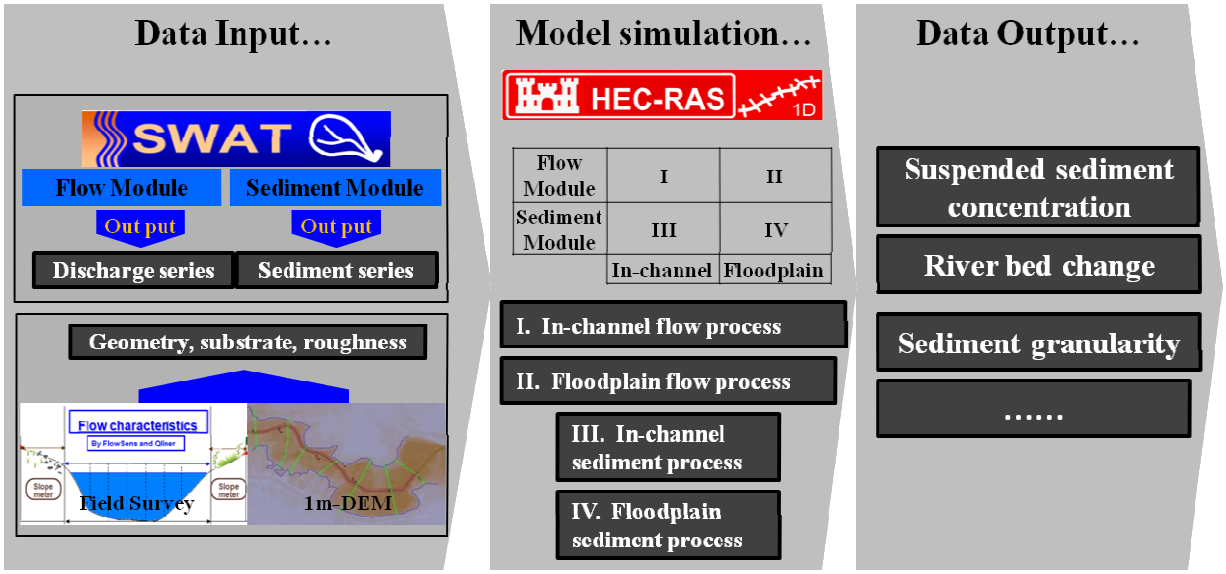

Fig. 5.2 Flow chart of the sediment model set up and simulation processes

5.2.2.2 **Data collection**

5.2.2.2.1 Field survey and data source

Ten river sections along the main Stör channel and its tributaries with each a length of 300 m were selected (Fig. 5.1). Seven cross sections evenly distributed along each of these 300 m river reaches were surveyed for the cross-sectional geometry data during a moderate water level period (September 2011). The geometries between bank stations were mapped manually and the topographic data of floodplains were automatically extracted from the Digital Elevation Model (DEM) with 1 m resolution (LVermGeoSH, 1995) using HEC–geoRAS, an ArcView extension capability developed by the USACE–HEC (USACE, 2010).

5.2.2.2.2 Gauge data

Hydrological data like water surface width, depth, flow velocity and discharge for each cross section were measured originally under moderate water level period (September 2011). Measurements were then repeated at the same cross sections during flood season (January 2012) and dry season (April 2012) for calibration purpose of the model. The hydrological data were measured mostly with Acoustic Doppler device called Qliner (ADQ, OTT Company, Kempten/Germany), and the FlowSens (SEBAHydrometrie, Kempten/Germany) was adopted when the water depth was not adequate (<25 cm). Both Qliner and FlowSens have been proven to be high accurate and efficient equipment (Song et al., 2012). Gauged data from 10 years (2001.01.01-2011.01.01) were gathered from the four hydrological stations for further calibration and validation (LKN-SH, 2012). Additionally, the bank vegetation and the grain size constitution of the channel sediment were noted during the field campaigns and then transformed into roughness values.

A suspended sediment gauge was set up using an automatic water sampler MAXX SP III© from 1th January 2010 until 1th January 2011 at the gauge Willenscharen. Twelve bottles, each with a capacity of 2.9 liters, were settled in the automatic water sampler, inside which the temperature was kept constant between 3 and 5°C. The sampler pumped 20 ml water into the bottle every 72 min, and 20 sub-samples were pumped into the same bottle to accomplish the 2 liter daily sample. The water sample for the following day was arranged in the neighborhood bottle, and so on. The samples were brought back every 10 or 11 days and analyzed in the laboratory of the Department of Hydrology and Water Resources Management at Christian-Albrechts-University Kiel. One liter of each sample was filtrated through the 0.45 µm filter paper to collect the suspended solids. The residuals were then dried at 105 °C and weighted to determine the total suspended sediment (TSS) concentration of the sample (Pott, 2014).

5.2.2.2.3 SWAT-model-based data

Sediment model input involves the flow and the corresponding sediment data. Flow series and the rating curve are necessarily needed. While in the sediment part, the suspended sediment load series, the particle size specification of the load and the particle accumulated frequency of the bed sediment are indispensable. The flow and sediment load series were generated by the SWAT model (Arnold et al., 1998), which has been setup and well calibrated until 2010 (Pott, 2014). The particle size specification and the accumulated frequency of the substrate for every cross section were sampled during the three field campaigns. A further modification to the substrate gradation was made based on the data from the official survey (SH, 2013).

The high quality of the modeled data makes the SWAT model a reliable data base for HEC-RAS. The measured and SWAT simulated flow series correlated with each other with the coefficient of determination (R^2) of 0.86 during calibration period and 0.84 during validation period. The Nash-Sutcliffe coefficients (NSE) were 0.85 and 0.83 respectively (Tab. 5.1). Analysis of the calibrated SWAT output and real measured sediment concentration yielded the R^2 of 0.56 and a NSE of 0.55. The averaged R^2 and NSE produced by validated data were 0.61 and 0.59 respectively (Tab. 5.1). Although a relatively wider discrepancy was outlined in the sediment results than in flow modeling, the sediment output can still represent the main trends of the sediment and provided an adequate data base for the HEC-RAS model.

Tab. 5.1 Calibration and validation of the total suspended sediment (Pott, 2014)

	Calibration				**Validation**			
	R^2	**NSE**	**PBIAS**	**RSR**	**R^2**	**NSE**	**PBIAS**	**RSR**
Flow	0.86	0.85	1.20	0.38	0.84	0.83	6.10	0.42
Sediment	0.56	0.55	23.3	0.67	0.61	0.59	4.20	0.64

5.2.3. Hydraulic models

5.2.3.1 **Model calibration**

The daily measured data of point S21 in 2010 from the automatic suspended sediment gauge station (Pott, 2014) was taken to calibrate the sediment model and the results are shown in Fig. 5.3. The Coefficient of Determination (R^2) and the NSE between the two suspended sediment concentration series were 0.78 and 0.77 respectively. The simulated data highly agree with the really measured data except at some peak points.

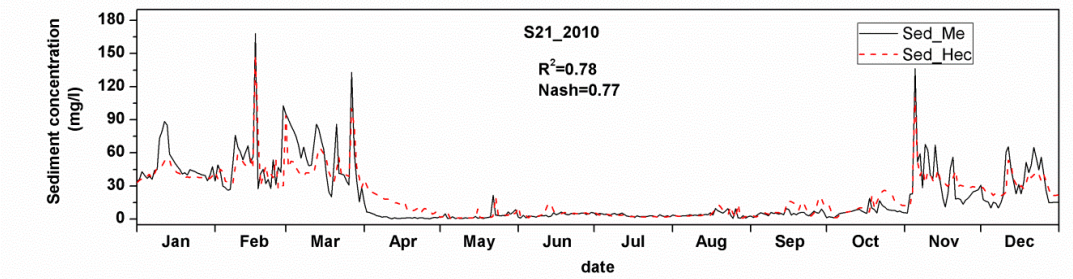

Fig. 5.3 The calibrated results of HEC-RAS model (daily simulated sediment concentration in S21 in 2010)

Note: Nash refers to the Nash-Sutcliffe efficiency. Sed_Me is the measured suspended sediment series and Sed_Hec is the modeled suspended sediment data from HEC-RAS model.

5.2.3.2 **Model validation**

Daily data was collected every month since 2001 until 2010 in point S09 and S21 (LKN-SH, 2012). High consistency between real measured and modeled sediment concentration series was apparently identified in the validated model in both points. The two data series correlated with each other with R^2 of 0.73 in S09 and 0.65 in S21. The NSEs were 0.70 and 0.52 respectively (Fig. 5.4 (a) and (b)). The modeled data in 2010 for all the points obviously showed highly agreement with the measured data, with a R^2 of 0.80 and a NSE of 0.81. The high validated model accuracy suggests that the SWAT model is a reliable data source and the HEC-RAS is the efficient model for the sediment transportation.

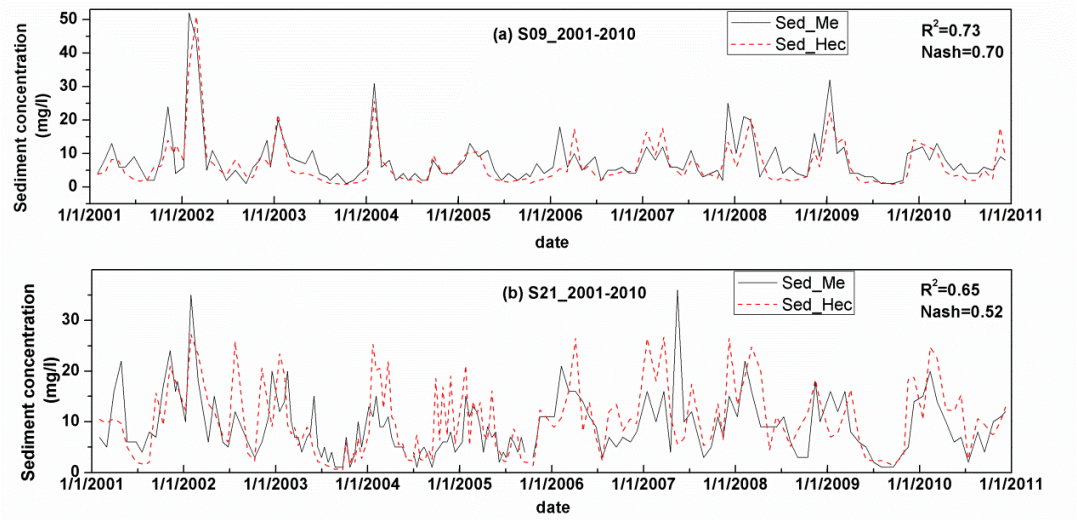

Fig. 5.4 The validation of simulated sediment concentration, (a) daily results from point S09; (b) daily results from point S21.

5.2.3.3 **Floodplain sediment**

In the sediment simulation module, the sedimentation process on the floodplain can be implemented by "bed change options". Specifically, we first simulated the sediment transportation in channel with the "no bed change allowed outside the movable bed limits" option, and then a simulation with "allow deposition outside of the movable bed limits" option was carried out. The difference of the two simulations represented the sedimentation on the floodplain. No flood event happened during 2000 - 2010 in river section S16, consequently the comparison of the sedimentation process within channel and on the floodplain was only available for the other nine river sections.

5.3 Model results

5.3.1. 10-years sedimentation trend

The simulation for the ten river sections with 10-years sediment load series (2000-2010) was completed with the 1-day computation step. The change of the bed elevation during the simulation time is shown in Fig. 5.5 Deposition processes dominated the Upper Stör catchment during the simulation time with an average sedimentation depth of 2.85 cm. The highest sedimentation depth appeared in S09 with 6.79 cm of sediment deposited on the channel bed, while in S03 and S20, the sedimentation depths were as low as 0.2 cm. In the other 7 river sections, the sediment deposited and accumulated to around 2-4 cm.

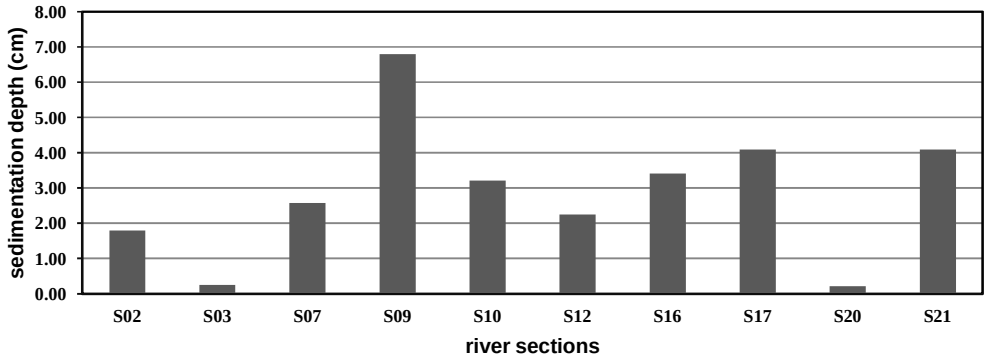

Fig. 5.5 The modeled sedimentation depth of the ten selected river sections in simulation time (2000-2010)

5.3.2. Sedimentation in-channel and on the floodplain

5.3.2.1 **Sedimentation amount**

The 10-year accumulation amount of the channelized and floodplain deposited sediment is shown in Tab. 5.2. The channelized sediment varied from 120 tons (S03) to nearly 3000 tons (S21), and averagely around 1358 tons of sediment deposited in the channel. Compared with the channel condition, the floodplains retained much less sediment, only 12 tons in each on average. Although there was 62.50 tons of overbank deposition in S20, most of the other floodplains captured less than two tons of sediment. The coefficient of variation (CV) revealed that the floodplain deposition was more complex and variable compared with the channelized sedimentation. The percentage of the floodplain deposition was also calculated and shown in the table. In general about 1% of the sediment was retained by the floodplain and the rest 99% deposited onto the channel bed.

Tab. 5.2 Channelized and floodplain sedimentation in the studied river sections (2000-2010)

	S02	**S03**	**S07**	**S09**	**S10**	**S12**	**S17**	**S20**	**S21**	**averaged**	**CV**
Channel (tons)	713.34	120.55	810.79	2808.54	955.65	1560.66	1300.83	957.11	2990.18	1357.52	0.71
Floodplain (tons)	1.70	1.08	0.19	0.48	1.75	10.17	0.82	62.50	27.20	11.77	1.78
Percentage of floodplain sediment (%)	0.24	0.89	0.02	0.02	0.18	0.65	0.06	6.13	0.90	1.01	1.93

5.3.2.2 **Sedimentation rate**

The HEC-RAS output of the channel sedimentation and floodplain sedimentation of river sections was converted into deposition rates (Fig. 5.6 (a)). The deposition rates in-channel varied from 0.28-2.79 g/m^2/d, and the averaged value was 1.75 g/m^2/d. Around 1.69 g of sediments deposited per unit area on the floodplain during every inundated day, which was the similar rate as in-channel flow. The deposition rate on the floodplain of each river section showed a wider value range. In S07, only 0.01 g of sediments deposited per unit area in the floodplain each flooded day, however, on the floodplain of S10, this value was 5.68 g/m^2/d. The coefficients of variation of in-channel and floodplain deposition rate were 0.51 and 1.17 respectively, which revealed the higher variation of the floodplain sedimentation process.

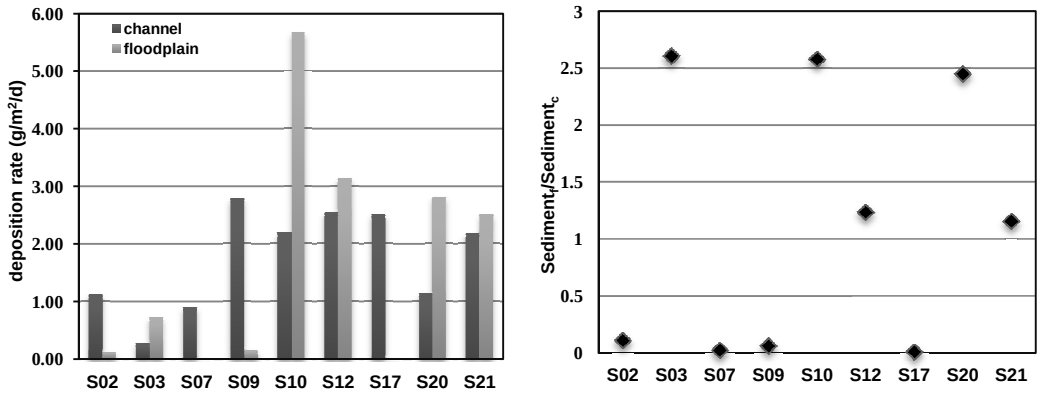

Fig. 5.6 The comparison of sedimentation processes in-channel and on the floodplain: (a) Deposition rates in-channel and on the floodplain; (b) and the ratios of deposition rates in-channel and on the floodplain

Note: Sediment$_f$ refers to the floodplain deposition rate and sediment$_c$ refers to the deposition rate in-channel

According to Fig. 5.6 (a), in five out of the nine sections, the floodplain deposition rates were higher than those in the channel, and in the other four sections, the opposite phenomenon occurred. In order to have a better understanding of the difference of sedimentation processes, the ratio of the deposition rate in-channel and on the floodplain were plotted and shown in Fig. 5.6 (b). Three levels of ratio were clearly shown on the plot. In S03, S10 and S20, the deposition rate on the floodplain were 2.5 times of that in-channel, while the amount of the sediments deposited on the floodplain were around 0.25 times more than the in-channel deposition in S12 and S21. The floodplain deposition rates were smaller than the in-channel deposition rates in the other four river sections, where the floodplain sediments accounted no more than 10% of the total sediment.

5.3.2.3 **Particle size distribution of the sediment**

Apart from the amount of the sediment, the particle size of the floodplain sediment and in-channel sediment is another attractive topic. The HEC-RAS model enables the simulation of the sediment process with different particle sizes. As shown in Fig. 5.7, the particle size of the sediment on the floodplain was smaller than that in the channel. No sediment with a diameter larger than 1 mm deposited on the

floodplain. The floodplain at river section S03captured only the fine silt and kept the smallest floodplain sediment. The grain sizes from silt to gravel can be transported and deposited on the floodplain adjacent to S12, which made up the coarsest floodplain sediment. On the floodplain of S20 and S21, the sediment was constituted by grains sized from silt to medium sand, and the percentages of every grain size were relatively even. Besides this, the particle size distribution of the floodplain sediment and in-channel sediment were similar in S20 and S21. The constitutions of the floodplain sediment of the other river sections were similar, mainly contained silt and sands.

The D50 and D90 of the sediment at each river section is given in Tab. 5.3. The median particle size (D50) of the channelized and floodplain sediment was 0.92 mm and 0.16 mm respectively. D90 of the channelized deposition was much coarser than D50, as high as 4.2 mm. On the floodplain, D90 was 0.32 mm, around twice of the diameter of the D50. According to the particle size classification, the sands sized from very fine-grained to coarse-grained constituted of half amount of the sediment. The standard deviation of the sediment particle size from the nine sub-catchments demonstrated that the constitution of the channelized sediment has a coarser and higher variability than the floodplain sediment.

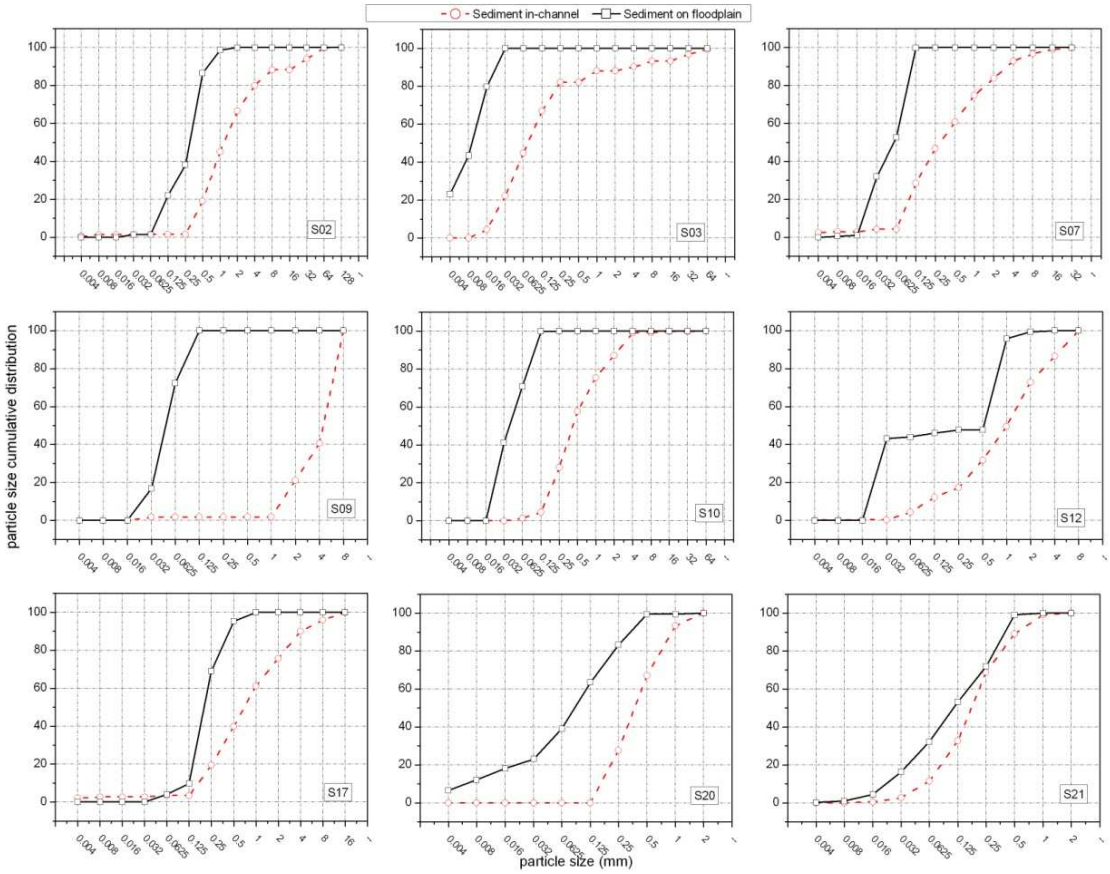

Fig. 5.7 Particle size distributions of the sediment in-channel and on the floodplain

Tab. 5.3 D50 and D90 of the sediment in the studied river sections

		S02	S03	S07	S09	S10	S12	S16	S17	S20	S21	averaged	STDEV
Channel	**d50 (mm)**	1.50	0.10	0.28	4.20	0.45	1.10	0.13	0.75	0.49	0.20	**0.92**	1.24
	d90 (mm)	8.00	4.00	3.80	6.00	2.10	8.50	4.20	4.00	0.95	0.45	**4.20**	2.70
Floodplain	**d50 (mm)**	0.40	0.01	0.06	0.05	0.04	0.50	—	0.20	0.10	0.11	**0.16**	0.17
	d90 (mm)	0.60	0.02	0.10	0.10	0.10	0.80	—	0.45	0.35	0.40	**0.32**	0.27

5.4 Discussion

5.4.1. Land use/cover and sedimentation process

The deposition and erosion processes depend on the intricate combination of the flow condition and the catchment land use condition. In this study we converted the land use condition to roughness factors. According to our field campaigns, the roughness of the pasture and arable land were relatively low, while the roughness of the forest and construction land roughness was higher (Tab. 5.4). Inversely proportional relationships were clearly shown between sediment amount, sediment rate and the floodplain roughness (Fig. 5.8 (a) and (b)). According to Fig. 5.8 (a) and (b), more sediment deposited on the river section adjacent with agriculture land. This might be because of the better capability of soil and water conservation of the forest than the agriculture land, due to the multistory canopy and extensive root system formed by forest (Zaimes et al., 2004) The erosion rate of pasture is higher than the forest but lower than the arable land (Zaimes et al., 2004). The construction land provided very little sediment into the river due to the high pavement rate.

Tab. 5.4 Characteristics of the selected ten sub-catchments

Site No.	Catchment size [km^2]	Land use/cover condition		Roughness of the floodplain	Altitude (m)
		LOB	ROB		
S02	70.09	C+P	F+P	0.09	331.6
S03	30.98	F+P	F	0.12	65.67
S07	33.29	C+P	F	0.10	179.84
S09	196.05	C+P	P	0.07	257.5
S10	32.34	P	C	0.08	41.33
S12	60.63	C+F	A+P	0.09	278.5
S16	32.33	A	A	0.07	0
S17	56.92	P	P	0.08	283.5
S20	203.02	P	A	0.08	1006.66
S21	461.74	P	P	0.09	710.83

Note: LOB is the left bank of the channel; ROB is the right bank of the channel. C refers to the construction land use; F means Forest; P is pasture land; A is arable land.

The deposition ratio increased with the growth of the floodplain roughness factor (Fig. 5.8 (c)). The lower sediment deposition ratio and higher sediment amount in the river section adjacent to the arable land sufficiently illustrate that the agriculture land is the provider of sediments. These results are in accordance

with the previous research. The erosion study pointed out that river banks and the adjacent agriculture fields were the main sediment input in Kielstau catchment (Kiesel et al., 2009b). The greatest stream bank erosion rate and total soil losses happened in the floodplain adjacent to row-crop fields, followed by continuously grazed pastures while the lowest erosion was in riparian forest buffers (Zaimes et al., 2004).

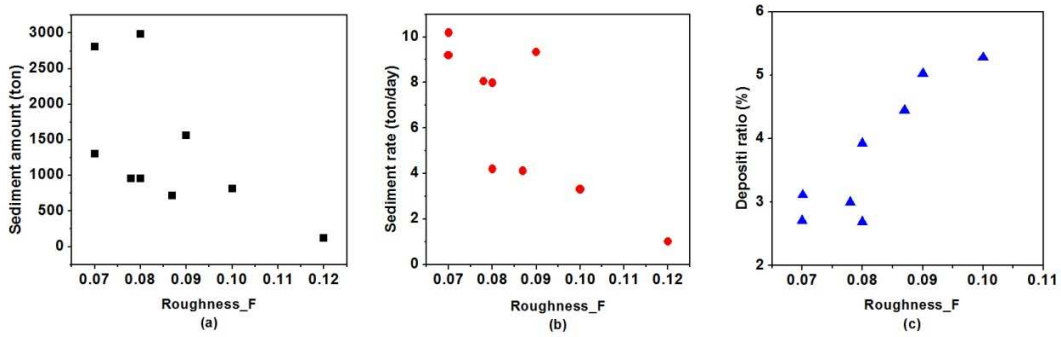

Fig. 5.8 The varying sedimentation characteristic with floodplain roughness factors among different catchments, (a) sediment amount, (b) sedimentation rate, (c) deposition ratio. Roughness_F refers to the roughness coefficient of the floodplain of every sub-catchment

5.4.2. Stream power and sedimentation process comparison

Previous research revealed that the flood energy accounts for around 1% - 10% of the total stream energy during the peak discharge from 2000 to 2010 (Song et al., 2014). The sediment distribution pattern along the cross section was calculated and suggested around 0% - 1.4% of all the sediment deposited on the floodplain. The ratio of the flood stream power and the ratio of the floodplain sediment highly correlated with each other (Fig. 5.9). It is reasonable to expect the higher stream power transport more suspended sediment to the floodplain, and part of the sediment deposited on the floodplain because of the loss of the energy.

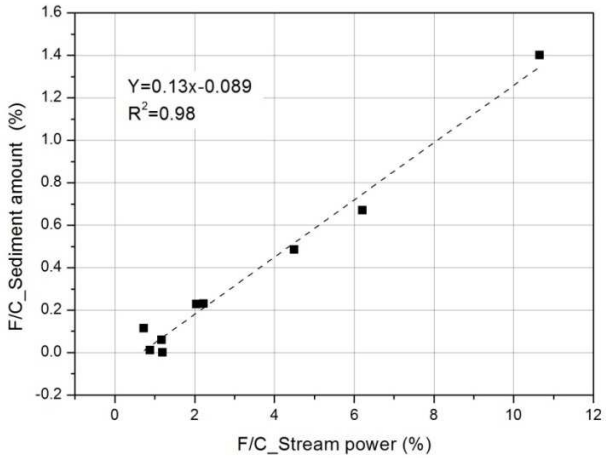

Fig. 5.9 The percentage of flood flow power against the percentage of sediment amount on the floodplain in every during 10years peak flood

Note: F/C_Sediment amount, the ratio of floodplain and channelized sediment amount; F/C_Stream power, the ratio of flood power and channel stream power; the dash line is the trend line of the F/C_Sediment amount

5.4.3. Sediment particle size

The sediment particle size in-channel and on the floodplain are positively correlated with the river section altitude and the flood stream power respectively (Fig. 5.10 (a) and (b)). In the higher altitude points like S02 and S03, the channelized D90 was nearly 8mm, while the outlet (S21) channelized D90 was around 0.5mm (Fig. 5.10 (a)). Despite the D90 of channelized sediment was smallest in point S21, the D90 of the floodplain sediment was largest among all the sub-catchments due to the highest floodplain stream power. It suggests that during the flood, the upper stream tributary with higher slope but shallower and narrower flows faster enough to reach the incipient velocity of the coarser sediments. But these coarser sediments tend to deposit onto the river bed of the upper stream sub-basin, instead of being transported downstream to the outlet of the Upper Stör catchment. Higher floodplain stream power is capable to transport coarser sediment to the floodplain, and most of them deposit onto the floodplain since the decrease of the velocity and the increase of the roughness.

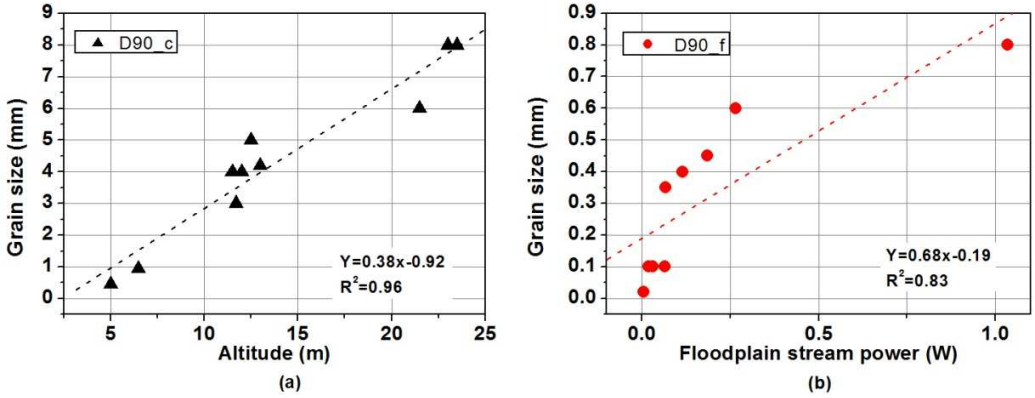

Fig. 5.10 The grain size sediment of different catchment, (a) D90 of channelized sediment at different altitude, (b) D90 of floodplain sediment against floodplain stream power during 10years peak flood

Note, D90_c refers to the D90 of channelized sediment, D90_f is the D90 of floodplain sediment, the dash line is the trend line of the grain size.

5.4.4. Reliability and accuracy of the results

The research in similar catchments would be a good reference to our study. The lower Mesa river section is located in Spain with about 30 km in length and a mean slope of 1.05%. The annual discharge of the Mesa river is 1.5 m^3/s, which is quite similar with our sub-catchment Brachenfeld (S02). The in-channel sedimentation in the lower reach of the River Mesa was observed from April 2003 to September 2009 (Auqué et al., 2013). The bed elevation change revealed the in-channel sedimentation rate of 2.05 mm every year, and in Brachenfeld the annual sedimentation depth was 1.80 mm. This means the models results of our catchment are reasonable (Tab. 5.5).

Tab. 5.5 The in-channel deposition rate of the Lower Mesa river and S02 river of the catchment

Catchment	Length (km)	Slope (%)	Discharge (m^3)	Duration	Deposition rate (mm/yr)
Lower Mesa river (Spain)	30	1.05	1.5	Apr. 2003- Sep. 2009	2.05
S02 (Stör - Brachenfeld)	**18**	**0.21**	**0.95**	**Jan. 2001-Dec. 2010**	**1.8**

The Duvenseebach catchment is located about 60km southeast of Upper Stör catchment in the Pleistocene landscape of Schleswig-Holstein, Germany. With a drainage area of 28 km^2, the Duvenseebach catchment is dominated by similar natural and geographical conditions to the Upper Stör catchment. A sediment trapping research during the spring flood 2011 in this catchment indicated that there was around 0.11 - 0.22 kg of sediment retained per unit area on the floodplain (Zhang, 2011). In contrast, in our study area the sedimentation rate varied from 0.01 to 0.23 $kg/m^2/yr$. Another field and laboratory experiment completed in a lowland river floodplain in Denmark (River Odense) provided a floodplain sedimentation rate ranged from 0.94 to 1.75 $kg/m^2/yr$ (Tab. 5.6), which was around 10 times higher than the value of our catchments (Kronvang et al., 2009). The catchment was inundated for 47-day during the study period, which was around four times longer than the average inundation period of our catchment. Considering this difference, the results of both catchments were quite similar to our study.

Tab. 5.6 The floodplain deposition rate of Duvenseebach, Odense and Upper Stör catchment

Catchment	Method	Annually inundated days	Deposition rate ($g/m^2/d$)
Duvenseebach (S-H)	Grass mats trapping	-	0.11 - 0.22
Odense (Denmark)	Grass mats trapping	47	0.94 - 1.75
Upper Stör	**Model**	**10**	**0.01 - 0.23**

5.5 Conclusion and outlook

In this study, we combined the geometry variation capability of the HEC-RAS model and the data generation advantage of the SWAT model for simulating the sediment processes of ten selected river sections in the Upper Stör catchment. Decadal sediment models for both channelized and floodplain deposition were completed with a daily computation step for every sub-catchments. Based on the output of the model, the decadal sediment trend was evaluated and the comparison of the channelized and floodplain sedimentation processes was investigated. The results clearly show that,

(1) in general, deposition processes dominated the Upper Stör catchment in the decadal time scale, with an average sedimentation depth of 2.85 cm. The different sedimentation amount and rate among different mainly due to the floodplain land use/cover condition.

(2) the stream power distribution in-channel and on the floodplain dominates the sediment distribution. The floodplain sedimentation process was more complex and has a higher variability than the channelized deposition, although the mean deposition rate was similar. Only 1% of the sediment was retained by the floodplain and the rest of 99% deposited onto the channel bed.

(3) the altitude of the river section dominates the channelized sediment grain size, while the floodplain sediment size depends mainly on the floodplain stream power. The constitution of the channelized sediment was coarser and has a higher variability than the floodplain sediment. The D50 of the channelized and floodplain sediment was 0.92 mm and 0.16 mm respectively, while the D90 of the sediment was 4.2 mm in channel and 0.32 mm on the floodplain.

Our study has been focusing on quantifying and comparing the channelized and floodplain sedimentation processes by means of the combination of the HEC-RAS and SWAT models. The distributed ecohydrological model SWAT provided reasonable daily discharge and sediment load information, which was unavailable at selected locations of different sub-basins. The real-time operational model HEC-RAS has been proven to be well performing in channel geometry simulation and sediment transportation. The sedimentation results of our catchment are comparable to that from lowland catchments worldwide and that under different methodology. This comparison proves the efficiency and applicability of the combined HEC-RAS and SWAT model strategy in sediment simulation. Due to the 1D characteristic of the HEC-RAS model, the spatial distribution of floodplain depositions was not examined here, which would be an interesting issue and will give more thoroughly overview about the floodplain deposition processes.

Chapter 6. Conclusion and discussion

6.1 Summarizing the key achievements

This dissertation was conducted in the Northern German lowland catchments, and some other catchments in Germany and China (Fig 1.3, 1.4, 1.5 and 1.6). The catchments have been chosen due to the criteria of the "maximum variety of the hydrological conditions", but the turbulence caused by large obstacles, dams or waterfalls have been avoided. These catchments located in different geographic regions, covered a wide range of soil properties, catchment sizes, land use types, river geometry, and meteorological conditions. The wide variety of the hydrological conditions provided comprehensive testing environment for the equipment and measurement methodology. Meanwhile, the different structure of the vertical flow profile caused by catchment characteristics can be clarified with data from representative catchments. Lowland catchments have been facing the challenge of higher frequency and magnitude of flood, which will strengthen the energy transfer and substance exchange process of the interactive lowland river-floodplain system (Dankers and Feyen, 2009; Kundzewicz et al., 2010). In order to focus on the energy transfer and sediment transportation both in channel and on the floodplain in lowland area, the flow and sediment models were set up only in Upper Stör catchment. The analysis of the results of the measurements and models provide satisfactory answers to our research questions posted in part 1.5. The main achievements are summarized as follows:

6.1.1. The accuracy of the Doppler equipment meter (ADQ)

Question 1: Can the emerging Doppler equipment (ADQ) and the measurement we took provide accurate results compared to the traditional flow meter? Whether the accuracy of the discharge and the velocity measured with ADQ are adequately reliable for the model setup?

The main aim of Chapter 2 is to answer this question. Based on the 366 measurements at 174 cross sections collected from 8 catchments of different sizes with various flow conditions, the accuracy, stability and sensitivity of velocity, depth and discharge measurements from an ADQ device were tested. Comparison between Doppler equipment (ADQ), point velocity ADC and the electromagnetic device FlowSens were made. The observations clearly show that compared with the electromagnetic device FlowSens, ADQ produced comparable results for depth, velocity and discharge. The consistency of the depth measurement was higher than discharge and velocity measurement. Strong agreement between measurements with all three instruments was observed in river mean velocity, vertical mean velocity, layer averaged and point velocity were revealed. River mean velocity agreed better than point velocity, while the mean vertical profile velocity expressed higher unity than the mean layer velocity. Repeated measurement at the same cross section and within the same river sections demonstrated the high

reproducibility of the ADQ measurements. The inner setting test of the equipment showed that the ratio between cell size and depth within 0.1-0.2 and a measuring time of 40-50 s are recommended for a reliable measurement. All these testing suggested that the ADQ is a reliable and accurate velocity and discharge measurement device, and the measurement methodology is suitable for the hydrodynamic sampling. The accuracy of the vertical depth, the river mean discharge and the vertical profile velocity are adequately reliable for the setting up of vertical profile models and hydrological models.

6.1.2. The model of vertical flow velocity profile

Question 2: Is it possible to use some easy-to-determine parameters to set up a simple and common distribution model for the flow velocity in vertical direction?

In Chapter 3 we try to modify the traditional vertical velocity distribution formula with parameters that can be measured and determined easily. The traditional logarithmic, power and parabolic formulas are widely used for vertical velocity distribution estimation. All the three formulas involve the friction velocity (u_*) and the depth (y) of the measured point. The friction velocity (u_*) is hard to measure directly, and the real depth (y) of the measured point is not comparable in different catchments. Hence, we proposed a new form of formula, in which the friction velocity (u_*) is substituted by the dimensionless relative flow velocity mean vertical velocity ($\bar{u}$), the real depth (y) of the measured point is substituted by the dimensionless relative water depth (y/H). Then the 248 vertical profiles collected from Upper Stör catchment (German lowland area), Kinzig catchment (German low mountainous catchment) and Changjiang catchment (Chinese mountainous catchment) were used to test the applicability of the new formulas. And the results show that the new logarithmic, power and parabolic formulas fit the real measured vertical distribution at a very high level. The averaged absolute error was 10% in logarithmic fitting, 11% in power fitting and 7% in parabolic fitting. The errors mainly appeared in the area near the water surface, and in the middle part of the profiles, all three new formulas perform very well. There is no uniform formula for all the catchments, the coefficients and the constants in the formulas are positively related to the catchment slope. This proved that the substitution of u_* and y in the so far used formulas with the easy-to-determine parameter $u/\bar{u}$ and y/H is efficient and applicable.

6.1.3. The lateral distribution of flow and steam power

Question 3: How do the discharge and stream power distribute in the channel and on the floodplain? What is the main cause of the different distribution among different sub-catchments?

The HEC-RAS models for ten selected river sections in the Upper Stör catchment were set up and calibrated in Chapter 4, to evaluate the flow and energy distribution in the lowland river-floodplain system. The output of the SWAT model of the same sub-catchments was adopted as data input source. Analysis of

the data from 2000-2010 clearly show the distribution pattern of the flow and stream power in channel and on the floodplain: 40-75% of the total discharge was located on the floodplain but they generated only around 1-10% of the stream power during 10year-peak flood, and more flood power were generated on the floodplain with lower slope; with the same increase of the discharge, the in-channel power grew 3 times faster than the floodplain power. The roughness factor was highly correlated with the different increase rate among different catchment; statistically, the 10-year-averaged discharge and unit power were around 1/3 of that during bankfull discharge condition, and the 10-year-peak discharge and unit power were nearly 1.6 times of the corresponding bankfull parameters.

6.1.4. The lateral distribution of the sediment

Question 4: How much sediment was deposited or eroded in the study area? What are the main differences between the sediment process in-channel and on the floodplain? Why does the sediment pattern among sub-catchments differ?

Question 4 is the main focus of Chapter 5, in which we simulated the sediment processes of ten selected river sections in the Upper Stör catchment in decadal time scale based on the HEC-RAS model and SWAT model. The geometry variation capability of the HEC-RAS model and the data generation advantage of the SWAT model were combined in the simulation. The output indicates that the deposition processes dominated the Upper Stör catchment in the decadal time scale with an average sedimentation depth of 2.85 cm, and the floodplain land use/cover condition affected the sedimentation amount in different sub catchments. The main difference of the channelized and floodplain sedimentation lies in the quantity and the grain size of the sediment. Around 1% of the sediment was retained by the floodplain and the remaining 99% deposited onto the channel bed. The floodplain sedimentation process was more complex and has a higher variability than the channelized deposition, although the mean deposition rate was similar. The altitude of the river section dominates the channelized sediment grain size, and the floodplain sediment size depends mainly on the floodplain stream power.

6.2 Discussion of the achievements

6.2.1. Uncertainty of the ADQ measurement

The new emerging Acoustic Doppler Qliner (ADQ) enables different inner settings for different measurements, like cell size and measurement time interval. Choosing the appropriate cell size and time interval is essential to minimize the measurement uncertainty. The measurement comparison suggests the performance of ADQ is more sensitive to the cell size setting than to the time interval setting. The recommended ratio between cell size and mean water depth should be within 0.1-0.2 in order to get a high quality result. With larger cell size depth ratio, the discharge tends to be overestimated. The time interval

test revealed the longer time needed for the flow with low velocity to assure an accurate measurement. According to the analysis, all the measurements from ADQ with different cell size and time interval settings provided errors within ±5% compared with the results from FlowSens, which reflects very high reliability of the equipment.

The vegetations and irregular substrates in river bed and bank influence the transmission of the sound waves. The negative correlation was found between measurement errors and the distances of vertical profiles from the river bank. The error of mean layer velocity was negatively proportional to the standard distance from the river bed. River bed seems to have a larger influence than river bank. This means the nearer the measured point to the bank or bed, the larger the measurement error will be. Due to the low velocity at the points near the river bed and bank, the error of from these have little impacts on the discharge results.

6.2.2. Vertical flow velocity formula

Although the three prediction formulas worked well in describing the water profile with averaged error around ±10%, there is no universal formula with unique coefficients and constants for the vertical profiles from different cross sections. Parabolic line fits the measured data better than logarithm formula and power formula. But the variability of the parabolic coefficients and constant are higher among all the sub-basins. The high correlations between the fitted coefficients and constants provide the opportunity to establish the simplified but relatively rough formula instead of a universal formula. The slope of the catchment tends to influence the coefficients of the formulas in a positive direction.

6.2.3. Model uncertainty

The main sources of the error in HEC-RAS simulations include the measurement uncertainty, the uncertainty of the SWAT-modeled data, the roughness and slope uncertainty of the channel bed and floodplain, etc.. In this dissertation, the accuracy of the measurement device and methodology have been proven in Chapter 2. Thus it is reasonable to exclude the measurement error, and the uncertainties caused by SWAT modeled data and the roughness and slope factor warrant detailed discussion.

Previous researchers have pointed out that the under- or overestimation of SWAT model are usually affected by the climate data, the number and size of sub-basins, the resolution of spatial input data and the algorithms used in SWAT (Garen and Moore, 2005; Inamdar and Naumov, 2006; Migliaccio and Chaubey, 2008). In our study, the uncertainty of the SWAT model in Upper Stör catchment has been discussed in the previous study (Pott, 2014). The well calibrated daily discharge model yielded the coefficient of determination (R^2) of 0.86 during calibration period and 0.84 during validation period compared with the real measured data, with Nash-Sutcliffe coefficients 0.85 and 0.83 respectively (Fig 1.8). Analysis of the calibrated daily output and real measured suspended sediment yielded the R^2 of 0.56 and the Nash-

Sutcliffe coefficient (NSE) of 0.55 (Fig 1.8). The averaged R^2 and Nash-Sutcliffe coefficient produced by daily validated data were 0.61 and 0.59 respectively. These model errors, especially in the sediment yield series might cause the uncertainty in the second-round simulation carried out in the HEC-RAS models in the sub-catchments without gauge stations.

The roughness and slope uncertainty is considered to have the most important impact on the prediction of water surface elevation (Pappenberger et al., 2005). Earlier research concluded that the roughness varies in values in different seasons attribute to differences in aquatic plant growth and the water depth (O'Hare et al., 2010; Shih and Rahi, 1982). The roughness factor was estimated in the field according to the empirical table (Chow, 1959), which might result to unavoidable error. The slope of the river bed was deduced from the geometry of the cross section and the 1-m DEM during model setup. During the model calibration process, the roughness and slope calibration were combined. Specifically, we fixed the roughness height and modified the slope value, or with fixed slope value and modified roughness, to get the most satisfied model results. The deficits of such a calibration are that a fixed inaccurate roughness would result additionally in a wrong slope value. In this dissertation the seasonal roughness factor was introduced, which provided a variable roughness factor for every month and reduced the error possibility concerning roughness. Correspondingly, the quality of the calibrated river slope improved substantially.

6.2.4. The flow/sediment processes in sub-catchments

The characteristics of the sub-catchment, such as the roughness, slope of the bed and floodplain, the land use/cover and the altitude of the study sites are correlated with the flow and sediment processes according to our study. Among all the spatially distributed catchment characteristics, the roughness factor of the river and floodplain plays the key role in the flow and sediment distribution pattern. The increase rate of the channelized and floodplain power and the deposition ratio were highly correlated with the roughness factor. Land use/cover mainly determined the amount of sediment of the sub-catchment. Forest has a better capability of soil and water conservation than agriculture land, while constructed areas delivered very little sediment into the river due to the high sealing rate. These findings are in accordance with previous research (Kiesel et al., 2009b; Zaimes et al., 2004). The altitude of the researched sub-catchment was positively correlated with the sediment particle size in-channel and on the floodplain. All these findings indicate that the better understanding of the characteristics of the sub-catchment would be the basic step to analyze the flow and sediment processes especially during the flood event.

6.3 Overall conclusion and outlook

This dissertation proves the accuracy and the reliability of the new discharge and velocity device (ADQ, OTT Qliner with acoustic Doppler technology) and the corresponding methodology for the discharge and velocity measurement in medium-sized river. Meanwhile the new structure of the vertical flow velocity

with easy-to-determine parameters is proven to be applicable and efficient. The lateral distribution of the flow, energy and sediment in the Upper Stör catchment in Northern German lowland area was evaluated based on the well calibrated HEC-RAS and SWAT model. The results provide some basic knowledge about the flow and sediment processes in lowland river-floodplain system. All the current findings and achievements of this dissertation are a significant baseline for the floodplain management, river development plan in the Upper Stör catchment or any further research in the similar area. More issues should be addressed in future studies for a comprehensive understanding of the lowland interactive hydrological, hydraulic and ecological processes:

(1) the improvement of the data input. The output of the HEC-RAS model provides adequate and acceptable information for the flow and sediment in-channel and on the floodplain, but due to the data accessibility problem, the modeled sediment input series were in satisfactory quality. Long-term continued daily measurement data of the suspended sediment would be expected in future studies for more realistic sediment output results.

(2) the flow and sediment processes simulation of the higher magnitude flood events, like 100years or 1000years flood would be interesting in the engineering and ecological study. High magnitude but low frequency floods are supposed to happen more often according to the analysis of climate change scenarios, which increases the need of flood process studies especially in lowland catchments.

(3) HEC-RAS model is capable of simulating the floodplain flow/sediment and channelized flow/sediment process individually, but it cannot provide insight into the inter-exchange process between river and floodplain, as a result we mainly focused on the amount and grain size distribution of the sediment. More experiments are needed to understand the sediment exchange during flood events.

(4) although this dissertation indicates that the pasture and the arable land are the main providers of the sediment, but the transportation processes of the sediment from each kind of land use/cover are still unclear. The river-section-scale based study previously included the basic sediment path and source information, but catchment-scale based studies were rarely found.

(5) non-point source pollution, such as Nitrogen and Phosphorus in lowland catchments has been considered to be one of the most important environmental problems especially in agricultural used lowland catchments. The flow/sediment lateral distribution analysis in this study would be a convenient data base for related pollution studies and the agricultural management in the Upper Stör catchment.

References

Afzal, N. (2001). Power law and log law velocity profiles in turbulent boundary-layer flow: equivalent relations at large Reynolds numbers. Acta Mech. *151*, 195–216.

Alfredsson, P.H., and Örlü, R. (2012). A New Way to Determine the Wall Position and Friction Velocity in Wall-Bounded Turbulent Flows. In Progress in Turbulence and Wind Energy IV, M. Oberlack, J. Peinke, A. Talamelli, L. Castillo, and M. Hölling, eds. (Springer Berlin Heidelberg), pp. 181–185.

Archer, D.R. (1989). Flood wave attenuation due to channel and floodplain storage and effects on flood frequency. Floods Hydrol. Sedimentol. Geomorphol. Implic. John Wiley Sons N. Y. 1989 P 37-46.

Arnold, J.G., Srinivasan, R., Muttiah, R.S., and Williams, J.R. (1998). Large Area Hydrologic Modeling and Assessment Part I: Model Development1. JAWRA J. Am. Water Resour. Assoc. *34*, 73–89.

Asselman, N.E.M., and Middelkoop, H. (1995). Floodplain sedimentation: Quantities, patterns and processes. Earth Surf. Process. Landf. *20*, 481–499.

Auqué, L., Arenas, C., Osácar, C., Pardo, G., Sancho, C., and Vázquez-Urbez, M. (2013). Tufa sedimentation in changing hydrological conditions: the River Mesa (Spain). Geol. Acta *11*, 85–102.

Baldwin, D.S., and Mitchell, A.M. (2000). The effects of drying and re-flooding on the sediment and soil nutrient dynamics of lowland river–floodplain systems: a synthesis. Regul. Rivers Res. Manag. *16*, 457–467.

Barker, D.M., Lawler, D.M., Knight, D.W., Morris, D.G., Davies, H.N., and Stewart, E.J. (2009). Longitudinal distributions of river flood power: the combined automated flood, elevation and stream power (CAFES) methodology. Earth Surf. Process. Landf. *34*, 280–290.

Bates, P.D., and De Roo, A.P.J. (2000). A simple raster-based model for flood inundation simulation. J. Hydrol. *236*, 54–77.

Beechie, T.J., Liermann, M., Pollock, M.M., Baker, S., and Davies, J. (2006). Channel pattern and river-floodplain dynamics in forested mountain river systems. Geomorphology *78*, 124–141.

Bergstrom, D.J., Tachie, M.F., and Balachandar, R. (2001). Application of power laws to low Reynolds number boundary layers on smooth and rough surfaces. Phys. Fluids 1994-Present *13*, 3277–3284.

BGR (1999). “Bodenübersichtskarte im Maßstab 1:200 000 (BÜK 200). Verbreitung der Bodengesellschaften”, Federal Institure for Geoscience and Natural Resources (Hannover, Germany).

BGR (2012). Bundesanstalt für Geowissenschaften und Rohstoffe: Bodenübersichtskarte 1:200.000 (BÜK 200).

BKG (2011). Bundesamt für Kartographie und Geodäsie: Digitales Landschaftsmodell (ATKIS).

Blench, T. (1966). Discussion of “Sediment transportation mechanics: initiation of motion.”J. Hydraul. Div. ASCE *92*, 287–288.

Bockelmann, B.N., Fenrich, E.K., Lin, B., and Falconer, R.A. (2004). Development of an ecohydraulics model for stream and river restoration. Ecol. Eng. *22*, 227–235.

Bowers, M.C., Tung, W.W., and Gao, J.B. (2012). On the distributions of seasonal river flows: Lognormal or power law? Water Resour. Res. *48*, n/a–n/a.

Brocca, L., Melone, F., and Moramarco, T. (2011). Distributed rainfall-runoff modelling for flood frequency estimation and flood forecasting. Hydrol. Process. *25*, 2801–2813.

Brunner, G.W. (1995). HEC-RAS River Analysis System. Hydraulic Reference Manual. Version 1.0.

Cameron, S.M. (2011). PIV algorithms for open-channel turbulence research: Accuracy, resolution and limitations. J. Hydro-Environ. Res. *5*, 247–262.

Chang, H. (2008). Case Study of Fluvial Modeling of River Responses to Dam Removal. J. Hydraul. Eng. *134*, 295–302.

Chapra, S.C., and Pelletier, G.J. (2003). QUAL2K: a modeling framework for simulating river and stream water quality: documentation and users manual. Civ. Environ. Eng. Dept Tufts Univ. Medford MA.

Chen, C. (1991). Unified Theory on Power Laws for Flow Resistance. J. Hydraul. Eng. *117*, 371–389.

Chen, S., Xiao, G., Zhao, Y., Zhang, J., and Wang, W. (1999). Study on velocity distribution function of river cross section (in Chinese). J. Hydraul. Eng. Chin. *4*, 70–74.

Cheng, N., and Chiew, Y. (1998). Modified Logarithmic Law for Velocity Distribution Subjected to Upward Seepage. J. Hydraul. Eng. *124*, 1235–1241.

Chiu, C.-L., and Tung, N.-C. (2002). Maximum velocity and regularities in open-channel flow. J. Hydraul. Eng. *128*, 390–398.

Chow, V. (1959). Open channel hydraulics (New York).

Christian, J., Duenas-Osorio, L., Teague, A., Fang, Z., and Bedient, P. (2013). Uncertainty in floodplain delineation: expression of flood hazard and risk in a Gulf Coast watershed. Hydrol. Process. *27*, 2774–2784.

Coffey, R., Cummins, E., Bhreathnach, N., Flaherty, V.O., and Cormican, M. (2010). Development of a pathogen transport model for Irish catchments using SWAT. Agric. Water Manag. *97*, 101–111.

Coleman, N. (1973). The velocity defect law and the sediment transfer coefficient in an open channel. SEDIMENT Transp. Vol. 1.

Craig, A., Muste, M., and McVay, J. (2009). Experimental Evaluation of Q-Liner Measurement Performance. (Vancouver, British Columbia, Canada),.

Daly, S.F., and Vuyovich, C.M. (2003). Modeling river ice with HEC-RAS. In Proceedings of the 12th CGU-HS CRIPE Workshop on River Ice, Edmonton, Alta,.

Dankers, R., and Feyen, L. (2009). Flood hazard in Europe in an ensemble of regional climate scenarios. J. Geophys. Res. Atmospheres *114*, n/a–n/a.

Darwish, M.A.G. (2010). Geochemical reconnaissance survey and environmental assessment for stream sediments of Wadi Um Gier, Southeastern Desert, Egypt. Environ. Earth Sci. *62*, 657–672.

Dickhudt, P.J., Friedrichs, C.T., Schaffner, L.C., and Sanford, L.P. (2009). Spatial and temporal variation in

cohesive sediment erodibility in the York River estuary, eastern USA: A biologically influenced equilibrium modified by seasonal deposition. Mar. Geol. *267*, 128–140.

DLR (1995). Landsat TM5-Szene aus dem Jahr 1995, Auflösung 25 × 25 m (Deutsches Zentrum für Luft- und Raumfahrt Köln.).

EEA (2000). Corine Landcover 250 m-Raster (Copenhagen, Denmark: European Environment Agency).

Estrany, J., Garcia, C., Martínez-Carreras, N., and Walling, D.E. (2012). A suspended sediment budget for the agricultural Can Revull catchment (Mallorca, Spain). Z. Für Geomorphol. Suppl. Issues *56*, 169–193.

Evans, I.S., Hengl, T., and Gorsevski, P. (2009). Chapter 22 Applications in Geomorphology. In Developments in Soil Science, Tomislav Hengl and Hannes I. Reuter, ed. (Elsevier), pp. 497–525.

Fan, C., Ko, C.-H., and Wang, W.-S. (2009). An innovative modeling approach using Qual2K and HEC-RAS integration to assess the impact of tidal effect on River Water quality simulation. J. Environ. Manage. *90*, 1824–1832.

Fleming, M.J., Gibson, S.A., and Pak, J.H. (2010). Modeling Watershed and Riverine Sediment Processes with HEC-HMS and HEC-RAS. In Watershed Management 2010, (American Society of Civil Engineers), pp. 1340–1349.

Fohrer, N., and Jähnig, S. (2009). Integrated modelling of the response of aquatic ecosystems to land use and climate change in the Poyang lake region, China. DFG Project Proposal.

Frąckiewicz, A. (2010). Water quality of the river Stör and its tributaries. Christian Albrecht's University of Kiel.

Frizell, K. warren, and Vermeyen, T.B. (2007). Comparing Apples and Oranges: Teledyne/RDI StreamPro ADCP and the OTT QLiner River Discharge Measurement System.

Fromin, N., Pinay, G., Montuelle, B., Landais, D., Ourcival, J.M., Joffre, R., and Lensi, R. (2010). Impact of seasonal sediment desiccation and rewetting on microbial processes involved in greenhouse gas emissions. Ecohydrology *3*, 339–348.

Garen, D.C., and Moore, D.S. (2005). Curve Number Hydrology in Water Quality Modeling: Uses, Abuses, and Future Directions1. JAWRA J. Am. Water Resour. Assoc. *41*, 377–388.

Geertz, J. (2012). Land use scenarios for the river Treene catchment in northern Germany. Bachelor thesis. University of Kiel.

George, W.K. (2007). Is there a universal log law for turbulent wall-bounded flows? Philos. Trans. R. Soc. Math. Phys. Eng. Sci. *365*, 789–806.

Gomani, M.C., Dietrich, O., Lischeid, G., Mahoo, H., Mahay, F., Mbilinyi, B., and Sarmett, J. (2010). Establishment of a hydrological monitoring network in a tropical African catchment: An integrated participatory approach. Phys. Chem. Earth Parts ABC *35*, 648–656.

González, J.A., Melching, C.S., and Oberg, K.A. (1996). Analysis of open-channel velocity measurements collected with an Acoustic Doppler Current Profiler. Proc RiverTech96 IWRA Chic. Ill. *2*, 838–845.

Goodbred Jr, S.L., and Kuehl, S.A. (1998). Floodplain processes in the Bengal Basin and the storage of Ganges–Brahmaputra river sediment: an accretion study using 137Cs and 210Pb geochronology. Sediment. Geol. *121*,

239–258.

Goode, J.R., Luce, C.H., and Buffington, J.M. (2012). Enhanced sediment delivery in a changing climate in semi-arid mountain basins: Implications for water resource management and aquatic habitat in the northern Rocky Mountains. Geomorphology *139–140*, 1–15.

Gunawan, B., Sterling, M., and Knight, D.W. (2010). Using an acoustic Doppler current profiler in a small river. Water Environ. J. *24*, 147–158.

Guo, J. (0). Modified log-wake-law for smooth rectangular open channel flow. J. Hydraul. Res. *0*, 1–14.

Hauet, A., Creutin, J.-D., and Belleudy, P. (2008). Sensitivity study of large-scale particle image velocimetry measurement of river discharge using numerical simulation. J. Hydrol. *349*, 178–190.

He, J., and Wang, H. (2003). Turbulence characteristics of non-uniform flow in a smooth open channel (in Chinese). J. Hohai Univ. Nat. Sci. *31*, 513–517.

Hervouet, J.-M. (2000). TELEMAC modelling system: an overview. Hydrol. Process. *14*, 2209–2210.

Hicks, F.E., and Peacock, T. (2005). Suitability of HEC-RAS for Flood Forecasting. Can. Water Resour. J. *30*, 159–174.

HMUELV (2011). Hessisches Ministerium für Umwelt, Energie, Landwirtschaft und Verbraucherschutz (2011): Beseitigung von kommunalen Abwässern in Hessen, Lagebericht 2010.

Hoffmann, T., Erkens, G., Gerlach, R., Klostermann, J., and Lang, A. (2009). Trends and controls of Holocene floodplain sedimentation in the Rhine catchment. Catena *77*, 96–106.

Horritt, M.S., and Bates, P.D. (2002). Evaluation of 1D and 2D numerical models for predicting river flood inundation. J. Hydrol. *268*, 87–99.

Hsieh, P.A., and Freckleton, J.R. (1993). Documentation of a computer program to simulate horizontal-flow barriers using the US Geological Survey's modular three-dimensional finite-difference ground-water flow model (US Department of the Interior, US Geological Survey).

HVBG (2011). Hessische Verwaltung für Bodenmanagement und Geoinformation: Digitales Geländemodell.

Inamdar, S., and Naumov, A. (2006). Assessment of Sediment Yields for a Mixed-landuse Great Lakes Watershed: Lessons from Field Measurements and Modeling. J. Gt. Lakes Res. *32*, 471–488.

Instruments R. D. (1996). Principles of Operation A Practical Primer. Available RDInstruments Com.

ISDSP (2013). International Scientific Data Service Platform: 30m Resolution Digital Elevation Model.

Jähnig, S.C., Lorenz, A., and Hering, D. (2008). Hydromorphological parameters indicating differences between single- and multiple-channel mountain rivers in Germany, in relation to their modification and recovery. Aquat. Conserv. Mar. Freshw. Ecosyst. *18*, 1200–1216.

Jähnig, S.C., Kuemmerlen, M., Kiesel, J., Domisch, S., Cai, Q., Schmalz, B., and Fohrer, N. (2012). Modelling of riverine ecosystems by integrating models: conceptual approach, a case study and research agenda. J. Biogeogr. *39*, 2253–2263.

Jain, S.K. (2010). Simulation of Runoff and Sediment Yield for a Himalayan Watershed Using SWAT Model. J. Water Resour. Prot. *02*, 267–281.

Jain, V., Preston, N., Fryirs, K., and Brierley, G. (2006). Comparative assessment of three approaches for deriving stream power plots along long profiles in the upper Hunter River catchment, New South Wales, Australia. Geomorphology *74*, 297–317.

James, C.S. (1985). Sediment transfer to overbank sections. J. Hydraul. Res. *23*, 435–452.

JCGM (2008). International vocabulary of metrology - Basic and general concepts and associated terms (VIM).

Johnson, R.M., Warburton, J., Mills, A.J., and Winter, C. (2010). Evaluating the Significance of Event Sediment Dynamics in a First Order Tributary Using Mutiple Sediment Budgets. Geogr. Ann. Ser. Phys. Geogr. *92*, 189–209.

Johnston, J.M., McGarvey, D.J., Barber, M.C., Laniak, G., Babendreier, J., Parmar, R., Wolfe, K., Kraemer, S.R., Cyterski, M., Knightes, C., et al. (2011). An integrated modeling framework for performing environmental assessments: Application to ecosystem services in the Albemarle-Pamlico basins (NC and VA, USA). Ecol. Model. *222*, 2471–2484.

Jowett, I.G. (1998). Hydraulic geometry of New Zealand rivers and its use as a preliminary method of habitat assessment. Regul. Rivers Res. Manag. *14*, 451–466.

Von Kármán, T.H. (1931). Mechanical similitude and turbulence.

Kasper, K. (2005). Accuracy of HEC-RAS to Calculate Flow Depths and Total Energy Loss With and Without Bendway Weirs in a Meander Bend. MS Plan-B Rep. Colo. State Univ. Dep. Civ. Eng. Fort Collins CO.

Kawahara, M., and Umetsu, T. (1986). Finite element method for moving boundary problems in river flow. Int. J. Numer. Methods Fluids *6*, 365–386.

Kiesel, J., Hering, D., Schmalz, B., and Fohrer, N. (2009a). A transdisciplinary approach for modelling macroinvertebrate habitats in lowland streams. IAHS Publ *328*, 24–33.

Kiesel, J., Schmalz, B., and Fohrer, N. (2009b). SEPAL – a simple GIS-based tool to estimate sediment pathways in lowland catchments. Advances in Geosciences *21*, 25–32.

Kiesel, J., Schmalz, B., Brown, G.L., and Fohrer, N. (2013). Application of a hydrological-hydraulic modelling cascade in lowlands for investigating water and sediment fluxes in catchment, channel and reach. J Hydrol Hydromech *61*, 334–346.

Knebl, M.R., Yang, Z.-L., Hutchison, K., and Maidment, D.R. (2005). Regional scale flood modeling using NEXRAD rainfall, GIS, and HEC-HMS/RAS: a case study for the San Antonio River Basin Summer 2002 storm event. J. Environ. Manage. *75*, 325–336.

Knight, D., and Shiono, K. (1996). River channel and floodplain hydraulics. Floodplain Process. *5*, 139–181.

Knighton, A.D. (1999). Downstream variation in stream power. Geomorphology *29*, 293–306.

Kronvang, B., Hoffmann, C.C., and Dröge, R. (2009). Sediment deposition and net phosphorus retention in a hydraulically restored lowland river floodplain in Denmark: combining field and laboratory experiments. Mar. Freshw. Res. *60*, 638–646.

Kuemmerlen, M., Domisch, S., Schmalz, B., Cai, Q., Fohrer, N., and Jähnig, S.C. (2012). Integrierte Modellierung von aquatischen Ökosystemen in China: Arealbestimmung von Makrozoobenthos auf Einzugsgebietsebene. Hydrol. Wasserbewirtsch. *56*, 185–192.

Kuemmerlen, M., Schmalz, B., Guse, B., Cai, Q., Fohrer, N., and Jähnig, S.C. (2014). Integrating catchment properties in small scale species distribution models of stream macroinvertebrates. Ecol. Model. *277*, 77–86.

Kundzewicz, Z.W., Lugeri, N., Dankers, R., Hirabayashi, Y., Döll, P., Pińskwar, I., Dysarz, T., Hochrainer, S., and Matczak, P. (2010). Assessing river flood risk and adaptation in Europe—review of projections for the future. Mitig. Adapt. Strateg. Glob. Change *15*, 641–656.

Lambert, C.P., and Walling, D.E. (1987). Floodplain Sedimentation: A Preliminary Investigation of Contemporary Deposition within the Lower Reaches of the River Culm, Devon, UK. Geogr. Ann. Ser. Phys. Geogr. *69*, 393–404.

LANU, S.H. (2006). Die Böden Schleswig Holsteins, Landesamt für Natur und Umwelt des Landes Schleswig Holstein, Kiel.

Lau, T.L., and Ghani, A.A. (2012). Sustainable solutions for global crisis of flooding, pollution and water scarcity. Int. J. River Basin Manag. *10*, 137–138.

Lehner, B., Döll, P., Alcamo, J., Henrichs, T., and Kaspar, F. (2006). Estimating the Impact of Global Change on Flood and Drought Risks in Europe: A Continental, Integrated Analysis. Clim. Change *75*, 273–299.

Lewin, J. (2013). Enlightenment and the GM floodplain. Earth Surf. Process. Landf. *38*, 17–29.

Lewin, J., and Hughes, D. (1980). Welsh floodplain studies: II. Application of a qualitative inundation model. J. Hydrol. *46*, 35–49.

Lin, B., and Falconer, R.A. (1995). Modelling sediment fluxes in estuarine waters using a curvilinear coordinate grid system. Estuar. Coast. Shelf Sci. *41*, 413–428.

Lisle, T.E. (1989). Sediment transport and resulting deposition in spawning gravels, north coastal California. Water Resour. Res. *25*, 1303–1319.

Lisle, T.E., Nelson, J.M., Pitlick, J., Madej, M.A., and Barkett, B.L. (2000). Variability of bed mobility in natural, gravel-bed channels and adjustments to sediment load at local and reach scales. Water Resour. Res. *36*, 3743–3755.

LKN-SH (2012). Landesbetriebs für Küstenschutz, Nationalpark und Meeresschutz Schleswig-Holstein: Discharge and water surface elevation data.

López-Tarazón, J.A., Batalla, R.J., and Vericat, D. (2011). In-channel sediment storage in a highly erodible catchment: the River Isabena (Ebro Basin, Southern Pyrenees). Z. Für Geomorphol. *55*, 365–382.

Lozano, D., and Mateos, L. (2009). Field evaluation of ultrasonic flowmeters for measuring water discharge in irrigation canals. Irrig. Drain. *58*, 189–198.

Lu, Y., and Lueck, R.G. (1999). Using a broadband ADCP in a tidal channel. Part II: Turbulence. J. Atmospheric Ocean. Technol. *16*.

Luo, Y., Arnold, J., Allen, P., and Chen, X. (2012). Baseflow simulation using SWAT model in an inland river basin

in Tianshan Mountains, Northwest China. Hydrol Earth Syst Sci *16*, 1259–1267.

LVA, S.-H. (1995). Digitales Geländemodell DHM50 für Schleswig-Holstein, Gitterweite 50×50 m.

LVermA (1995). Digitales Geländemodell DHM50 für Schleswig-Holstein (Kiel, Germany.).

LVermGeoSH (1995). Landesamt für Vermessung und Geoinformation Schleswig-Holstein: Digitales Geländemodelle 1 (DGM 1).

Macklin, M.G., Brewer, P.A., Balteanu, D., Coulthard, T.J., Driga, B., Howard, A.J., and Zaharia, S. (2003). The long term fate and environmental significance of contaminant metals released by the January and March 2000 mining tailings dam failures in Maramureş County, upper Tisa Basin, Romania. Appl. Geochem. *18*, 241–257.

Marchi, L., Borga, M., Preciso, E., and Gaume, E. (2010b). Characterisation of selected extreme flash floods in Europe and implications for flood risk management. J. Hydrol. *394*, 118–133.

Marchi, L., Borga, M., Cavalli, M., and Gaume, E. (2010a). Stream power of selected recent flash floods in Europe. In EGU General Assembly Conference Abstracts, p. 10226.

Markowska, J., Markowski, J., and Drabiński, A. (2012). Application of HEC-RAS model for estimating changes in watercourse geometry during floods. Stud. Geotech. Mech. *34*, 63.

Marriott, S. (1992). Textural analysis and modelling of a flood deposit: River severn, U.K. Earth Surf. Process. Landf. *17*, 687–697.

Mc Gahey, C., Samuels, P. g., Knight, D. w., and O'Hare, M. t. (2008). Estimating river flow capacity in practice. J. Flood Risk Manag. *1*, 23–33.

Meurer, J. (2012). Modeling the Impact of Climate Change on Hydrology and Sediment Balance in a Low Mountain Range River Basin. Master. University of Kiel.

Middelkoop, H., and Asselman, N.E.M. (1998). Spatial variability of floodplain sedimentation at the event scale in the Rhine–Meuse delta, The Netherlands. Earth Surf. Process. Landf. *23*, 561–573.

Middelkoop, H., Daamen, K., Gellens, D., Grabs, W., Kwadijk, J.C.J., Lang, H., Parmet, B.W. a. H., Schädler, B., Schulla, J., and Wilke, K. (2001). Impact of Climate Change on Hydrological Regimes and Water Resources Management in the Rhine Basin. Clim. Change *49*, 105–128.

Migliaccio, K., and Chaubey, I. (2008). Spatial Distributions and Stochastic Parameter Influences on SWAT Flow and Sediment Predictions. J. Hydrol. Eng. *13*, 258–269.

Mitsch, W.J., and Gosselink, J.G. (2007). Wetlands (New York: John Wiley & Sons, Inc).

MLUR (2004). Landesinterne Berichte zur Bestandsaufnahme der Gewässer: Teileinzugsgebiet Elbe (C-Bericht).

Mouri, G., Minoshima, D., Golosov, V., Chalov, S., Seto, S., Yoshimura, K., Nakamura, S., and Oki, T. (2013). Probability assessment of flood and sediment disasters in Japan using the Total Runoff-Integrating Pathways model. Int. J. Disaster Risk Reduct. *3*, 31–43.

Müller-Wohlfeil, D.-I., Bürger, G., and Lahmer, W. (2000). Response of a River Catchment to Climatic Change: Application of Expanded Downscaling to Northern Germany. Clim. Change *47*, 61–89.

Muste, M., Kim, W., and Fulford, J.M. (2008). Developments in hydrometric technology: new and emerging instruments for mapping river hydrodynamics. World Meteorol. Organ.

Muste, M., Ho, H.-C., and Kim, D. (2011). Considerations on direct stream flow measurements using video imagery: Outlook and research needs. J. Hydro-Environ. Res. *5*, 289–300.

Muste, M., Kim, D., and Merwade, V. (2012). Modern Digital Instruments and Techniques for Hydrodynamic and Morphologic Characterization of River Channels. In Gravel-Bed Rivers, M. Church, P.M. Biron, and A.G. Roy, eds. (John Wiley & Sons, Ltd), pp. 315–341.

NaLaMa-nt (2014). Nachhaltiges Landmanagement im Norddeutschen Tiefland.

Navratil, O., Albert, M.-B., Hérouin, E., and Gresillon, J.-M. (2006). Determination of bankfull discharge magnitude and frequency: comparison of methods on 16 gravel-bed river reaches. Earth Surf. Process. Landf. *31*, 1345–1363.

Nezu, I., and Sanjou, M. (2011). PIV and PTV measurements in hydro-sciences with focus on turbulent open-channel flows. J. Hydro-Environ. Res. *5*, 215–230.

Nicholas, A.P., Walling, D.E., Sweet, R.J., and Fang, X. (2006). Development and evaluation of a new catchment-scale model of floodplain sedimentation. Water Resour. Res. *42*.

Nittrouer, J.A., Shaw, J., Lamb, M.P., and Mohrig, D. (2012). Spatial and temporal trends for water-flow velocity and bed-material sediment transport in the lower Mississippi River. Geol. Soc. Am. Bull. *124*, 400–414.

NLWKN (2011). Niedersächsischer Landesbetrieb für Wasserwirtschaft, Küsten- und Naturschutz. Betriebsstelle Brake-Oldenburg.

O'Hare, M.T., McGahey, C., Bissett, N., Cailes, C., Henville, P., and Scarlett, P. (2010). Variability in roughness measurements for vegetated rivers near base flow, in England and Scotland. J. Hydrol. *385*, 361–370.

Oberg, K. (2002). In Search of Easy-to-Use Methods for Calibrating ADCPs for Velocity and Discharge Measurements. In Hydraulic Measurements and Experimental Methods 2002, (American Society of Civil Engineers), pp. 1–11.

OTT (2008). OTT ADC white paper.

OTT (2010). Mobile river discharge measurement system OTT Qliner –Operating instructions.

OTT (2011). OTT ADC instruction.

Pappenberger, F., Beven, K., Horritt, M., and Blazkova, S. (2005). Uncertainty in the calibration of effective roughness parameters in HEC-RAS using inundation and downstream level observations. J. Hydrol. *302*, 46–69.

Parajuli, P.B., Nelson, N.O., Frees, L.D., and Mankin, K.R. (2009). Comparison of AnnAGNPS and SWAT model simulation results in USDA-CEAP agricultural watersheds in south-central Kansas. Hydrol. Process. *23*, 748–763.

Parhi, P.K. (2013). HEC-RAS Model for Mannnig's Roughness: A Case Study. Open J. Mod. Hydrol. *03*, 97–101.

Parhi, P.K., Sankhua, R., and Roy, G. (2012). Calibration of Channel Roughness for Mahanadi River,(India) Using HEC-RAS Model. J. Water Resour. Prot. *4*.

Pasquale, N., Perona, P., Schneider, P., Shrestha, J., Wombacher, A., and Burlando, P. (2011). Modern comprehensive approach to monitor the morphodynamic evolution of a restored river corridor. Hydrol. Earth Syst. Sci. *15*.

Perlin, A., Moum, J.N., Klymak, J.M., Levine, M.D., Boyd, T., and Kosro, P.M. (2005). A modified law-of-the-wall applied to oceanic bottom boundary layers. J. Geophys. Res. Oceans *110*, n/a–n/a.

Petrow, T., and Merz, B. (2009). Trends in flood magnitude, frequency and seasonality in Germany in the period 1951–2002. J. Hydrol. *371*, 129–141.

Pizzuto, J.E. (1987). Sediment diffusion during overbank flows. Sedimentology *34*, 301–317.

Posey, J. (2009). The determinants of vulnerability and adaptive capacity at the municipal level: Evidence from floodplain management programs in the United States. Glob. Environ. Change *19*, 482–493.

Pott, C.A. (2014). Integrated monitoring, assessment and modeling of nitrogen and phosphorus pollution in a lowland catchment in Germany - A long-term study on water quality. doctor thesis. University of Kiel.

Rantz, S.E. (1982). Measurement and computation of streamflow, volume 1. Measurement of stage and discharge, volume 2. Computation of discharge. US Geol. Surv. Water-Supply Pap. *2175*, 631.

Reckendorfer, W., Funk, A., Gschöpf, C., Hein, T., Schiemer, F., and Arnott, S. (2013). Aquatic ecosystem functions of an isolated floodplain and their implications for flood retention and management. J. Appl. Ecol. *50*, 119–128.

Reniers, A.J.H.M., Thornton, E.B., Stanton, T.P., and Roelvink, J.A. (2004). Vertical flow structure during Sandy Duck: observations and modeling. Coast. Eng. *51*, 237–260.

Rhoads, B.L. (1987). Stream Power Terminology. Prof. Geogr. *39*, 189–195.

Rimkus, A. (2012). Structure of Turbulent Vortices in a Compound Channel. Arch. Hydro-Eng. Environ. Mech. *59*, 113–135.

Ripl, W., and Hildmann, C. (2000). Dissolved load transported by rivers as an indicator of landscape sustainability. Ecol. Eng. *14*, 373–387.

Rodriguez, L.B., Cello, P.A., Vionnet, C.A., and Goodrich, D. (2008). Fully conservative coupling of HEC-RAS with MODFLOW to simulate stream–aquifer interactions in a drainage basin. J. Hydrol. *353*, 129–142.

Rosenfeld, J., Hogan, D., Palm, D., Lundquist, H., Nilsson, C., and Beechie, T.J. (2010). Contrasting Landscape Influences on Sediment Supply and Stream Restoration Priorities in Northern Fennoscandia (Sweden and Finland) and Coastal British Columbia. Environ. Manage. *47*, 28–39.

Rücker, K., and Schrautzer, J. (2010). Nutrient retention function of a stream wetland complex—A high-frequency monitoring approach. Ecol. Eng. *36*, 612–622.

Rudorff, C.M., Melack, J.M., and Bates, P.D. (2014). Flooding dynamics on the lower Amazon floodplain: 1. Hydraulic controls on water elevation, inundation extent, and river-floodplain discharge. Water Resour. Res. *50*, 619–634.

Samani, J., and Mazaheri, M. (2010). An Analytical Model for Velocity Distribution in Transition Zone for Channel Flows over Inflexible Submerged Vegetation. J. Agric. Sci. Technol. *11*, 573–584.

Sarma, K., Lakshminarayana, P., and Rao, N. (1983). Velocity Distribution in Smooth Rectangular Open Channels. J. Hydraul. Eng. *109*, 270–289.

Schmalz, B., and Fohrer, N. (2009). Comparing model sensitivities of different landscapes using the ecohydrological SWAT model. Adv. Geosci. *21*, 91–98.

Schmalz, B., Tavares, F., and Fohrer, N. (2008). Modelling hydrological processes in mesoscale lowland river basins with SWAT—capabilities and challenges. Hydrol. Sci. J. *53*, 989–1000.

Schmalz, B., Kuemmerlen, M., Strehmel, A., Song, S., Cai, Q., Jähnig, S., and Fohrer, N. (2012). Integrierte Modellierung von aquatischen Ökosystemen in China: Ökohydrologie und Hydraulik. Hydrol. Wasserwirtsch. HW *56*, 169–184.

Schulz, M., Kozerski, H.-P., Pluntke, T., and Rinke, K. (2003). The influence of macrophytes on sedimentation and nutrient retention in the lower River Spree (Germany). Water Res. *37*, 569–578.

Schulze, K., Hunger, M., and Döll, P. (2005). Simulating river flow velocity on global scale. Adv. Geosci. *5*, 133–136.

SEBA (2010). Mobile discharge measurement in rivers, channels, sewer flow, fresh-, waste- and saline water.

Seckin, G., and Atabay, S. (2005). Experimental backwater analysis around bridge waterways. Can. J. Civ. Eng. *32*, 1015–1029.

SH, D.-W. (2013). Digitales Anlagenverzeichnis Schleswig-Holstein. Wasser- und Bodenverbände des Landes Schleswig-Holstein und Land Schleswig-Holstein.

Shih, S.F., and Rahi, G.S. (1982). Seasonal variations of Manning's roughness coefficient in a subtropical marsh. Trans ASAE *25*, 116–119.

Simões, F.J.M., and Yang, C.T. (2008). GSTARS computer models and their applications, Part II: Applications. Int. J. Sediment Res. *23*, 299–315.

Singh, V.P., Marini, G., and Fontana, N. (2013). Derivation of 2D Power-Law Velocity Distribution Using Entropy Theory. Entropy *15*, 1221–1231.

Smith, L.C., and Pavelsky, T.M. (2008). Estimation of river discharge, propagation speed, and hydraulic geometry from space: Lena River, Siberia. Water Resour. Res. *44*.

Song, S., Schmalz, B., Hörmann, G., and Fohrer, N. (2012). Accuracy, reproducibility and sensitivity of acoustic Doppler technology for velocity and discharge measurements in medium-sized rivers. Hydrol. Sci. J. *57*, 1626–1641.

Song, S., Schmalz, B., and Fohrer, N. (2014). Simulation and comparison of in-channel flow and floodplain flow in a German lowland area based on the HEC-RAS model. J. Hydrol. Hydromech. Accept. 022014.

SonTek (2000). Doppler velocity log for ROV/AUV applications. SonTek Newsl. *6*.

Sowiski, M. (2006). An uncertainty analysis of the flood-stage upstream from a bridge.

Sponseller, R.A., Grimm, N.B., Boulton, A.J., and Sabo, J.L. (2010). Responses of macroinvertebrate communities to long-term flow variability in a Sonoran Desert stream. Glob. Change Biol. *16*, 2891–2900.

Stacey, M.T., Monismith, S.G., and Burau, J.R. (1999). Observations of Turbulence in a Partially Stratified Estuary. J. Phys. Oceanogr. *29*, 1950–1970.

Stewart, M.D., Bates, P.D., Anderson, M.G., Price, D.A., and Burt, T.P. (1999). Modelling floods in hydrologically complex lowland river reaches. J. Hydrol. *223*, 85–106.

Stone, M.C., and Hotchkiss, R.H. (2007). Evaluating velocity measurement techniques in shallow streams. J. Hydraul. Res. *45*, 752–762.

Storlazzi, C.D., Field, M.E., and Bothner, M.H. (2011). The use (and misuse) of sediment traps in coral reef environments: theory, observations, and suggested protocols. Coral Reefs *30*, 23–38.

Strehmel, A. (2011). Model-based Hydraulic Analysis of Flow and Sediment Transport in the Changjiang Basin in the Poyang Lake Region, China. University of Kiel.

Sun, D., Wang, E., Dong, Z., and Li, G. (2004). Discussion and application of velocity profile in open channel with rectangular cross-section (in Chinese). J. Hydrodyn. Chin. *19*, 144–151.

Talebizadeh, M., Morid, S., Ayyoubzadeh, S.A., and Ghasemzadeh, M. (2009). Uncertainty Analysis in Sediment Load Modeling Using ANN and SWAT Model. Water Resour. Manag. *24*, 1747–1761.

Thandaveswara (2011). River Flow Measurements.

Thuiller, W. (2003). BIOMOD – optimizing predictions of species distributions and projecting potential future shifts under global change. Glob. Change Biol. *9*, 1353–1362.

Tockner, K., Malard, F., and Ward, J.V. (2000). An extension of the flood pulse concept. Hydrol. Process. *14*, 2681–2883.

Tockner, K., Malard, F., Uehlinger, U., and Ward, J.V. (2002). Nutrients and organic matter in a glacial river-floodplain system (Val Roseg, Switzerland). Limnol. Oceanogr. *47*, 266–277.

USACE (2010). HEC-RAS River Analysis System. User's Manual. Version 4.1. U.S. (Davis, CA: Army Corps of Engineers Hydrologic Engineering Center).

Vedula, S., and Achanta, R. (1985). Bed Shear From Velocity Profiles: A New Approach. J. Hydraul. Eng. *111*, 131–143.

Venohr, M. (2000). Einträge und Abbau von Nährstoffen in Fliessgewässern der oberen Stör. University of Kiel.

Vocal Ferencevic, M., and Ashmore, P. (2012). Creating and Evaluating Digital Elevation Model-Based Stream-Power Map as a Stream Assessment Tool. River Res. Appl. *28*, 1394–1416.

Walling, D.E., and He, Q. (1998). The spatial variability of overbank sedimentation on river floodplains. Geomorphology *24*, 209–223.

Walling, D.E., and Owens, P.N. (2003). The role of overbank floodplain sedimentation in catchment contaminant budgets. Hydrobiologia *494*, 83–91.

Walling, D.E., Owens, P.N., Carter, J., Leeks, G.J.L., Lewis, S., Meharg, A.A., and Wright, J. (2003). Storage of sediment-associated nutrients and contaminants in river channel and floodplain systems. Appl. Geochem. *18*, 195–220.

Wang, X.J., Milner, T.E., and Nelson, J.S. (1995). Characterization of fluid flow velocity by optical Doppler tomography. Opt. Lett. *20*, 1337–1339.

Ward, J.V., and Stanford, J.A. (1995). Ecological connectivity in alluvial river ecosystems and its disruption by flow regulation. Regul. Rivers Res. Manag. *11*, 105–119.

Wei, T., Schmidt, R., and McMurtry, P. (2005). Comment on the Clauser chart method for determining the friction velocity. Exp. Fluids *38*, 695–699.

Weitbrecht, V., Seol, D.-G., Negretti, E., Detert, M., Kühn, G., and Jirka, G.H. (2011). PIV measurements in environmental flows: Recent experiences at the Institute for Hydromechanics in Karlsruhe. J. Hydro-Environ. Res. *5*, 231–245.

Wellman, J.C., Combs, D.L., and Cook, S.B. (2000). Long-Term Impacts of Bridge and Culvert Construction or Replacement on Fish Communities and Sediment Characteristics of Streams. J. Freshw. Ecol. *15*, 317–328.

Wiberg, P.L., and Smith, J.D. (1991). Velocity distribution and bed roughness in high-gradient streams. Water Resour. Res. *27*, 825–838.

Wilson, A.J., Walling, D.E., and Leeks, G.J.L. (2004). In-channel storage of fine sediment in rivers of southwest England. V. Golosov, V. Belyaev, and D.E. Walling, eds. (IAHS Publication 288), pp. 291–299.

Wohl, E.E., and Cenderelli, D.A. (2000). Sediment deposition and transport patterns following a reservoir sediment release. Water Resour. Res. *36*, 319–333.

Wu, N., Tang, T., Fu, X., Jiang, W., Li, F., Zhou, S., Cai, Q., and Fohrer, N. (2010). Impacts of cascade run-of-river dams on benthic diatoms in the Xiangxi River, China. Aquat. Sci. *72*, 117–125.

Wu, N., Schmalz, B., and Fohrer, N. (2011). Distribution of phytoplankton in a German lowland river in relation to environmental factors. J. Plankton Res. *33*, 807–820.

Xiang, L., Lu, X.X., Higgitt, D.L., and Wang, S.M. (2002). Recent lake sedimentation in the middle and lower Yangtze basin inferred from 137Cs and 210Pb measurements. J. Asian Earth Sci. *21*, 77–86.

Yan, J., Wang, E., Sun, D., and Dong, Z. (2005). Experiment study velocity distribution characteristics in rectangular cross-section (in Chinese). Eng. J. Wuhan Univ. *38*, 58–60.

Yang, H.-C., and Chang, F.-J. (2005). Modelling combined open channel flow by artificial neural networks. Hydrol. Process. *19*, 3747–3762.

Yang, J., Townsend, R.D., and Daneshfar, B. (2006). Applying the HEC-RAS model and GIS techniques in river network floodplain delineation. Can. J. Civ. Eng. *33*, 19–28.

Yang, S.L., Milliman, J.D., Li, P., and Xu, K. (2011). 50,000 dams later: Erosion of the Yangtze River and its delta. Glob. Planet. Change *75*, 14–20.

Yeager, K.M., and Santschi, P.H. (2003). Invariance of isotope ratios of lithogenic radionuclides: more evidence for their use as sediment source tracers. J. Environ. Radioact. *69*, 159–176.

Yorke, T.H., and Oberg, K.A. (2002). Measuring river velocity and discharge with acoustic Doppler profilers. Flow Meas. Instrum. *13*, 191–195.

Yuan, X., Yin, K., Harrison, P.J., Cai, W.-J., He, L., and Xu, J. (2010). Bacterial production and respiration in subtropical Hong Kong waters: influence of the Pearl River discharge and sewage effluent. Aquat. Microb. Ecol. *58*, 167–179.

Zagarola, M.V., and Smits, A.J. (1998). Mean-flow scaling of turbulent pipe flow. J. Fluid Mech. *373*, 33–79.

Zaimes, G.N., Schultz, R.C., and Isenhart, T.M. (2004). Stream bank erosion adjacent to riparian forest buffers, row-crop fields, and continuously-grazed pastures along Bear Creek in central Iowa. J. Soil Water Conserv. *59*, 19–27.

Zanoun, E.-S., Durst, F., and Nagib, H. (2003). Evaluating the law of the wall in two-dimensional fully developed turbulent channel flows. Phys. Fluids 1994-Present *15*, 3079–3089.

Zeng, W., and Beck, M.B. (2003). STAND, a dynamic model for sediment transport and water quality. J. Hydrol. *277*, 125–133.

Zhang, H. (2011). Sedimentation and Phosphorus Deposition in a Wetland Stream Complex (Duvenseebachniederung, Ritzerau). University of Kiel.

Zhang, X. (2008). Comparison and study of the open channel turbulent velocity distribution formula (in Chinese). Master. Hohai University, China.

Zhang, Z., and Dong, Z. (1998). Viscous fluid mechanics. 358.

Zhang, B., Geiger, W.F., Kaden, S., Kutzner, R., and Wang, Z. (2006). Overall-effective measures for sustainable water resources management in the coastal areas of Shandong Province, China. J. Ocean Univ. China *5*, 339–344.

Zhu, C., and Li, S. (2009). Study on vertical velocity distribution with extra fine sediment. In International Conference on Test and Measurement, 2009. ICTM '09, pp. 260–263.

Zorn, T.G., and Wills, T.C. (2012). A Reconnaissance Survey of the Effects of Sediment Traps on Michigan Streams. North Am. J. Fish. Manag. *32*, 1005–1016.

Appendix

Appendix 1. The description of the point names

Point name	Interpretation
h15	Point 15 in catchment Hunte
h31	Point 31 in catchment Hunte
h34	Point 34 in catchment Hunte
ks100111	Measurement taken on Jan. 10th, 2011in river Kielstau
ks120111	Measurement taken on Jan. 12th, 2011in river Kielstau
n23	Point 23 in catchment Nuthe
n24	Point 24 in catchment Nuthe
O1	Point O1 in catchment Kinzig
S070111	Point 31 in catchment Hunte
S130111	Measurement taken on Jan. 10th, 2011in river Kielstau
S5	Point S5 in catchment Stör
t03	Measurement taken on July 03rd, 2011 in river Treene
t060111	Measurement taken on Jan. 06th, 2011 in river Treene
t09	Measurement taken on July 09th, 2011 in river Treene
t110111	Measurement taken on July 03rd, 2011 in river Treene

Acknowledgements

It is the beginning of my 43th month in Germany, when I finished writing this dissertation. It is not only the ending of my PhD study, but also the closure to my student life, which has been lasting for 22years and half. At this special moment, I definitely have so… many thanks to express.

First and foremost, I would like to give my sincere thanks to dear Prof. Dr. Nicola Fohrer, who gives me the opportunity to study as a PhD student in this warm and lovely working group. During my stay in Germany, and even before I came to Germany, she always supports me, supervises me and provides all kinds of help I need. Without her patience and constructive guidance in reviewing and improving my manuscripts throughout the research, the dissertation would not go so well.

I also want to thank Prof. Dr. Joachim Schrautzer, who has provided a lot of equipment for my field work, and would like to serve as the second reviewer of this dissertation. And the other members of the defense committee, Prof. Dr. Athanasios Vafeidis, Prof. Dr. Felix Müller and Prof. Dr. Hans-Rudolf Bork, who have arranged some time for my defense and provided lots of valuable comments and suggestions for the modification of this dissertation.

I would like to say “Thank you” to my second supervisor both in scientific work and everyday life, Dr. Britta Schmalz. She watched every step and progress of my work and life since the 1st day I arrived in Germany, and contributed so much to this dissertation. Quite often, I was impressed by her friendly, attentive and considerate thought to work and friends.

Sincere gratitude goes the CSC (Chinese Scholarship Council) for providing me the economic support during 2010.09 to 2013.08, for my PhD study in Germany.

Big thanks go to Dr. Cristiano Pott, who has prepared very good SWAT database for this dissertation. Thanks also go to Dr. Georg Hömann and Dipl. Jens Kiesel, who have provided so much technical support concerning the office computer and Arcgis software. Great thanks go to M.Sc. Alexander Strehmel and M.Sc. Yang Yu for the translation of the abstract, hosting me when I was homeless, as well as providing so much encouragement and supporting especially in the last few months. Special thanks go to B.Sc. Jan-Peer Oliver Peers for revising the language of this dissertation, and the help offered to me during my stay in Germany...

A lot of gratitude goes to my colleague in the Department of Hydrology and Water Resources Management. Whenever I think about the colleague who has helped me in blazing sunshine, in freezing winter, in strong storm or hailstone, I feel so touched and grateful. How could my job finished without all the nice help from all of you. The gathering with some colleague in spare time provided me the chance to experience the Germany life, which was really cherished and enriched my life here.

I would like to express my thanks to all my friends in Kiel. They have offered so much help and support, especially at the first and last few months. It is my friends, who brought me out of the lioness and

trepidation at the beginning of my study. It is my friends, who hosted me when I have no place to stay. It is my friends, who prepared the food and forced me to eat, when I was in sickness or totally under stress. It is my friends, who shared my happiness and unhappiness all the time and provided accompany when I needed….

I want to give my very special thanks to one my uncles, Qingliang Wang. He provided me the opportunity to pursue higher education when my family was in a terrible situation. During my study in the last 22years and half, he gave me considerable care and security, both economically and psychologically.

Finally, I would like to give my most special thanks to my parents and brother, who have been protecting me, supporting me and worrying me all the time. Although I know they have always been trying their best to love me, and they really did a great job. But still, sometimes I was shocked when I felt how much they love me, which is much much more than I expected. Sorry for making them worry me for that long time. I want to express my extreme love and thanks to them and tell them: It is my turn to protect you, like what you have done to me in the last 28 years!

Erklärung

Hiermit erkläre ich, dass ich die vorliegende Dissertation, abgesehen von der Beratung durch meine Betreuer, selbständig verfasst habe und keine weiteren Quellen und Hilfsmittel als die hier angegebenen verwendet habe. Diese Arbeit hat weder ganz noch in Teilen bereits an anderer Stelle einer Prüfungskommission zur Erlangung des Doktorgrades vorgelegen. Ich erkläre, dass die vorliegende Arbeit gemäß der Grundsätze zur Sicherung guter wissenschaftlicher Praxis der Deutschen Forschungsgemeinschaft erstellt wurde.

Kiel, Februar 2014

(Song Song)